3-22-2012

An Inquiry: Effectiveness of the Complex Empirical Mode Decomposition Method, the Hilbert-Huang Transform, and the Fast-Fourier Transform for Analysis of Dynamic Objects

Kristen L. Wallis

AN INQUIRY: EFFECTIVENESS OF THE COMPLEX EMPIRICAL MODE DECOMPOSITION METHOD, THE HILBERT-HUANG TRANSFORM, AND THE FAST-FOURIER TRANSFORM FOR ANALYSIS OF DYNAMIC OBJECTS

THESIS

Kristen L. Wallis, Second Lieutenant, USAF

AFIT/GE/ENG/12-42

DEPARTMENT OF THE AIR FORCE
AIR UNIVERSITY

AIR FORCE INSTITUTE OF TECHNOLOGY

Wright-Patterson Air Force Base, Ohio

AFIT/GE/ENG/12-42

AN INQUIRY: EFFECTIVENESS OF THE COMPLEX EMPIRICAL MODE DECOMPOSITION METHOD, THE HILBERT-HUANG TRANSFORM, AND THE FAST-FOURIER TRANSFORM FOR ANALYSIS OF DYNAMIC OBJECTS

THESIS

Presented to the Faculty

Department of Electrical and Computer Engineering

Graduate School of Engineering and Management

Air Force Institute of Technology

Air University

Air Education and Training Command

In Partial Fulfillment of the Requirements for the

Degree of Master of Science in Electrical Engineering

Kristen L. Wallis, BSEE

Second Lieutenant, USAF

March 2012

AFIT/GE/ENG/12-42

AN INQUIRY: EFFECTIVENESS OF THE COMPLEX EMPIRICAL MODE DECOMPOSITION METHOD, THE HILBERT-HUANG TRANSFORM, AND THE FAST-FOURIER TRANSFORM FOR ANALYSIS OF DYNAMIC OBJECTS

Kristen L. Wallis, BSEE
Second Lieutenant, USAF

Approved:

//signed//	22 Feb 2012
Andrew J. Terzuoli, PhD (Chairman)	Date
//signed//	22 Feb 2012
Lt Col Geoffrey A. Akers, PhD (Member)	Date
//signed//	22 Feb 2012
Peter J. Collins, PhD (Member)	Date
//signed//	22 Feb 2012
Mark E. Oxley, PhD (Member)	Date

Abstract

A review of current signal analysis tools show that new techniques are required for an enhanced fidelity or data integrity. Recently, the Hilbert-Huang transform (HHT) and its inherent property, the Empirical Mode Decomposition (EMD) technique, have been formerly investigated. The technique of Complex EMD (CEMD) was also explored. The scope of this work was to assess the CEMD technique as an innovative analysis tool. Subsequent to this, comparisons between applications of the Hilbert transform (HT) and the Fast-Fourier transform (FFT) were analyzed. MATLAB® was implemented to model signal decomposition and the execution of mathematical transforms for generating results. The CEMD technique successfully decomposed the data into its oscillatory modes. After comparative graphical analysis of the HT and FFT, application of the HT provided marginal enhancements of the data modeled previously by the FFT. Altogether, the HHT could not be determined as a helpful analysis tool. Nevertheless, the CEMD technique, an inherent component of the HHT, exhibited a possible improvement as an analysis tool for signal processing data. Further evaluation of the CEMD technique and the HHT is needed for ultimate determination of their usefulness as an analysis tool.

To my loving fiancée,
I could never have finished this without you!

Acknowledgments

I would like to thank Dr Andrew Terzuoli for his support and guidance over the course of the development of this research. Without his reassurances over the course of this research effort, I do not know how I would have stayed sane while working on my thesis. I would also like to thank my research committee members, Lt Col Geoffrey Akers, PhD; Dr Peter Collins; and Dr Mark Oxley. Without their individual expertise in the various aspects of my thesis, I would not have thought to include or address certain topics that needed my attention. The time they sacrificed to attend my research briefings and provide feedback was extremely valuable. In addition, I would like to thank my co-sponsors, Rich Davis and Alan Frazier, who helped me immensely when I hit the "engineering wall," especially where my code was concerned, in order to complete my thesis objectives. Finally, and most importantly, I am extremely grateful for my fiancée, who has sacrificed so much and endured my random discussions of my thesis topic or coding stumbles. It is because of him that I am as successfully in accomplishing this academic achievement as I have been.

Kristen L. Wallis

Table of Contents

Page

Abstract iv

Acknowledgments vi

Table of Contents vii

List of Figures x

List of Tables xv

List of Nomenclature xvi

I. Problem Statement 1

1.1. Background 1
1.1.1. Benefits of Investigating the EMD Technique 2
1.1.2. History of the Hilbert-Huang Transform 2
1.1.3. Explanation of the Empirical Mode Decomposition Technique 4
1.1.4. Primary Focus of the Hilbert-Huang Transform 5
1.1.5. Complex Extensions of the Empirical Mode Decomposition Technique 6
1.2. Statement of Problem 8
1.3. Justification for Research 8
1.4. Approach/Methodology 9
1.4.1. Data Collection 9
1.4.2. Explanation of Chosen Algorithm 10
1.4.3. Qualitative Data to be Analyzed 10
1.5. Overview of Chapters 11

II. Literature Review 12

2.1. Introduction 12
2.2. Literature Review Structure 13
2.3. The Hilbert-Huang Transform 13
2.3.1. Pre-Existing Non-Stationary Methods 14
2.3.2. Method Developed by Huang et al. 16
2.3.3. Intrinsic Mode Functions 16
2.3.4. The Empirical Mode Decomposition Method 17
2.3.5. The Sifting Process 20
2.3.6. The Hilbert Transform 20
2.3.7. The Hilbert Spectrum 21

2.4. Algorithm Variations 23
2.4.1. Algorithmic Variations 23
2.4.2. Performance Elements 24
2.5. Empirical Mode Decomposition as a Filter Bank 25
2.5.1. Fractional Gaussian Noise 25
2.5.2. Flandrin et al. Conclusions 25
2.6. EMD Applications 26
2.6.1. Seismic Application 26
2.6.2. Heart Rate Variability Application 27
2.6.3. Seismic Reflection Application 27
2.6.4. Cycle and Trend Mode Application 29
2.6.5. Petrophysical Model Application 29
2.7. Extending EMD into the Complex Domain 30
2.7.1. Complex Traces and Instantaneous Frequency 31
2.8. Methods for Empirical Mode Decomposition in Complex Domain 32
2.8.1. Complex Empirical Mode Decomposition 32
2.8.2. Rotation Invariant Complex Empirical Mode Decomposition 35
2.8.3. Bivariate Empirical Mode Decomposition 36
2.9. Comparison of EMD and Complex EMD Extensions 39
2.9.1. Realization of Complex EMD 39
2.9.2. Characteristics of Complex EMD 39
2.9.3. Numerical Experiments 40
2.10. Applications for Complex EMD 41
2.10.1. Multichannel Information Fusion 41
2.10.2. Single Vector Sensor Application 43
2.10.3. Multiscale Image Fusion Application 45
2.11. Multivariate EMD Application 47
2.12. Conclusions 48

III. Algorithm Design and Implementation 50

3.1. Overview 50
3.2. Data Collection 51
3.3. Algorithm Design and Components 54
3.3.1. The Empirical Mode Decomposition 54
3.3.2. Complex Extension of Empirical Mode Decomposition 56
3.3.3. The Hilbert Transform 62
3.3.4. The Fourier Transform 66
3.5. Implementation of the Algorithms 69
3.5.1. Unsuccessful Coding Attempts 70
3.5.2. Bivariate Empirical Mode Decomposition Explanation 70
3.5.3. Final CEMD Algorithm Implementation 70
3.6. Chapter Summary 77

IV. Results and Data Analysis 78

4.1. Overview 78
4.2. Evaluation of CEMD Method 78
4.3. Analysis of Decomposed Data Before and After the Hilbert Transform 82
4.3.1. Original Signal Plot Analysis 83
4.3.2. IMF Plot Analysis 85
4.4. Analysis of the FFT Plots Before and After the Hilbert Transform Application 91
4.4.1. Original Signal FFT Plot Comparisons 92
4.4.2. IMF FFT Plot Comparisons 94
4.5. Analysis of Doppler-Time-Intensity Plots Prior to and After the Hilbert Transform 103
4.5.1. Doppler-Time-Intensity (DTI) Plots 103
4.5.2. Original Signal DTI Plot Comparison 103
4.5.3. IMF DTI Plot Comparisons 105
4.5.4. DTI Plot Comparison Conclusions 116
4.6. Chapter Summary 117

V. Conclusions and Future Work 119

5.1. Overall Summary 119
5.2. Key Results 119
5.3. Concluding Thoughts 122
5.4. Future Work 123

Appendix A 125

Appendix B 127

Appendix C 135

Appendix D 137

Bibliography 139

Vita 142

List of Figures

Page
Figure 1: Cylinder with two end caps, on Styrofoam pylon 52
Figure 2: Cylinder with one end cap and one open end, "cavity", on Styrofoam pylon . 52
Figure 3: Cone-Sphere, on Styrofoam pylon 52
Figure 4: Dihedral Spherical Corner Reflector, on Styrofoam pylon 53
Figure 5: The signal enclosed in its 3D envelope. The black thick lines stand for the envelope curves that are used to derive the mean. 57
Figure 6: Illustration of the first definition of the mean of the complex-valued signal... 58
Figure 7: Illustration of the second definition of the mean of the complex-valued signal. 58
Figure 8: CEMD Magnitude of Closed-Cap Cylinder 79
Figure 9: CEMD Magnitude of Real-World Signal--IMF #2 79
Figure 10: CEMD Magnitude of Closed-Cap Cylinder 80
Figure 11: CEMD Magnitude of Real-World Signal--IMF #2 80
Figure 12: CEMD Magnitude of Cone-Sphere 81
Figure 13: CEMD Magnitude of Dihedral Corner Reflector 82
Figure 14: CEMD Magnitude of Real-World Signal—IMF #3 82
Figure 15: CEMD Magnitude of Original Signal 83
Figure 16: HHT Magnitude of Original Signal 83
Figure 17: CEMD Phase of Original Signal 84
Figure 18: HHT Phase of Original Signal 84
Figure 19: EMD Magnitude of IMF #1 85

Figure 20: HHT Magnitude of IMF #1 85
Figure 21: CEMD Magnitude of IMF #2 86
Figure 22: HHT Magnitude of IMF #2 86
Figure 23: CEMD Magnitude of IMF #5 87
Figure 24: HHT Magnitude of IMF #5 87
Figure 25: CEMD Magnitude of IMF #6 88
Figure 26: HHT Magnitude of IMF #6 88
Figure 27: CEMD Magnitude of IMF #7 89
Figure 28: HHT Magnitude of IMF #7 89
Figure 29: CEMD Magnitude of IMF #8 89
Figure 30: HHT Magnitude of IMF #8 89
Figure 31: CEMD Magnitude of IMF #9 90
Figure 32: HHT Magnitude of IMF #9 90
Figure 33: CEMD Magnitude of IMF #10 90
Figure 34: HHT Magnitude of IMF #10 90
Figure 35: CEMD Magnitude of IMF #11 91
Figure 36: HHT Magnitude of IMF #11 91
Figure 37: FFT of CEMD Magnitude of Original Signal 92
Figure 38: FFT of HHT Magnitude of Original Signal 92
Figure 39: FFT of CEMD Phase of Original Signal 93
Figure 40: FFT of HHT Phase of Original Signal 94
Figure 41: FFT of CEMD Magnitude of IMF #1 95
Figure 42: FFT of HHT Magnitude of IMF #1 95

Figure 43: FFT of CEMD Magnitude of IMF #2 95
Figure 44: FFT of HHT Magnitude of IMF #2 95
Figure 45: FFT of CEMD Magnitude of IMF #3 96
Figure 46: FFT of HHT Magnitude of IMF #3 96
Figure 47: FFT of CEMD Magnitude of IMF #4 96
Figure 48: FFT of HHT Magnitude of IMF #4 96
Figure 49: FFT of CEMD Magnitude of IMF #5 97
Figure 50: FFT of HHT Magnitude of IMF #5 97
Figure 51: FFT of CEMD Magnitude of IMF #6 98
Figure 52: FFT of HHT Magnitude of IMF #6 98
Figure 53: FFT of CEMD Magnitude of IMF #7 98
Figure 54: FFT of HHT Magnitude of IMF #7 98
Figure 55: FFT of CEMD Magnitude of IMF #8 99
Figure 56: FFT of HHT Magnitude of IMF #8 99
Figure 57: FFT of CEMD Magnitude of IMF #9 99
Figure 58: FFT of HHT Magnitude of IMF #9 99
Figure 59: FFT of CEMD Magnitude of IMF #10 100
Figure 60: FFT of HHT Magnitude of IMF #10 100
Figure 61: FFT of CEMD Magnitude of IMF #11 100
Figure 62: FFT of HHT Magnitude of IMF #11 100
Figure 63: FFT of CEMD Phase of IMF #1 101
Figure 64: FFT of HHT Phase of IMF #1 101
Figure 65: FFT of CEMD Phase of IMF #5 101

Figure 66: FFT of HHT Phase of IMF #5 101
Figure 67: FFT of CEMD Phase of IMF #7 102
Figure 68: FFT of HHT Phase of IMF #7 102
Figure 69: FFT of CEMD Phase of IMF #11 102
Figure 70: FFT of HHT Phase of IMF #11 102
Figure 71: DTI Magnitude of Original Signal 104
Figure 72: DTI HHT Magnitude of Original Signal 104
Figure 73: DTI Magnitude of IMF #1 106
Figure 74: DTI HHT Magnitude of IMF #1 106
Figure 75: DTI Magnitude of IMF #2 107
Figure 76: DTI HHT Magnitude of IMF #2 107
Figure 77: DTI Magnitude of IMF #5 109
Figure 78: DTI HHT Magnitude of IMF #5 109
Figure 79: DTI Magnitude of IMF #6 110
Figure 80: DTI HHT Magnitude of IMF #6 110
Figure 81: DTI Magnitude of IMF #7 111
Figure 82: DTI HHT Magnitude of IMF #7 111
Figure 83: DTI Magnitude of IMF #8 112
Figure 84: DTI HHT Magnitude of IMF #8 112
Figure 85: DTI Magnitude of IMF #9 114
Figure 86: DTI HHT Magnitude of IMF #9 114
Figure 87: DTI Magnitude of IMF #10 115
Figure 88: DTI HHT Magnitude of IMF #10 115

Figure 89: DTI Magnitude of IMF #11 116
Figure 90: DTI HHT Magnitude of IMF #11 116
Figure 91: BEMD Algorithm by Dr. Flandrin 126
Figure 92: Section B.1 Modified BEMD Algorithm 127
Figure 93: Section B.2 Modified BEMD Algorithm 127
Figure 94: Section B.3 Modified BEMD Algorithm 128
Figure 95: Section B.4 Modified BEMD Algorithm 129
Figure 96: Section B.5 Modified BEMD Algorithm 130
Figure 97: Section B.6 Modified BEMD Algorithm 131
Figure 98: Section B.7 Modified BEMD Algorithm 133
Figure 99: Section B.7 Modified BEMD Algorithm 134
Figure 100: CEMD_FIX function 136
Figure 101: DTI Magnitude of IMF #3 137
Figure 102: DTI HHT Magnitude of IMF #3 137
Figure 103: DTI Magnitude of IMF #4 138
Figure 104: DTI HHT Magnitude of IMF #4 138

List of Tables

Page

Table 1: The EMD Algorithm 4

Table 2: Flandrin et al. EMD Algorithm 18

Table 3: Analytic Expression of Given Signal 31

Table 4: Algorithm 1 for EMD Bivariate Extension 38

Table 5: Algorithm 2 for EMD Bivariate Extension 38

Table 6: Algorithm 2 Reformulation for EMD Bivariate Extension 59

Table 7: Hilbert Transform Pairs 64

Table 8: MATLAB® Hilbert Algorithm [22] 66

List of Nomenclature

Term	Abbreviations
AFIT **L**ORE **P**rocessing **IN**tegrated **E**nvironment	ALPINE
Bivariate Empirical Mode Decomposition	BEMD
Complex Empirical Mode Decomposition	CEMD
Discrete Fourier Transform	DFT
Doppler-Time-Intensity	DTI
Empirical Mode Decomposition	EMD
Fast-Fourier Transform	FFT
Graphical User Interface	GUI
Hilbert-Huang Transform	HHT
Intrinsic Mode Function(s)	IMF(s)
Multivariate Empirical Mode Decomposition	MEMD
Radar-Cross Section	RCS
Rotational Invariant Complex Empirical Mode Decomposition	RICEMD
Signal-to-Noise	SNR
Standard Deviation	SD
Vector Hilbert-Huang Transform	VHHT

Mathematical Symbol	Meaning
*	Conjugate
Re(•)	Real-value of signal

AN INQUIRY: EFFECTIVENESS OF THE COMPLEX EMPIRICAL MODE DECOMPOSITION METHOD, THE HILBERT-HUANG TRANSFORM, AND THE FAST-FOURIER TRANSFORM FOR ANALYSIS OF DYNAMIC OBJECTS

I. Problem Statement

1.1. Background

The effectiveness of the Hilbert-Huang transform (HHT), and more specifically the complex extension of the Empirical Mode Decomposition (EMD) technique within the HHT, as analysis tools for complex radar-cross section (RCS) data collected from dynamic objects were being investigated. In addition to assessing the use of the HHT for complex RCS data, both the Fast-Fourier transform (FFT) and Hilbert transform were applied to the data that has been analyzed using the Complex Empirical Mode Decomposition (CEMD) algorithm. Once results have been generated for both transforms based on the decomposed complex data, the outputs from the two transforms were compared to determine whether the HHT can provide information or better fidelity not previously provided by the FFT of the decomposed complex data.

In addition to assessing the EMD technique of the HHT, the EMD technique was extended into the realm of complex-valued signals and complex-valued data to provide a more accurate output of the data being processed by the FFT and the Hilbert transform of the decomposed complex data. While the original EMD method analyzes only the real-valued or magnitude portion of the data, the use of an algorithm that allows the analysis of complex data was implemented as part of assessing and examining the usefulness of the HHT.

1.1.1. Benefits of Investigating the EMD Technique

The benefits of the findings were weighed prior to beginning the research, especially when determining their validity and usefulness as a possible tool. This particular problem does not require the use of expensive equipment or many undeveloped concepts, but there is a cost concerning manpower and time devoted to researching existing topics and determining how the new topic will be approached.

For the task of assessing the CEMD technique and HHT as analysis tools, as well as determining the usefulness compared with the FFT, the benefits will outweigh the time spent in the research and development towards the problem. Due to the previous research done in the field of knowledge and development of the EMD technique, there is a good foundation for the development of the CEMD coding that will be necessary for assessment of the CEMD method and the use of the HHT. The largest benefit of assessing the use of the CEMD method and the HHT presently is determining its potential for future.

1.1.2. History of the Hilbert-Huang Transform

Historically, analysis of data collected from dynamic objects has been done using the Fourier spectral analysis, consisting of the Discrete Fourier transform (DFT) and the Fourier transform. In the mid-1960s, after the development of the FFT, analysis in computationally intense fields was revolutionized. Even though the Fourier transform had been used in data analysis for years prior to the introduction of the FFT, implementation of the FFT algorithm allowed those working with the Fourier spectral analysis for data processing experienced an expedited form of signal processing. For the past 50 years, the FFT has been the primary analysis tool for signal processing. Even

though the FFT has provided an acceptable analysis procedure for linear and stationary (or periodic) data sets, Fourier analysis has some constraints and drawbacks inherent to the method.

The primary drawback inherent to Fourier analysis, and by extension the FFT algorithm, is a limitation founded upon the analysis of linear and stationary data. The property of analysis of linear and stationary data is due to the FFT employing a known and predefined set of basis functions that maps the inputted data from the time domain to the frequency domain. Consequently, analysis of nonlinear (such as shockwave data or turbulence data) and non-stationary data is nearly impossible with the FFT.

As a result of the constraint on the FFT method, other mathematical tools are receiving consideration from analysts in the intelligence community. In recent years, an innovative technique for analyzing dynamic objects has been investigated in other fields of study. The specific mathematical tool that was analyzed, scrutinized, and assessed throughout this thesis is the HHT, a more recent analysis tool that contains the EMD technique and the Hilbert transform.

Dr. Huang [1] claimed that the HHT is more suitable to analyze nonlinear and non-stationary objects, resulting in an interest of investigating the capabilities and possibilities of using the HHT as an analysis tool. The HHT performs the decomposition of the signal into its oscillatory modes using the EMD technique and applies the Hilbert transform to these modes, which results in the Hilbert spectrum representation of the signal.

1.1.3. Explanation of the Empirical Mode Decomposition Technique

The EMD algorithm is an adaptive technique, in which a given signal is decomposed into a set of oscillating basis functions through use of the sifting process. These oscillatory components of the decomposed signal are called the Intrinsic Mode Functions (IMFs) and are representations of the oscillating nature embedded in the data [1]. The Fourier transform has a predefined set of basis functions, yet the IMFs that are decomposed from the data are considered the basis functions for the given signal.

More precisely, the EMD performs the following decomposition through various steps:

$$x(k) = \sum_{i=1}^{N} c_i(k) + r(k) \tag{1}$$

where $c_i(k), i = 1, ..., N$ denote the IMFs and $r(k)$ denotes the residual. The IMF is characterized by two properties: (1) the upper and lower envelopes are symmetric; and (2) the number of zero-crossings and the number of extrema are exactly equal [2].

To extract the IMFs from a given signal, the following sifting algorithm is employed, as detailed in Table 1 [1].

Table 1: The EMD Algorithm

1. Find the locations of all the extrema of the given signal, $x'(k)$
2. Interpolate (using the cubic spline interpolation) between all the minima and respective maxima to obtain the signal envelope passing through the minima $e_{\min}(k)$ and respective maxima $e_{\max}(k)$
3. Compute the local mean $m(k) = \left(e_{\min}(k) + e_{\max}(k)\right)/2$
4. Subtract the local mean from the signal to obtain the "oscillating" signal $s(k) = x'(k) - m(k)$
5. If the resulting signal obeys the stopping criterion, $d(k) = s(k)$ becomes an IMF; otherwise, set $x'(k) = s(k)$ and repeat the process from Step 1

The stopping criterion for the final step is the normalized squared difference between two successive iterates, $s_n(k)$ and $s_{n-1}(k)$, or as follows:

$$\sum_{i=0}^{N} \frac{\left\| s_{i-1}(k) - s_i(k) \right\|^2}{s_{i-1}^2(k)} \leq SD, \tag{2}$$

where *N* represents the total number of samples in the original signal $x(k)$, and the standard deviation (SD) is set within the range of (0.2-0.3) [1].

Once the sifting algorithm is implemented, the Hilbert transform is applied to each individual IMF. The resulting equation upon application of the Hilbert transform, is given by, representing the Hilbert spectrum is as follows:

$$X(t) = \sum_{i=1}^{N} a_i(t) e^{j\theta_i(t)}, \tag{3}$$

where $a_i(t)$ is the time-dependent amplitude and $\theta_i(t)$ is the phase function. The instantaneous radial frequency can be defined by

$$\omega_i(t) = \frac{d\theta_i(t)}{dt} \tag{4}$$

and can be plotted against the amplitude, in which the resulting plot is the Time-Frequency Amplitude, representing the Hilbert spectrum. The combination of the instantaneous frequency concept, detailed in (4), and the EMD technique, detailed in (1), makes the HHT a powerful tool in both signal decomposition and signal analysis [2].

1.1.4. Primary Focus of the Hilbert-Huang Transform

The HHT consists of the EMD technique and Hilbert transform, in which the primary focus of assessing the use of the HHT to analyze RCS data is the EMD technique

portion. The Hilbert spectrum results from the Hilbert transform application and is used in comparing the generated graphical results. The EMD technique has been investigated extensively by numerous researchers [3]-[8]; therefore, for purposes of data analysis in this evaluation, the EMD extension into the complex domain will be explored as applied to complex RCS data. The CEMD method has become more relevant in fields where the data collected contains a phase component (such as signal processing).

1.1.5. Complex Extensions of the Empirical Mode Decomposition Technique

Several complex extensions of the EMD technique have been developed recently. Such complex methods include CEMD [9], RICEMD [10], and BEMD [11]. Throughout literature, the term CEMD is ambiguous, referring to the method described in [9] or in reference to the process of extending the EMD technique to the complex domain.

The first extension introduced for extending the EMD technique in the complex domain was termed CEMD by Tanaka and Mandic [9]. The authors used the relationship that exists between the positive and negative frequency components of the complex signal. Rather than viewing the result as one signal consisting of these two frequency components, Tanaka and Mandic view the IMFs extracted as independent of each other. Then, by applying the EMD technique to the negative and positive frequency components, the two sets of IMFs were created, which corresponded to the negative and positive frequency components. This method works well for the low-dimensional (such a single dimensional) case, but when applied to a higher-dimensional case, the analysis degrades due to the rigorous mathematical nature of the algorithm and the non-intuitive extension from the original EMD algorithm. [9]

A second complex EMD extension proposed by Umair Bin Altaf et al. is RICEMD [10]. This method differs from the CEMD method developed by Tanaka and Mandic [9], where the RICEMD method operates completely in the complex domain. As a result, the steps to accomplish the EMD method are performed in the complex domain rather than the real domain. The only difference between the original EMD method and this proposed complex extension exists in determining the extrema and the envelope of the signal. Other than these two steps of the EMD algorithm being changed, the RICEMD and the original EMD methods are accomplished in the same manner.

One final method proposed for the realization of the complex EMD analysis is called BEMD [11] developed by Rilling et al. This method is based on the idea of "bivariate signal = fast rotations + slow rotations." In order to discriminate between the "fast" and "slow" rotations, the idea is to define the "slow" component as the mean of the defined "envelope." The envelope for the bivariate signal is now three dimensional rather than two dimensional, as in the univariate signal case. After the data points for analysis of the signal are selected, the issue of defining the mean arises. The preferred definition for the mean is the intersection of two straight lines, where the lines intersecting correspond to the two horizontal tangents and the two vertical tangents [11].

The desired goal for defining the mean was the same as the original EMD method: a smooth curve with as few oscillations as possible. The interpolation scheme employed by the BEMD technique is a cubic spline. The cubic spline was employed due to its minimum curvature property and fits the purpose of the EMD algorithm best.

The BEMD method was employed to extract the complex IMFs because the idea of projecting the signal into specific directions to extract the extrema, as well as

connecting the points to create the desired envelope is intuitive and similar to the original EMD method. The bivariate time series in the algorithms is treated as a complex-valued time series. Given an angle direction, the bivariate extensions are defined by the EMD algorithm, only with new sifting elementary operators defined by S^{B1} and S^{B2},which correspond to the two algorithms [11].

For the purposes of this thesis, the BEMD method proposed by Rilling et al. was employed to analyze the complex RCS data provided by the sponsor, as well as the simulated data collected at the RCS range.

1.2. Statement of Problem

The problem addressed in this research effort consisted of two parts. The first part was assessing the use of the CEMD technique of the HHT as an analysis tool on complex RCS data created by dynamic objects. Next, the decomposed signal after implementation of the CEMD method was analyzed after the applications of the FFT and Hilbert transform to determine whether the HHT provided enhanced analysis of the signal as compared with analysis provided previously from the FFT.

1.3. Justification for Research

Traditional data analysis tools, such as the Fourier transform and wavelet analysis, depend on the mapping of a pre-existing and known signal being transformed from the time domain to the frequency domain or from the scale domain to the dilation domain, respectively. Such tools are limited to the analysis of linear and stationary signals, leading to problems when a need to analyze nonlinear and non-stationary data arises. Most data collected fall within this category of nonlinear and non-stationary data,

for the sake of simplicity, there is a standing assumption that the data are linear and stationary. Recently, there has been interest in analyzing the data collected from dynamic objects using the CEMD technique and the HHT. Because the data are nonlinear and non-stationary, applying this recent adaptive data-driven analysis tool may provide novel insights about the data. The assessment of implementing the CEMD method as an analysis tool will be investigated through use of both real-world and simulated data. Then, in comparing the plotted IMFs resulting from employment of the CEMD method both before and after the application of the Hilbert transform using various mathematical transforms, the final decision will be made about the use of the CEMD method and the HHT as analysis tools.

1.4. Approach/Methodology

The methodology that will be used to complete the research will be described in greater detail in the methodology chapter, but a brief overview is provided in the following paragraphs.

1.4.1. Data Collection

The first data set evaluated was the real-world data set provided by the sponsor. In addition to this data set, four sets of simulated data collected at AFIT's RCS range were used in comparing with the decomposed real-world data set after the CEMD method is employed. These four sets of simulated data included: a cylinder with two end caps; a cylinder with one end cap and one open end (or cavity cylinder); an ogive; and a dihedral corner reflector. Once all data was collected, it will be calibrated using the MATLAB® graphical user interface (GUI) called ALPINE© [18]. Then, it will be converted into a

MAT-file that can be read into MATLAB®. At this point, the algorithm introduced in the following paragraph will be employed.

1.4.2. Explanation of Chosen Algorithm

Research has been done concerning methods that presently exist in the realm of analyzing complex-valued data sets that extend the EMD technique. Of the three methods that are most recognized by the academic community, the method that was employed in the data analysis for this work was the BEMD method developed by Rilling and Flandrin [11]. The BEMD method was used as a model, but there were some modifications to use the method on the dynamic object data set provided. Once the BEMD algorithm was created, the analysis of the data was accomplished.

After the BEMD algorithm was refined and tested on code provided, the real-world and simulated data were analyzed by the BEMD code developed for this research effort. After the data was analyzed by the BEMD technique code, three different transforms were applied to the resulting IMFs. First, the Hilbert transform was applied to the decomposed data. Second, the FFT was applied to the decomposed data both before and after the Hilbert transform application. Finally, the windowed FFT was applied to the decomposed data both before and after the Hilbert transform, represented as a Doppler-Time-Intensity (DTI) plot. For all three applied transforms, the IMFs of the complex RCS data were plotted and recorded, being used in the data analysis portion of the research.

1.4.3. Qualitative Data to be Analyzed

The analyzed data was qualitative data, in the form of graphs created in MATLAB®. The plotted IMFs resulting from the application of the Hilbert transform,

the FFT, and the Windowed FFT were the graphs compared for data analysis. These plotted IMFs were compared and distinct features, to include differences, similarities, and unique points, were documented. The sets of plotted IMFs from the three mathematical transformed mentioned earlier in this paragraph were the data analyzed.

1.5. Overview of Chapters

The remaining chapters of the thesis include the following components: the literature review section; the methodology section; the data analysis and results section; and the conclusions section. The literature review will contain analysis of work already done on the topic of the EMD technique and the HHT, including articles relevant to the research for the problem being investigated. The methodology section details the approach to complete the research and method employed to create the qualitative data to be analyzed in the data analysis section. The main idea of the methodology is to qualitatively represent the problem as graphs, as well as provide a way to assess the use of the CEMD method and the HHT as analysis tools. After the methodology is explained, the plotted data sets will be discussed and analyzed in the data analysis section. The resulting plotted IMFs created by the data will be analyzed and compared in order to determine whether the CEMD algorithm and the HHT provide enhanced fidelity than the FFT. The thesis will continue with a discussion of the data created by the CEMD coding. Concluding thoughts will be made in the final section as to the assessment of the CEMD algorithm and the HHT as possible analysis tools, as well as how the Hilbert transform compares with the FFT analysis of dynamic object data sets.

II. Literature Review

2.1. Introduction

Traditionally, the use of "Fourier spectral analysis" [1] through application of the Fourier transform, as well as the faster algorithm of the FFT, has been used to quantify various sets of data in the signal analysis department. The restrictive nature of the Fourier transform primary need for a linear system and strictly periodic or stationary data [1], other transforms have been researched as possible supplemental or replacement analysis tools in the fields where nonlinear and non-stationary data exist.

More recently, investigation into a newer mathematical transforms have been conducted. One transform called the HHT was introduced by Dr. Huang et al. [1] and has since been used in numerous fields of science and engineering, ranging from seismic analysis to heartbeat patterns [3], [4], [6], and [14]. The HHT consists of two components: (1) the Empirical Mode Decomposition (EMD) method and (2) the Hilbert transform.

The EMD method is an adaptive technique in which a given signal is decomposed into a set of oscillating components through use of the sifting process. The oscillatory components are called the IMFs of the given signal and are representations of the oscillating nature embedded in the data. The FFT has a defined set of basis functions; however, the IMFs that are decomposed from the data are considered the basis functions for the signal. The EMD technique and application of the Hilbert transform to create the Hilbert spectrum comprise the HHT.

The EMD accepts only real-valued signals and could lead to the loss of some information provided by the signal. Therefore, research has been performed in the past

five years to create a way to extend the EMD technique to analyze complex-valued signals, consisting of the real-valued and imaginary-valued data. Several researchers [9,10,11] have also developed methods that fall under the topic of the CEMD; they have extended the EMD technique to incorporate complex-valued data sets rather than only the real-valued components of the data.

2.2. Literature Review Structure

The work accomplished by Dr. Huang et al. [1] is analyzed by the various ways the HHT and EMD technique have been adapted into a number of fields of study [3]-[4], [6], [14] and will conclude with the more recent developments for the CEMD technique [9]-[11], [15]-[17], as well as multivariate signals [12]. Over the course of approximately 15 years of research, many breakthroughs and discoveries concerning the use of the HHT have occurred, more specifically concerning the EMD technique inherent to the HHT. Upon completing this literature review, a greater understanding of the HHT and EMD technique is expected.

2.3. The Hilbert-Huang Transform

Where the details of the HHT are concerned, Dr. N. E. Huang is a leading authority in the field. Huang et al. wrote introduced "[t]he empirical mode decomposition and the Hilbert spectrum for nonlinear and non-stationary time series analysis" [1] in 1998 and introduced a new method for analyzing nonlinear and non-stationary data, known as the HHT. There are two components of the HHT, as stated above, but the key part of the HHT is the EMD technique. Huang et al. claimed that, through the application of the EMD technique, "any complicated data set can be

decomposed into a finite and…small number of 'intrinsic mode functions' that admit well-behaved Hilbert transforms" [1]. Much interest has been shown for use of the EMD technique due to its adaptive nature and the claim that it is also "highly-efficient" [1] due to that adaptiveness. Another important trait the EMD technique possesses is its ability to be applied to a localized region. In order to apply the EMD to nonlinear and non-stationary time series, the necessary conditions of the data are that of (1) locality and (2) adaptivity.

2.3.1. Pre-Existing Non-Stationary Methods

In preparing for the explanation of the development of the EMD technique and Hilbert spectrum, Huang et al. present various pre-existing non-stationary data processing methods [1]. The following methods work for non-stationary (or non-periodic) data, but depend heavily on Fourier analysis, leading the applications of these methods to be limited to linear data.

The first method discussed is the most basic method called the spectrogram. Huang et al. claim that the spectrogram "is nothing but a limited time window-width Fourier spectral analysis" [1]. Because it depends on Fourier analysis, it is not used for the analysis of nonlinear and non-stationary data.

The next approach is the wavelet analysis, an adjustable window Fourier analysis, defined by the following equation:

$$W(a,b;X,\psi) = |a|^{-1/2} \int_{-\infty}^{\infty} X(t)\psi^*\left(\frac{t-b}{a}\right)dt \tag{5}$$

where $\psi^*(\bullet)$ is the wavelet function, a is the dilation factor and b is the translation of the origin. The physical explanation of (5) is that $W(a,b;X,\psi)$ is the "energy" of X of

scale a at $t = b$ [1]. The continuous wavelet analysis is of an analytic form, in which the problem employing it occurs with the Morlet wavelet as an example, making the "quantitative definition of the energy-frequency-time distribution difficult" [1]. Even though the wavelet analysis contains difficulties, Huang et al. use the wavelet analysis in the validation of the Hilbert spectrum.

A third method, called the Wigner-Ville distribution, is also sometimes referred to as the Heisenberg wavelet. By definition, the Wigner-Ville distribution is the Fourier transform of the central covariance function, defined by the following equation:

$$V(\omega,t) = \int_{-\infty}^{\infty} C_c(\tau,t) e^{-i\omega\tau} d\tau \,, \tag{6}$$

where

$$C_c(\tau,t) = X\left(t - \frac{1}{2}\tau\right) X^*\left(t + \frac{1}{2}\tau\right). \tag{7}$$

The problem with the Wigner-Ville distribution occurs with the cross terms that result from the negative energy components, thus resulting in a windowed Fourier analysis [1]. The Fourier analysis limitations are forced upon the Wigner-Ville distribution analysis, primarily the linearity condition.

Another method is the evolutionary spectrum, where the classical Fourier analysis is extended to a more generalized basis. Thus, a method is sought to define the basis, $\{\phi(\omega,t)\}$, without defining it prior to the application of the method.

The final method introduced by Huang et al. prior to the EMD technique and Hilbert spectrum was the empirical orthogonal function (EOF) expansion. EOF

expansion states, for any real signal, $z(x,t)$, the application of the EOF will reduce the signal to:

$$z(x,t) = \sum_{k=1}^{n} a_k(t) f_k(x) \quad (8)$$

The expansion basis for EOF is derived from the data, showing it as adaptive. Notwithstanding, its main problem is the uncertainty of its true meaning where non-stationarity and nonlinearity are concerned, alluding to the conclusion. EOF is not an effective improvement from those methods dependent upon Fourier analysis.

2.3.2. Method Developed by Huang et al.

The method introduced by Huang et al. is a general method that consists of two steps. The first is the decomposition of the data through the EMD technique, where the data are decomposed into a number of IMFs. The next step is to apply the Hilbert transform to those IMFs, resulting in the Hilbert spectrum. Contained within the Hilbert spectrum are the instantaneous (or local) frequency and instantaneous energy, and are used for analysis rather than the global frequency and energy as defined by Fourier analysis [1].

2.3.3. Intrinsic Mode Functions

Huang et al. proposed a "class of functions designated as intrinsic mode functions," [1] where the formal definition is as follows:

> "An intrinsic mode function (IMF) is a function that satisfies two conditions: (1) in the whole data set, the number of extrema and the number of zero crossing must either equal or differ at most by one; and (2) at any point, the mean value of the envelope defined by the local maxima and the envelope defined by the local minima is zero" [1].

The first condition, as stated above, is similar to the narrowband requirements for a stationary process. The second condition presented takes the global requirement from a stationary data set and adapts it to the local level for non-stationary data sets. The ideal requirement is for the local mean of the given data set to be zero. The IMFs represent the oscillatory modes that are embedded in the data and can be in the form of either amplitude-modulated signals or frequency-modulated signals.

2.3.4. The Empirical Mode Decomposition Method

The EMD method is also commonly referred to as the sifting process. This new method is used with both nonlinear and non-stationary data. In order to help with the analysis of nonlinear and non-stationary signals, the EMD method has successfully been used in applications of various disciplines due to its versatile data-driven signal analysis ability. The EMD method is a new technique, pioneered specifically for the purposes of adaptively representing nonlinear and non-stationary signals as sums of zero-mean amplitude- and frequency-modulated components. The one new feature of this method, when compared to previously existing methods, is that the EMD technique is "intuitive, direct, *a posteriori* and adaptive, with the basis of the decomposition based on…the [given] data" [1].

The main idea of the EMD technique is to decompose the signal into its oscillatory modes. As long as the two conditions stated in the IMF definition in section 2.2.3 are satisfied, the EMD method can use the envelopes defined by the maxima and minima separately. After the extrema are identified, the local maxima are connected with a cubic spline as the upper envelope. The same process is performed for the lower

envelope. Sifting is a similar process, in which the finest local mode is separated from the rest of the data [1].

The EMD method is designed to "reduce non-stationary, multicomponent signals to a series of amplitude- and frequency-modulated contributions" [6] and can be used to gain significant information inherent to the signal. Although other methods exist for non-stationary analysis, the EMD method differs from wavelet decomposition in which the "filters of the filter band do not correspond to sub-band filtering but instead to signal-dependent, time-variant filters" [6].

The EMD technique operates in the time-domain and adaptively decomposes a signal into a set of basis functions called the IMFs, and data can be considered to be mapped onto a space spanned by the IMFs [10]. By applying the Hilbert transform to the IMFs, the "instantaneous frequency" is introduced.

To apply the technique of EMD, the given signal must be considered at the local oscillation level. The algorithm that Flandrin et al. employs is the algorithm described in Table 2 [8].

Table 2: Flandrin et al. EMD Algorithm

Given a signal $x(t)$:
1. Identify all extrema of $x(t)$
2. Interpolate between minima and respective maxima, ending up with some envelope $e_{\min}(t)$ and its respective $e_{\max}(t)$.
3. Compute the mean: $m(t) = \frac{1}{2}\left(e_{\min}(t) + e_{\max}(t)\right)$
4. Extract the detail: $d(t) = x(t) - m(t)$
5. Iterate on the residual: $m(t)$

In the above algorithm, the detail, denoted by $d(t)$, corresponds to the oscillation terminating at the two minima and passing through the maximum value of the oscillating wave, existing between the two extrema. The local trend, denoted by $m(t)$, corresponds to the low-frequency part. The sifting process is employed on the signal, where an IMF and residual are extracted and the iterative algorithm is performed on the residual portion. The sifting process is applied to $d(t)$ until $d(t)$ can be considered as zero-mean, according to the stopping criterion [8].

The method of EMD considers a signal at the scale of its local oscillations and attempts to formalize the idea that "signal = fast oscillations superimposed on slow oscillations" [11]. The EMD technique is designed to define local "low frequency" components as the local trend, $m_1[x](t)$, where this local trend then supports a local "high frequency" component as a zero-mean oscillation, or local detail, $d_1[x](t)$.

The signal is represented by the following expression:

$$x(t) = m_1[x](t) + d_1[x](t), \tag{9}$$

where $d_1[x](t)$ corresponds to an IMF. The sifting process is performed on (9) and the signal expression becomes:

$$x(t) = m_k[x](t) + \sum_{k=1}^{K} d_k[x](t). \tag{10}$$

Once the convergence criterion has been met, the local detail and local trend are represented as, $d_1[x](t) = S^n[x](t)$ and $m_1[x](t) = x(t) - d_1[x](t)$, respectively [11].

2.3.5. The Sifting Process

Huang et al. suggested a data-adapted method in which an oscillating wave is extracted from a given signal [13]. Each oscillating wave is defined as an IMF that satisfies the two conditions outlined by Huang et al. [1]. The sifting process is an iterative process, meaning that if the two conditions outlined by Huang et al. are not met, then the sifting procedure will be repeated until the two conditions are satisfied [13]. A "stopping rule" [13] is applied when all that remains of the original input signal is the residual after the IMFs have been extracted from the given signal.

2.3.6. The Hilbert Transform

For a real signal, $x(t)$, the analytic signal is defined as

$$z(t) = x(t) + jy(t) \tag{11}$$

In (11), $y(t)$ represents the Hilbert transform of the real signal, where

$$y(t) = \frac{1}{\pi} P \int_{-\infty}^{\infty} \frac{x(s)}{t-s} ds \tag{12}$$

and P is the Cauchy principal value. To describe the instantaneous frequency in its correct form, the analytic signal must be defined by polar coordinates, leading to the analytic signal being defined as:

$$z(t) = a(t)\exp(j\theta(t)) \tag{13}$$

In (13), $a(t)$ is the amplitude and defined as follows:

$$\|z(t)\| = \sqrt{(x(t))^2 + (y(t))^2} \tag{14}$$

and $\theta(t)$ represents the phase, defined by

$$\theta(t) = \tan^{-1}\left(\frac{y(t)}{x(t)}\right). \tag{15}$$

Finally, the instantaneous frequency as time-varying phase is defined as,

$$\omega = \frac{d\theta(t)}{dt}. \tag{16}$$

2.3.7. The Hilbert Spectrum

When given a non-stationary signal with variable frequency and amplitude change over a period of time, there is a need to have a more adaptive and flexible notion of frequency. The concept of the Hilbert spectrum and instantaneous frequency were detailed by Huang et al. [1] through the application of the Hilbert transform.

Once the IMFs have been decomposed from the original signal, the Hilbert transform can be applied to each of the IMFs individually, resulting in the components of the Hilbert spectrum. After applying the Hilbert transform and computing the instantaneous frequency using (16), the data set can now be expressed as:

$$X(t) = \sum_{k=1}^{n} a_k(t)\exp\left(j\int \omega_k(t)dt\right), \tag{17}$$

where a_k represents the amplitude of each component as a function of time and ω_k represents the instantaneous frequency of each component as a function of time.

In comparison, the Fourier representation would be expressed as:

$$X(t) = \sum_{k=1}^{n} a_k e^{j\omega_k t}, \tag{18}$$

where the amplitude a_k and frequency ω_k are both constants, rather than variable with time.

By using the IMF expansion rather than the Fourier expansion, the restrictions of expansion on a linear and stationary data set disappears and the function can now handle variable amplitude- and frequency-modulation, leading to an easier analysis of the nonlinear and non-stationary data sets.

Once the instantaneous frequency is calculated, the Hilbert spectrum can be represented by the triplet of $\{t, \omega_i(t), A_i(t)\}$ (or time-frequency-amplitude) in the time-frequency plane, where $A_i(t)$ is the amplitude of the analytic signal, corresponding to the instantaneous frequency $\omega_i(t)$.

The original EMD performs the mapping expressed below:

$$x[n] = \sum_{k=1}^{K} d_k[n] + r[n], \tag{19}$$

From this expression, the IMFs, denoted by $d_k[n]$, represent a unique time-frequency analyzer allowing for analysis of the instantaneous frequency. The combination of the concept of instantaneous frequency and the EMD technique makes the EMD framework so powerful for time-frequency signal analysis [9].

2.4. Algorithm Variations

In the article "On Empirical Mode Decomposition and its Algorithms," [5] by Rilling et al., a new data-driven technique of EMD is presented and issues related to its effective implementation are discussed. The technique of EMD is faced with the difficulty of not having an analytic form, being defined only by an algorithm, making theoretical analysis and performance evaluation nearly impossible [5]. In addition to presenting the problems inherent in the EMD technique, Rilling et al. also propose some variations on the EMD algorithm. Results were obtained from numerical simulations in order to support an interpretation of the method in terms of adaptive constant-Q filter banks [5].

2.4.1. Algorithmic Variations

The aim of Rilling et al. in presenting these algorithmic variations [5] was to make the choices made by the user more precise and to recommend specific rationales behind the decisions that the user makes prior to implementing the EMD algorithm. There are two variations that Rilling et al. present in this paper. The first is the Local EMD and the second is the On-line EMD.

The Local EMD algorithmic variation includes a variation made concerning the initial EMD algorithm formulation. The authors introduce an intermediate step in the sifting process, where the large error zeros exist. The sifting process eliminates the problem of over-iterating the entire signal by targeting the zeros that cause the largest error [5]. In the algorithm, the extra iterations performed are denoted by a weighting function, $w(t)$.

This weighting function is introduced in Step 4 of the original EMD algorithm detailed in Table 2, such that the new definition of the detail is now:

$$d(t) = x(t) - w(t)m(t) \quad (20)$$

The second variation, referred to as the On-line EMD, is based on the fact that the sifting step relies on the interpolation between the local extrema. Rilling et al. claim that because the interpolation of the extrema requires only a finite number of interpolations, "that the extraction of a mode could therefore be possible *blockwise*, without the necessary knowledge of the whole signal (or previous residual)" [5]. In order to realize this algorithmic variation, a sliding window was implemented on the original EMD algorithm, as described in Table 4.

2.4.2. Performance Elements

In addition to introducing the previous two algorithmic variations on the EMD algorithm, Rilling et al. also identify some performance elements causing problems when implementing the EMD algorithm. Because the EMD technique is defined by an algorithm, performance evaluation is difficult and requires simulation experiments [5]. The first problem they address is the idea of tones and sampling. The EMD is expected to be the identity operator with only one tone and no residual; however, in actuality, this is not a true statement. The issue arises from the fact that tone estimation depends heavily on the tone frequency, the application of the EMD technique results in a number of IMFs, as well as a residual component.

2.5. Empirical Mode Decomposition as a Filter Bank

Flandrin et al. presented [8], in which they reported on experiments involving fractional Gaussian noise to better understand how the EMD technique behaves in situations involving broadband noise. They conclude that the technique of EMD acts as a dyadic filter bank, resembling filters existing in wavelet decomposition [8].

2.5.1. Fractional Gaussian Noise

The final form of the EMD results in the representation as follows:

$$x(t) = \sum_{i=1}^{N} c_i(t) + r(t), \tag{21}$$

where $r(t)$ stands for the residual trend of the entire signal and $c_i(t)$ represents the IMFs throughout the decomposition [8].

Less attention has been given to realistic situations involving noise, where most studies have been performed based on simulations, resulting in less understanding of the decomposition that EMD can achieve when applied to a stochastic (or intrinsically non-deterministic) process. In order to help explain applying the EMD technique to such processes that involve noise, Flandrin et al. performed extensive realistic simulations in order to show that the EMD technique performs like a dyadic filter when applied to noise processes [8].

2.5.2. Flandrin et al. Conclusions

As a result of their research efforts, Flandrin et al. were able to report on the "first numerical experiments aimed at supporting the claim: "…the built-in adaptivity of EMD makes it behaves spontaneously as a 'wavelet-like' filter bank" [8]. The technique of

EMD naturally copes when there are superimposed IMFs and the benefits of the EMD method are similar to those of wavelet-based methods [8].

2.6. EMD Applications

The applications described in the following section employ only real-valued data, rather than complex-valued data.

2.6.1. Seismic Application

Magrin-Chagnolleau and Baraniuk [7] propose a new technique called the EMD is described and applied to the investigation of a seismic trace, where the IMFs and instantaneous frequency were studied. They also applied the EMD technique to a seismic section, resulting in new time-frequency attributes.

The topic in which Magrin-Chagnolleau and Baraniuk applied the EMD technique was that of seismic signals. Much like many real-world signals, seismic signals have the property that they are non-stationary [7]. Due to the inability of Fourier analysis to analyze non-stationary and nonlinear signals, Fourier analysis provides unsatisfying results due to the frequency changes that occur with respect over time of the seismic signal. Because the EMD method is an adaptive decomposition technique that decomposes the signal into its oscillating components, this new technique has potential in analyzing seismic signals when compared with Fourier-based analysis tools.

In their paper, Magrin-Chagnolleau and Baraniuk proposed a new way of decomposing a seismic trace into its IMFs and extracting the instantaneous frequency of each IMF. The next step in their research would be to extract other time-frequency

attributes based on different calculations in the time-frequency plane represented by the triplet, $\{t, \omega_i(t), A_i(t)\}$.

2.6.2. Heart Rate Variability Application

Balocchi et al., in "Deriving the respiratory sinus arrhythmia from the heartbeat time series using Empirical Mode Decomposition," explored an application of the EMD technique [3]. Heart-rate variability (HRV) is a well-known phenomenon and is of great clinical relevance in pathophysiologic investigations. However, analyzing HRV is difficult because it is the result of many nonlinear interacting processes. Any linear analysis tool that is applied to the HRV has the potential of underestimating or missing information. Therefore, researchers have applied EMD analysis to decompose the heartbeat interval series into their IMFs in order to identify the modes associated with breathing [3]. For comparison purposes, Balocchi et al. recorded the respiratory signal simultaneously with the tachogram (or EKG) signal.

As previously stated, the EMD method allows the analysis of nonlinear and non-stationary time series through the analysis of their IMFs. In this application performed by Balocchi et al., the authors were able to demonstrate the association of the first IMF extracted from a tachogram with the simultaneously recorded respiratory signal [3].

2.6.3. Seismic Reflection Application

The article "Application of the Empirical Mode Decomposition and Hilbert-Huang Transform to seismic reflection data," written by Battista et al., applied the technique of EMD to the study of seismic reflection data [6]. There have been advancements in the field of signal processing providing possibly improved imaging and analysis of "complex geologic targets found in seismic reflection data" [6]. The EMD

technique has yet to be recognized as a standard analysis tool by the seismic community. Therefore, the reasoning behind this experiment is to demonstrate the ability of the EMD technique and HHT to improve seismic reflection data quality.

The HHT allows for signals that are described as stochastic (or intrinsically non-deterministic) processes to be analyzed by using instantaneous attributes, such as frequency or displacement, in the time-frequency domain. Two reasons the authors applied the HHT to the data were: (1) to assess the ability of the EMD and HHT to quantify geologic information in the time and time-frequency domain and (2) to develop superior filters by using the instantaneous attributes. The main objective of the experiment was to determine whether HHT allows for filter design using its empirically-derived attributes [6].

For this application, the HHT was first used to compare the filtering in time-frequency domain against that of the frequency domain using Fourier transform. Then, the instantaneous attributes of the HHT were compared to those produced by the Hilbert transform, where the EMD technique was not performed with the Hilbert transform. By performing these two comparisons with well-known transforms, the authors were able to demonstrate the strength of using the time-frequency domain filtering and the necessity of using EMD with the Hilbert transform [6].

EMD and HHT were not presented as a replacement for existing methods, but the objectives of the study were met. The HHT is an impressive analysis tool due to its ability to preserve phase and amplitude while empirically separating the signal from noise. Battista et al. determine that future goals include integrating HHT with "amplitude-versus offset processing of gas hydrates" [6].

2.6.4. Cycle and Trend Mode Application

Ehlers and Way discussed the usefulness of an objective scientific approach for the identification of cycle or trend modes in the market [14]. While a number of tools are already available to provide distinction between the two modes, in this paper a unique new approach will be used to help determine the market mode called Empirical Mode Decomposition.

Ehlers and Way determined that cycle mode components of market activity can be identified using a band pass filter. An uptrend, which represents a cycle market mode, can be identified as the positive average of the filtered data over cycle periods and in a similar manner, a downtrend, representing a trend market mode, is identified by the negative average of the filtered data over cycle periods [14]. Finally, the delineation between cycle and trend modes can be made by the trend line deriving using the Empirical Mode Decomposition.

2.6.5. Petrophysical Model Application

Huang and Milkereit explore another use for the EMD method because of the importance of spectral analysis for seismic data processing and interpretation [4]. Due to the fact that the frequency contents of seismic data vary with time, the medium is a non-stationary one. The advantage of the HHT and EMD is they do not require presumed set of functions as previous methods, allowing the projection of non-stationary and nonlinear signals onto a time-frequency plane using the Intrinsic Mode Functions. Huang and Milkereit compare the findings of applying EMD method with those of applying the wavelet transform and the S-transform. In previous papers in the seismic community, spectral decomposition in seismic exploration produced a continuous time-frequency

expression of a seismic trace [4]. The EMD method generates necessary adaptive bases from data.

Huang and Milkereit present two applications for the EMD technique in their paper. The first application presented is the synthetic time series, where they applied the EMD method to three time series similar to applications used in three pre-existing papers [4]. After the first application, they concluded, the EMD method provides superior results to complex wavelet transform and S-transform in terms of temporal and spectral resolution.

The authors also applied the EMD method to decompose well-log data. The instantaneous power spectrum density function provided the "depth varying stochastic properties which can be used to simulate a time series of heterogeneous medium at every depth" [4]. Finally, the authors determined that a combination of two-dimensional slices yields a heterogeneous three-dimensional earth model adaptive to non-stationary along the borehole. In conclusion, Huang and Milkereit decided that the EMD method is a helpful tool when analyzing the seismic data used.

2.7. Extending EMD into the Complex Domain

Applications in the previous sub-section employ only real-valued data, as opposed to complex-valued data. In the following section, complex-valued data was used.

2.7.1. Complex Traces and Instantaneous Frequency

Given a real signal $x(t)$, the corresponding analytic signal (or complex trace) is expressed as:

$$X(t) = x(t) + jH\{x(t)\}, \tag{22}$$

where $H\{x(t)\}$ denotes the signal corresponding to $x(t)$ and was obtained using the Hilbert transform, where P is the Cauchy principle value of the integral [7], and is expressed as follows:

$$H\{x(t)\} = \frac{1}{\pi} P\int_{-\infty}^{\infty} \frac{x(\tau)}{t-\tau} d\tau . \tag{23}$$

Another way that the analytic signal can be obtained is detailed below in Table 3 [7].

Table 3: Analytic Expression of Given Signal

Given the real signal $x(t)$:
1. Take the Fourier transform of $x(t)$
2. Zero the amplitude for the negative frequencies and double the amplitude for the positive frequencies
3. Take the inverse Fourier transform of the resulting signal

In polar coordinates, the analytic signal can be expressed as:

$$X(t) = A(t)e^{j\theta(t)}, \tag{24}$$

where, $A(t)$ is the instantaneous amplitude and $\theta(t)$ is the instantaneous phase.

To determine the instantaneous radial frequency, the following equation is implemented:

$$\omega(t) = \frac{d\theta(t)}{dt} . \tag{25}$$

2.8. Methods for Empirical Mode Decomposition in Complex Domain

2.8.1. Complex Empirical Mode Decomposition

Tanaka and Mandic were the first to propose a method for extending the EMD method into the complex domain [9]. They proposed to achieve the complex extension for the EMD using a filter bank interpretation of the EMD mapping and by use of the positive and negative frequency components of the Fourier spectrum. This method yield complex-valued IMFs, facilitating the extension of the standard EMD to the complex domain.

The authors claim that the EMD method is a "novel signal analysis tool, whereby the underlying notion of instantaneous frequency provides an insight into the time-frequency signal features" [9]. Through the research accomplished by Huang et al. [1], the EMD technique is an established tool for analyzing non-stationary and nonlinear data. Yet, the EMD method was developed only for real-valued data, leading to difficulties in analysis where complex-valued data structures exist.

While Tanaka and Mandic claim a "simple way" to extend EMD to the complex domain would be to apply the EMD technique separately to the real and imaginary parts of a complex-valued signal; however, the mutual information from a complex quantity is lost when the signal is split into two quantities (real and imaginary). Instead, the authors introduce as their proposed CEMD the concept of complex IMFs that act as a dyadic

filter and operate directly in the complex domain, where the signal is divided into the positive and negative frequencies [9]. The only requirement for this method is that the CEMD preserves the filter on the average value.

To derive the CEMD, the complex-valued data set must first be decomposed into its positive and negative frequency components. In preparing for the explanation of the method Tanaka and Mandic proposed, let $\{x[n]\}$ represent a complex-valued time sequence and $X(e^{j\omega})$ represent the discrete-time Fourier transform of $x[n] \in \mathbb{C}$. There are two possibilities for obtaining the desired real time sequence form $x[n]$, where $x[n]$ is generally not analytic, making one of the above mentioned possibilities unusable.

The other possibility, where $x[n]$ is not assumed to be analytic, is the method used for extending the original EMD method into the complex domain. To extract the positive and negative frequency component from $x[n]$, an ideal bandpass filter, denoted by $BP(e^{j\omega})$, is applied to the original signal.

The ideal bandpass filter used for this analysis is expressed as

$$BP(e^{j\omega}) = \begin{cases} 1, 0 \le \omega < \pi \\ 0, -\pi \le \omega < 0 \end{cases} \tag{26}$$

By applying the bandpass filter, two analytic signals are generated:

$$\begin{aligned} X_{+}(e^{j\omega}) &= BP(e^{j\omega}) X(e^{j\omega}) \\ X_{-}(e^{j\omega}) &= BP(e^{j\omega}) X^{*}(e^{j\omega}) \end{aligned}, \tag{27, 28}$$

where $X^{*}(e^{j\omega})$ represents the complex conjugate of the signal.

Once the bandpass filter has been applied, the inverse Fourier transform is employed:

$$\begin{aligned} x_+[n] &= \mathrm{Re}\left\{F^{-1}\left[X_+(e^{j\omega})\right]\right\} \\ x_-[n] &= \mathrm{Re}\left\{F^{-1}\left[X_-(e^{j\omega})\right]\right\}, \end{aligned} \tag{29, 30}$$

where $\Re$ denotes the real-part of the signal and $F^{-1}[\bullet]$ represents the inverse Fourier transform of the signal. The IMFs can be obtained using the following summations of (27) and (28):

$$\begin{aligned} x_+[n] &= \sum_{i=1}^{N} x_i[n] + r_+[n] \\ x_-[n] &= \sum_{i=-N_-}^{-1} x_i[n] + r_-[n], \end{aligned} \tag{31, 32}$$

The reconstruction of the decomposed complex signal is as follows:

$$x[n] = \left(x_+[n] + jH\left[x_+[n]\right]\right) + \left(x_-[n] + jH\left[x_-[n]\right]\right)^*, \tag{33}$$

where $H[\bullet]$ represents the Hilbert transform of the signal. To obtain the i th complex IMF of the complex process $x[n]$, the following equation is employed:

$$y_i[n] = \left\{ \begin{array}{c} x_i[n] + jH\left[x_i[n]\right], i = 1,\ldots,N_+ \\ \left(x_i[n] + jH\left[x_i[n]\right]\right)^*, i = -N_-,\ldots,-1 \end{array} \right\}. \tag{34}$$

Therefore, the final algorithm representation of the proposed Complex EMD method is:

$$x[n] = \sum_{i=-N_-, i\neq 0}^{N_+} c_i[n] + r[n]. \tag{35}$$

Tanaka and Mandic concluded that the CEMD method can be achieved based on some inherent properties of the complex signals. In addition, the authors have been able

to apply the standard EMD to corresponding analytic components of complex-valued data used in their paper [9].

2.8.2. Rotation Invariant Complex Empirical Mode Decomposition

Umair Bin Altaf et al. propose a new method for extending the EMD technique into the complex domain is proposed. In contrast to a previous method proposed by Tanaka and Mandic [9], this method is achieved in a generic way so that the mathematical development mirrors that of the original EMD method [10]. Through this method, the IMFs are complex by design and shown to provide consistent framework for handling real and imaginary data.

Traditional time-frequency analysis methods are based on "a priori" mapping from time to frequency domains, where that mapping is defined by "basis functions" [10]. However, this "a priori" mapping poses problems for nonlinear and non-stationary signals that have time varying statistical characteristics, and a single basis function fails due to its limited accountability for the variations. In addition, this "a priori" mapping also compromises the physical significance of the signal analysis of nonlinear and non-stationary signals [10].

The authors proposed a new way to decompose a complex signal using the method of EMD and was achieved by making use of the complex spline. Using the complex spline makes it possible to carry out the arithmetic and algebraic operations of the algorithm in the complex domain, leading to a single set of IMFs contained in the complex domain [10].

Before describing their proposed method, the authors describe the method that Tanaka and Mandic proposed CEMD [9]. Concerning their method, Umair Bin Altaf et

al. claim this method is a "natural and generic way to extend EMD to the complex domain would be to operate in the complex domain" [10]. The same steps for the original EMD method are followed, but are carried out in the complex domain with various modifications.

The issue that arises is the definition of an extrema in the complex domain and a method for determining it. After describing a number of definitions, the definition of an extrema that is used for the method is: "a locus where the angle of the first derivative (first-order differential vector) changes its sign" [10]. The authors have assumed that each local maximum is followed by a local minimum and vice versa, and in order to prove this assumption true, the average of the envelopes is used. Envelopes for the complex signal can be estimated as spline interpolations of the local maxima, and minima, where the average can be computed. This complex spline is obtained by computing the real and imaginary parts separately [10].

The final steps of the complex algorithm are performed like the original EMD algorithm. The claimed advantage of the proposed CEMD method is that it does not split the signal into two parts and has the potential to be extended into higher-dimensional cases easily [10], unlike the method proposed by Tanaka and Mandic [9].

Umair Bin Altaf et al. conclude that the analysis of real-world complex-valued data shows that the proposed method provides new insights into time-frequency analysis of nonlinear and non-stationary signals, which was not possible before [10].

2.8.3. Bivariate Empirical Mode Decomposition

Rilling et al. present a new method for extension of the original EMD method to the complex domain in their paper [11]. Initially, the method of EMD was limited to the

analysis of real-valued time series; therefore, an extension to analysis of complex-value time series is proposed that is designed to extract zero-mean rotating components from the signal, where the original EMD extracts zero-mean oscillating components [11].

The basic idea underlying the proposed BEMD is that a "bivariate signal = fast rotations superimposed on slower rotations" [11]. The slowly rotating component has to be defined as the mean of some "envelope," where the envelope is represented by a three-dimensional tube tightly enclosing the signal. Given a set of points on the tube, there are at least two ways to define the mean of the envelope: (1) define the mean as the barycenter of four points, each having unit mass and (2) define the mean as the intersection of two lines, one being halfway between the two horizontal tangents and the other being halfway between the two vertical tangents [11]. Due to the second definition being less prone to errors, it is a more preferred method. The goal for the bivariate interpolation is the same as with the original EMD: smooth interpolation with as few "bumps" as possible, calling for the use of a cubic spline.

Given an angle direction that performs uniform sampling around the unit circle, the bivariate extensions are defined by the EMD algorithm, only with new sifting elementary operators defined by S^{B1} and S^{B2},which correspond to the algorithms in Tables 4 and 5 [11].

Table 4: Algorithm 1 for EMD Bivariate Extension

1. Given an angle direction: $\rho_k = \frac{2k\pi}{N}$ for $1 \le k \le N$ complete steps 2 through 4
2. Project the complex-valued signal $x(t)$ on direction $\rho_k : \partial_{\rho_k} = \mathrm{Re}[e^{j\rho_k} x(t)]$
3. Extract the locations $\{t_i^k\}$ (time corresponding to the angle direction and IMF) of the maxima of ∂_{ρ_k}
4. Interpolate the set $\{t_i^k, x(t_i^k)\}$ to obtain the envelope curve in direction $\rho_k : e_{\rho_k}(t)$
5. Compute the mean of all envelope curves: $m(t) = \frac{1}{N}\sum_k e_{\rho_k}(t)$
6. Subtract the mean to obtain $S^{B1}x(t) = x(t) - m(t)$

Table 5: Algorithm 2 for EMD Bivariate Extension

1. Given an angle direction: $\rho_k = \frac{2k\pi}{N}$ for $1 \le k \le N$ complete steps 2 through 4
2. Project the complex-valued signal $x(t)$ on direction $\rho_k : \partial_{\rho_k} = \mathrm{Re}[e^{j\rho_k x(t)}]$
3. Extract the locations $\{t_i^k, \partial_i^k\}$ of the maxima of ∂_{ρ_k}
4. Interpolate the set $\{t_i^k, e^{j\rho_k}\partial_i^k\}$ to obtain the partial (or partial differential equation of the) envelope curve in direction $\rho_k : e'_{\rho_k}(t)$
5. Compute the mean of all tangents: $m(t) = \frac{2}{N}\sum_k e'_{\rho_k}(t)$
6. Subtract the mean to obtain $S^{B2}x(t) = x(t) - m(t)$

The BEMD was designed so that the signals rotating around zero are the outputs, where the two algorithms for BEMD generally accept two types of solutions: (1) rotating signals, as intended, and (2) where the method fails to extract the rotating components and the output signals are ones that wander around zero in a more complicated manner [11].

Rilling et al. conclude, from extensive simulations, that the outputs of the two algorithms for BEMD are very similar when the data clearly contains rotating components, but may differ when they fail to extract the rotating components [11].

2.9. Comparison of EMD and Complex EMD Extensions

Yunchao et al. present the fact that CEMD is a powerful tool [15]. The HHT is the method developed by Huang et al. [1] for analyzing nonlinear and non-stationary data, due to the EMD technique not imposing any prior assumptions to the data [15].

2.9.1. Realization of Complex EMD

As developed by Huang et al. [1], the original EMD method is based on a characteristic time scale defined by the local extrema. Yet, the original EMD method is applicable only for real-valued time series and it is necessary to extend the application of EMD into the complex domain. There have been three different methods proposed for the realization of CEMD and while all three have their merits, the algorithm proposed by Rilling et al. [11] is used by Yunchao et al. due to the claim that it is more intuitive [15].

2.9.2. Characteristics of Complex EMD

From the simulations performed, the authors study of the IMFs characteristics, following a method proposed by Zhaohua et al. A couple conclusions that Yunchao et al. make from these simulations were that: (1) CEMD is an effective dyadic filter just like the original EMD method, (2) the power spectrum of the resulting complex-valued IMFs are subject to a normal distribution, and (3) the frequency features are the same for the real and imaginary part of the same IMF [15].

2.9.3. Numerical Experiments

In addition to simulations on white noise, the authors performed numerical experiments on a two-dimensional (or velocity and pressure) vector sensor. From these numerical experiments, Yunchao et al. claim that the decomposed results from the CEMD are better than the original EMD method [15]. There are three main differences from the original EMD to the CEMD. First, the number of IMFs is identical for the real and imaginary parts with the CEMD, where the original EMD method can have superimposed IMFs, resulting in an incorrect number of IMFs. The second difference is that, for the CEMD, the frequency characteristic is the same between the same order IMFs of the imaginary and real parts while the original EMD method does not possess this characteristic. This distinction between the CEMD and the original EMD methods is due to the CEMD observing the changes in the two variables of the signal. Finally, it is obvious from the experiments that the characteristics of the IMFs from the analytic (or complex) signal are better resolved in the frequency domain than the real signal [15].

From the numerical experiments performed by Yunchao et al., it can be concluded that, if the signal is long enough and the intricacy can be ignored, the analytic signal is a good choice for the application of the CEMD method; however, if the signal is short or the system is a real-time system, it is better to choose the less intricate complex signal [15].

Yunchao et al. conclude that CEMD is consistent for the frequency characteristics of the IMFs for the real and imaginary parts. Additionally, the results decomposed by the CEMD method are more legible than those decomposed by the EMD method, and the estimations done by the CEMD are more accurate. A final conclusion the authors make

is that one can choose the analytic signal or less intricate complex signal for application of the CEMD method in different conditions [15].

2.10. Applications for Complex EMD

2.10.1. Multichannel Information Fusion

Mandic et al. wrote about information "fusion" via signal "fission" in the framework of EMD [2]. The fission part occurs first where the signal is decomposed into its oscillatory components, then the fusion occurs when the IMFs are combined in an ad-hoc fashion to provide knowledge about the process [2]. Mandic et al. claims that extension of EMD into the complex domain is especially important for phase-dependent processes; however, extending EMD into the complex domain is not straightforward and depends heavily on the criterion for finding the local extrema of the signal.

Complex representation of a signal can be both intuitive and useful because the amplitude and phase can be modeled simultaneously [2]. There are many fields of study that use only real-valued data structures, but several important signal processing areas use complex-valued data structures. EMD is a data driven time-frequency analysis technique that is useful in the analysis of nonlinear and non-stationary signals.

One well-established information fusion model is the waterfall model. The method of EMD also performs both signal conditioning and feature extraction, key components of the waterfall model. EMD provides the framework for unifying information fission and fusion; therefore, the aim of the paper is to provide justification for the use of EMD, both real and complex, in knowledge extraction and information fusion [2].

The most intuitive way to extend EMD into the complex domain would be to apply EMD to the real and imaginary parts separately; however, in performing this, any mutual information, such as phase, that existed between the original components is ignored and lost. Therefore, this paper examines the effectiveness of two of the three introduced CEMD algorithms: (1) CEMD [9] based on the direct use of the Hilbert transform properties and (2) RICEMD [10] a generic expression of the real EMD.

Mandic et al. applied the CEMD method to data and came up with certain advantages and disadvantages for this method. The primary advantages that were found for this method were that it has a straightforward and intuitive math derivation, acting as a dyadic filter bank. However, with this method, the disadvantages seem to outweigh the advantages. Not only does this method fail to reveal any synchronized events between the data streams, but the IMFs are deprived of their physical connection with the original data set. An ambiguity exists at the zero frequency due to the way the math derivation is formed and, finally, this method cannot be extended to higher dimensions due to the limitation of representing a signal by its positive and negative frequencies [2].

In addition to applying the CEMD method, Mandic et al. also analyzes the RICEMD method and explain the advantages and disadvantages inherent in the method. The method operates fully in the complex domain and uses complex cubic splines for analysis of the signal in the complex domain. Unlike the CEMD method, the RICEMD method creates an equal number of IMFs for the real and imaginary parts and retains the physical interpretation of the signal. One disadvantage is the choice of criterion for finding the extrema of the complex signal is not unique, the extracted complex IMFs do possess physical interpretation [2].

2.10.2. Single Vector Sensor Application

Yunchao et al. introduced CEMD to improve processing from a single vector sensor of complex sound data using HHT [16]. Yunchao et al. claim that CEMD is a powerful tool for analyzing complex data and the results yielded in this paper show that CEMD is better in using the information between the correlative signals. In addition, the analytic signal is beneficial to direction estimation with different targets.

Vector sensors are sensors that can measure the pressure P and orthogonal components of the particle velocity, V_x and V_y, simultaneously, and vector sensors can also improve target detection capability. The HHT has been utilized to identify the multi-targets using the signals from the single vector sensor based on the frequency feature of the HHT. This use of the HHT has led to the development of the Vector HHT (VHHT) and the application of the VHHT was analyzed in this paper, as well as the improvement CEMD performs on the VHHT [16].

In two-dimensional circumstances, the vector sensor can simultaneously measure the pressure and orthogonal components of the velocity, V_x and V_y. From this process, the target's direction can be obtained as follows:

$$\theta = \arctan\left(\frac{PV_y^*}{PV_x^*}\right), \tag{36}$$

where the P represents the pressure component of the vector sensor, and V_x and V_y represent the orthogonal components of the velocity along the x-axis and y-axis.

By using the EMD to decompose the pressure and velocity components into their respective IMFs, the real-valued and imaginary-valued IMFs are obtained. The analytic signals of the resulting IMFs are represented below:

$$Z_{Pj}(t) = A_{Pj}(t)\exp\left(j\phi_{Pj}(t)\right), \tag{37}$$

$$Z_{V_x j}(t) = A_{V_x j}(t)\exp\left(j\phi_{V_x j}(t)\right), \tag{38}$$

and

$$Z_{V_y j}(t) = A_{V_y j}(t)\exp\left(j\phi_{V_y j}(t)\right). \tag{39}$$

The instantaneous sound energy flows corresponding to the x-axis and y-axis are represented by the multiplication of the complex conjugate of the velocity components analytic signal and the pressure analytic signal,

$$S_{PV_x j}(t) = \left(Z_{Pj}(t)\right)\left(Z_{V_x j}^{*}(t)\right), \tag{40}$$

and

$$S_{PV_y j}(t) = \left(Z_{Pj}(t)\right)\left(Z_{V_y j}^{*}(t)\right). \tag{41}$$

Finally, the instantaneous azimuth of the acoustic signal is represented by the following equation:

$$\theta_j(t) = \arctan\left(\frac{\mathrm{Re}\left\{S_{PV_y j}(t)\right\}}{\mathrm{Re}\left\{S_{PV_x j}(t)\right\}}\right). \tag{42}$$

CEMD is an extension of EMD in the complex plane. The method employed in this paper was the method proposed by Rilling et al. [11]. In this article, a number of characteristics of the CEMD method are discovered. Just a few of those characteristics include: (1) that CEMD is shown to act as a dyadic filter, (2) that the period of the IMF increases when the order increases and the center frequency decreases, (3) the frequency feature of the real and imaginary parts of the same IMF are the same, and (4) that the CEMD algorithm is adaptive like the original EMD algorithm [16].

Through the experiments performed, Yunchao et al. concluded that CEMD takes full advantage of the information between the relevant signals in the acoustic vector sensors. There are three separate aspects of the findings that show how well the CEMD works in the field of vector sensors. First, the order and frequency feature of the real and imaginary parts of the IMFs are identical. Second, the CEMD is better than EMD in noise suppression and reducing the mode-mixing. And last, that the analytic signal is more suitable for high signal-to-noise (SNR) and the simple complex signal is better in low SNR [16].

2.10.3. Multiscale Image Fusion Application

Looney and Mandic propose a solution to the problem of uniqueness when performing fusion of data from multiple and heterogeneous sources [17]. The proposed

solution relies heavily on using complex extensions of the data-driven technique of EMD, a new analysis technique proposed by Huang et al. [1].

In the data and information fusion community, there is a significant challenge when different focal points are observed [17]. The technique of EMD has been proposed for data fusion, where only the "relevant" IMFs are recombined into a restored signal. Due to its adaptivity, it is natural to consider the use of the EMD method for the problem of heterogeneous image fusion; however, there is still a problem of uniqueness when using the EMD method. Therefore, extensions into the complex domain of the EMD method have been proposed to help with the uniqueness of the resulting IMFs [17]. While there have been three complex extension of EMD recently proposed, the method employed in this paper BEMD [11].

The local and data-driven nature of EMD leads to two problems. First, that the uniqueness of decomposition-signals gives different IMFs, and second, that mode-mixing of the IMFs occurs [17]. The problem of uniqueness can be addressed by stopping the decomposition once a specific number of IMFs has been obtained. If the number of IMFs from each source is equal in number, then the problem of mode-mixing is also fixed. So, in order to fix both problems, Looney and Mandic propose to apply the BEMD method to decompose heterogeneous complex data simultaneously, rather than decomposing one part of the signal at a time [17].

To show the effectiveness of using EMD, and specifically BEMD, simulations were performed by Looney and Mandic on generated complex data and real-world fusion data. An automatic fusion algorithm is also proposed that is based on the BEMD algorithm [17]. The robustness of the analysis of the generated data guarantees a

meaningful comparison between the scales and forms the basis for the proposed image fusion algorithm and will be used for the real-world data analysis. By applying the BEMD algorithm to real-world image fusion data, it is illustrated that the problems of mode-mixing and uniqueness can be easily overcome [17].

Looney and Mandic conclude that the potential for BEMD for information fusion is verified, as well as a set of common frequency scales can be determined by simultaneously decomposing sources using the BEMD method [17]. In addition, the application of BEMD enables the proposed approach to overcome the uniqueness and mode-mixing problems. For future work, Looney and Mandic propose that higher dimensional extensions should be developed in order to enable the fusion of more than two images [17].

2.11. Multivariate EMD Application

Mutlu and Aviyente present the importance of quantifying the phase synchrony between signals is stated for different applications [12]. However, current techniques used to measure and quantify the phase synchrony suffer from constraints inherent to the wavelet transform and Hilbert transform. Therefore, in order to address such constraints on the analysis of the signals, a recently introduced multivariate empirical mode decomposition (MEMD) in order to assist in the quantification of multivariate phase synchrony.

Mutlu and Aviyente propose to use MEMD for quantifying the phase synchrony between multiple time series [12]. The original EMD method acts as a dyadic filter, thus a "pre-filtering tool" for the Hilbert transform-based phase synchrony analysis. The goal

of Mutlu and Aviyente's research is to extend the measures of correlation for multiple variables from statistics for quantifying multivariate synchronization. Mutlu and Aviyente claim: (1) the MEMD might be used to define pairwise synchrony between multiple time series across the same frequency, and (2) MEMD can extend the notion of bivariate synchrony to multivariate synchronization [12].

From their research, a new approach for quantifying multivariate phase synchronization within a group of oscillators. The new approach is based on the application of MEMD for extracting time and frequency dependent phase information [12]. MEMD method results in two improvements discovered from their research. First, MEMD is data-driven and eliminates the need for chosen bandpass filters and second, the MEMD extends the current state of the art-phase synchrony analysis from quantified bivariate relationships to the multivariate case [12]. Mutlu and Aviyente propose for future work that focuses on the extension of the methods proposed using different multivariate analysis technique.

2.12. Conclusions

Rilling et al. conclude that the EMD technique is a promising tool but it needs to be better understood. They call for further studies devoted to a theoretical approach and closed-form solution, due to the EMD definition by an algorithm rather than a closed-form solution. Additionally, Kim and Oh conclude that the IMFs that are decomposed from the EMD technique "provide a multi-resolution tool and spectral analysis given local information with time-varying amplitude and phase" [13].

The CEMD method takes full advantage of the information between the relevant signals in the acoustic vector sensors [16]. In addition, the results decomposed by the CEMD method are more legible than those decomposed by the EMD method, and the estimations done by the CEMD are always more accurate [15].

Concerning the three CEMD methods, conclusions have been made about the possibilities inherent to each one and the disadvantages for each method. The first complex method, ambiguously called CEMD, presented conclusions that the CEMD method can be achieved based on some inherent properties of the complex signals [9]. For the RICEMD method, Umair Bin Altaf et al. conclude that the analysis of real-world complex-valued data shows that the proposed method provides new insights into time-frequency analysis of nonlinear and non-stationary signals, which was not possible before [10]. The authors of the BEMD method conclude that the outputs of the two algorithms for BEMD are very similar when the data clearly contains rotating components, but may differ when they fail to extract the rotating components [11].

Through all the papers written for the EMD technique, each application of the method shows that the method proves worthwhile when applied to the data sets. There are some restraints still inherent to the original EMD method; various authors then extend the method into the complex domain, which helps with some of the issues found in the real domain. Overall, the investigation into the HHT developed by Huang et al. [1], and more specifically the EMD technique, displays information not accessible by the FFT and that new information can help in the analysis of many natural phenomena that are nonlinear and non-stationary in nature.

III. Algorithm Design and Implementation

3.1. Overview

This chapter presents the methodology used in achieving the objective of the research. The objective of this research was two-fold. First, the assessment of using the CEMD technique inherent to the HHT as a signal processing analysis tool was investigated. Secondly, the results from the application of the Hilbert transform and the FFT on the decomposed data sets using the CEMD technique were compared. The comparisons of the resulting graphs from the application of the two separate mathematical transforms were sought to deliver insight into determining which of the transforms provided enhanced fidelity of the real-world data set. Additionally, the analysis of the HHT was compared with the analysis provided from the FFT to determine how the application of the HHT affects a RCS data set.

The approach used to satisfy the two requirements stated above concerning the problem statement, was conducted primarily using the MATLAB® computer program, where the Signal Processing and Spline Toolboxes were employed. In addition to using MATLAB® and the two above mentioned toolboxes, code that was written by Dr. Flandrin and available on his website was implemented, as detailed in BEMD [11].

The method for collection of the data will be discussed, as well as the components of the designed algorithm will be presented and explained. Finally, a detailed explanation of the implementation of the algorithm used will be discussed, with detailed explanations of the various components used in completion of the methodology.

3.2. Data Collection

There were two separate data collections employed for the completion of this evaluation. The first data set was provided by the sponsor, also referred to as the "real-world data set" during the methodology portion of this thesis. This set of data was obtained through determining the complex RCS data from a rotating object. Measurement of a target's RCS is performed at a radar reflectivity range or scattering range. One type of RCS range is an outdoor range, where the target is positioned on a specially shaped low RCS pylon some distance down-range from the transmitters. Such a range eliminates the need for placing radar absorbers behind the target; however, multi-path interactions with the ground must be mitigated. There are instances, as with the real-world data set, in which an object exists in the atmosphere and pulses are sent from the radar to the object, recording the radar return from the object. The real-world data set collected consisted of at least two revolutions of the object, while the second set of data consisted of only one extremely-finely sampled revolution of the object. For the real-world object, the approximate shape was a cylinder with one end enclosed, with the other end open, or a "cavity" cylinder.

The second data collected consisted of using the RCS range owned by AFIT called an anechoic chamber. In such a room, the target is placed on a rotating pillar in the center, and the entire background is covered with radar absorbing material. These absorbers prevent corruption of the measurement due to reflections. A compact range is an anechoic chamber with a reflector to simulate far-field conditions. There were a variety of shapes used over the course of the data collection, but upon further analysis of the real-world object, four specific sets of data were chosen for comparison with the

decomposed real-world data set. These four data sets were: (1) a cylinder with two end caps, refer to Figure 1; (2) a cylinder with one end cap and one open "cavity", refer to Figure 2; (3) a cone-sphere, or an object with a roundly tapered end, refer to Figure 3; and (4) a dihedral corner reflector configuration, refer to Figure 4.

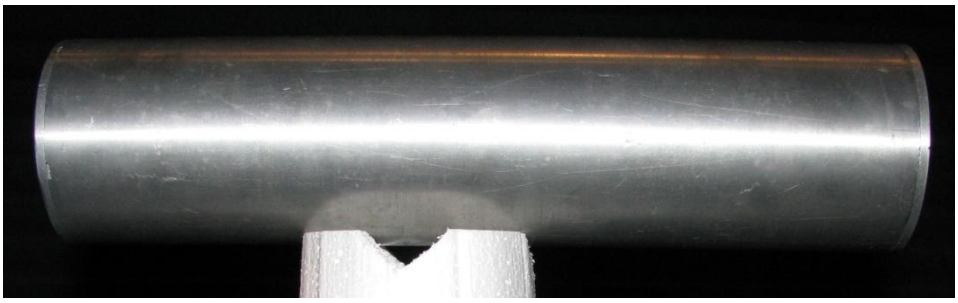

Figure 1: Cylinder with two end caps, on Styrofoam pylon

Figure 2: Cylinder with one end cap and one open end, "cavity", on Styrofoam pylon

Figure 3: Cone-Sphere, on Styrofoam pylon

Figure 4: Dihedral Spherical Corner Reflector, on Styrofoam pylon

The four data sets detailed above were considered the simulated (or theoretical) data to help assess whether the CEMD technique worked properly for a signal composed of various canonical objects, such as the dynamic object represented by the real-world data set. To assess the usefulness and workability of the CEMD algorithm, the real-world data set was decomposed and compared with the RCS values of the simulated objects to determine whether those components were possibly detected in the decomposed real-world signal.

To work with a complex-valued data set in the same manner as the real-world data set, the simulated data collected in the anechoic chamber had to be calibrated. This calibration was accomplished using a MATLAB® GUI called ALPINE©, version 3.1.1, designed by AFIT professor Dr. Peter Collins [18]. Through the use of two specific modules of the ALPINE© GUI, the `calibrateRCS` and the `plotGlobalRCS` modules, the data input and calibration was user-friendly and accomplished quickly. Access to this GUI saved hours of individual code creation and analysis. The calibration results were stored in a MATLAB® MAT-file, enabling the flexibility to load the data into any desired program.

Once the data was calibrated and placed in a useable format, the data was able to be analyzed using the CEMD algorithm developed by Dr. Flandrin [11], followed by the application of both the FFT and the Hilbert transform to the IMFs decomposed using the CEMD algorithm.

3.3. Algorithm Design and Components

Traditionally, signal processing data, such as the RCS data collected for this thesis, was analyzed using Fourier spectrum analysis [1]. However, the technique of the EMD method and use of the complete HHT have been receiving more attention for use in the analysis of signal processing data. More specifically, the CEMD algorithm was employed for the decomposition of the signals analyzed in this thesis. In this section, the original EMD algorithm was explored, as well as the complex extension of the EMD algorithm. Once these two items have been discussed, explanation of the components in the algorithm employed for the thesis will be detailed.

3.3.1. The Empirical Mode Decomposition

EMD is defined as an exploratory analysis technique. EMD is an adaptive technique used to decompose a given signal into its oscillatory modes [2]. This decomposition is accomplished through a process referred to as the sifting algorithm. The sifting algorithm, which defines the EMD process, was detailed previously in Table 1 [1].

Once the sifting algorithm was applied to the given signal, the resulting oscillatory components are called IMFs [2]. These IMFs represent the oscillatory nature embedded in the data. In addition, these IMFs also represent the basis functions of the

signal and are derived from the data, rather than a pre-defined set of basis functions that exist in such transforms as Fourier and wavelets [1].

The algorithm detailed previously in Table 1 was utilized to perform the EMD decomposition as follows:

$$x(k) = \sum_{i=1}^{N} c_i(k) + r(k), \tag{43}$$

in which the IMFs are denoted by $c_i(k)$ and the residue is represented by $r(k)$.

Once the sifting algorithm was applied to the given signal, the IMFs are in a form that can be linearly transformed. More specifically, the FFT and Hilbert transform were applied to the IMFs of the decomposed data. Through application of the Hilbert transform, the given real-valued signal was transformed into a complex-valued signal, where the analytic representation of (43) is given by:

$$X(t) = \sum_{i=1}^{N} a_i(t) e^{j\theta_i(t)}. \tag{44}$$

In (44), the residue $r(t)$ was omitted due to its lack of oscillatory behavior [2]. The analytic signal was created using the IMF to represent the real part and employing the Hilbert transform to represent the imaginary part, such that $x + j\mathrm{H}(x)$ becomes the new representation of the signal [2]. The aim for creating this analytic, time-dependent signal was to extract the time-dependent amplitude $a_i(t)$ and the phase function, $\theta_i(t)$, components more easily [2]. Finally, the instantaneous frequency, denoted by,

$$\omega(t) = \frac{d\theta(t)}{dt}, \tag{45}$$

can also be extracted, used to create a Time-Frequency-Amplitude representation of the signal called the Hilbert spectrum [2].

3.3.2. Complex Extension of Empirical Mode Decomposition

The original formulation of the EMD algorithm by Huang et al. [1] restricts its application to real-valued signals. However, many fields of study use complex-valued data sets, whereby ignoring the imaginary components can cause important information to be lost, as well as the analysis of the signal incompletely presented. Since introduction of the EMD algorithm by Huang et al. in 1998, there have been three complex extensions proposed [9,10,11]. In Chapter II section 2.7, more detailed descriptions of the CEMD [9] and the RICEMD [10] methods are located. The third complex extension, BEMD [11], was revisited due to its involvement in the research and the decomposition of given complex RCS data sets.

3.3.2.1 Bivariate Empirical Mode Decomposition

The method proposed by Rilling et al. [11] was followed to study the characteristics of the IMFs of the given data sets. The other two complex extensions discussed in Chapter II employed the original EMD algorithm and decomposed complex-valued signals similar to real-valued signals; however, the BEMD algorithm "adapts the rational underlying the EMD to the bivariate [or complex-valued] framework" [11]. Dr. Flandrin's BEMD paper provided free MATLAB® code [11] for implementation of the CEMD algorithm, Hilbert transform, and Fast-Fourier transform.

The original EMD algorithm is based on the natural oscillation related to the signal extrema. Nevertheless, for a complex-valued signal, defining extrema in the same manner as a real-valued signal is more confusing and unclear. Therefore, Rilling et al. proposed the notion of "rotation" and is considered a three-dimensional interpretation of the real-valued notion of oscillation [11]. The underlying idea of the complex extension

to EMD proposed by Rilling et al. is that the "bivariate signal = fast rotations superimposed on slower rotation" [11], whereas the original EMD algorithm is based upon the idea that the "signal = fast oscillations superimposed on slower oscillations" [11]. As with the original EMD algorithm, the BEMD algorithm uses the idea of an "envelope," where the envelope of the BEMD algorithm is now a three-dimensional tube enclosing the signal [11] (refer to Figure 5).

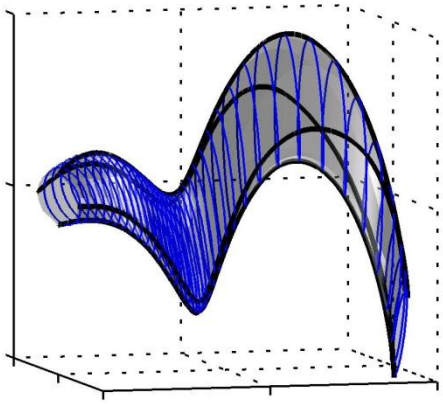

Figure 5: The signal enclosed in its 3D envelope. The black thick lines stand for the envelope curves that are used to derive the mean.

Using this idea of how the envelope is created, the slowest rotating component is defined as the center of the tube. There are two ways of defining the mean value of the tube: (1) define the mean as the barycenter (or center of mass) of the four points considering each to have unit mass (refer to Figure 6), or (2) define the mean as the intersection of two straight lines, one being halfway between the two horizontal tangents and the other one halfway between the two vertical tangents (refer to Figure 7) [11].

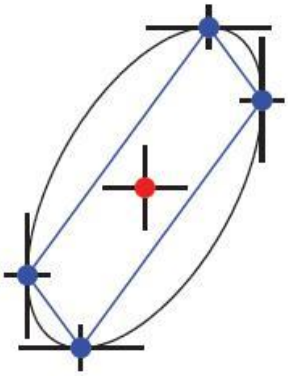

Figure 6: Illustration of the first definition of the mean of the complex-valued signal.

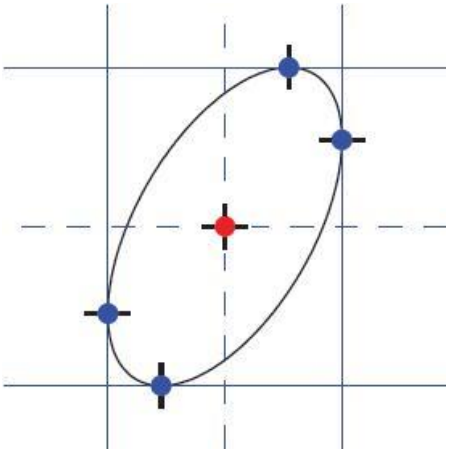

Figure 7: Illustration of the second definition of the mean of the complex-valued signal.

Due to its natural robustness to sampling errors, scheme two for defining the mean value of the tube is preferred in practice. These sampling errors should be taken seriously since the original EMD is sensitive to sampling, leading to the idea that the BEMD algorithm will also be sampling sensitive [11].

The desired interpolation is defined as: "a smooth interpolation, with as few 'spurious bumps' as possible" [10]. To satisfy this definition, a cubic spline was employed. The interpolation of the BEMD algorithm is performed in a similar manner to the EMD algorithm. Wolfram-*MathWorld* defines a cubic spline as:

> "A spline constructed of piecewise third-order polynomials which pass through a set of m control points. The second derivative of each polynomial is commonly set to zero at the endpoints, since this provides a boundary condition that completes the system of $m-2$ equations. This produces a so-called 'natural' cubic spline and leads to a simple tri-diagonal system which can be solved easily to give the coefficients of the polynomials" [19].

The proposed complex extension of the BEMD algorithm led to the complex EMD algorithm detailed previously in Tables 4 and 5. The proposed algorithms used the same algorithm as the EMD, where the only difference was the new sifting operators, S^{B1} and S^{B2}, representing the fast and slow oscillations.

The reformulation of the second complex algorithm allowed the sifting operator to be represented as a univariate (or real-valued) EMD sifting operator, shown below in Table 6. This reformulation allowed the behavior of the algorithm to be studied in a similar method as the original EMD algorithm [11].

Table 6: Algorithm 2 Reformulation for EMD Bivariate Extension

1. Given an angular direction: $\rho_k = \frac{2k\pi}{N}$ for $1 \le k \le N$ complete steps 2 through 3
2. Project the complex-valued signal $x(t)$ on direction $\rho_k : \partial_{\rho_k} = \mathrm{Re}[e^{j\rho_k} x(t)]$
3. Compute the partial estimate in direction ρ_k: $s_{\rho_k} = e^{-j\rho_k} \mathrm{P}[\partial_{\rho_k}](t)$
4. Subtract the mean to obtain $S^{B2}(t) = \frac{2}{N} \sum_k s_{\rho_k}(t)$

3.3.2.2. Bivariate Intrinsic Mode Functions (IMFs)

The BEMD algorithm proposed by Rilling et al. was designed so "that signals rotating around zero are admissible outputs" [11]. Rilling et al. clarified this vague notion of "rotating around zero" by asking: "what signals the algorithms actually consider

admissible outputs" [11]. In other words, $x(t)$ is considered a "fixed point of the sifting operator" [11], or

$$\begin{aligned} S^{B1}x(t) &\approx x(t) \\ S^{B2}x(t) &\approx x(t)\cdot \end{aligned} \tag{46, 47}$$

To explain the outputs that resulted from the BEMD algorithm, Rilling et al. explained various simulations. Both algorithms presented by Rilling et al. state two types of solutions are generally accepted. The first solution corresponded to the rotating signals, as expected, and the second occurred in cases where the method fails to extract the rotating components. In the latter case, the outputs "wander around zero" was more complicated than the first case [11]. The second types of solutions were encountered when the signal was not a clearly rotating signal, whereas solutions of the first type were signals with unchanging local rotation [11].

Rotating "around zero," as stated by Rilling et al., was clarified by considering the simple case where the signal performs one rotation around zero per period, or

$$\psi(t+T) = \psi(t) + 2\pi, \tag{48}$$

where T is the period of the signal. The clarification allows the understanding that only one maximum value exists per period. Thus, all of the envelope curves are constants with respect to time, allowing the mean to be derived analytically. Consequently, the envelope curve associated with the angular direction, $\rho_k = {2k\pi}/{N}$, is equal to the maximum signal value in that specific direction, where the phase of the derivative is equal to the definition in (48).

For the two separate algorithms existing in the BEMD method, Rilling et al. showed the means are equivalent to each other [11]. The mean for the first algorithm presented in Table 4 is defined as:

$$m^{B1}(t) = \frac{1}{N}\sum_k x\left(\psi^{-1}\left(\frac{2\pi k}{N} + \frac{\pi}{2}\right)\right), \tag{49}$$

with the limit of the algorithm resulting in:

$$m^{B1}(t) = \frac{1}{2\pi}\int_0^{2\pi} x\left(\psi^{-1}(\rho)\right)d\rho = \frac{1}{2\pi}\int_0^T x(t)\frac{d\psi}{dt}dt, \tag{50}$$

representing the mean of the signal over a period with a weight function of $\frac{d\psi}{dt} > 0$. The weighting conveys that the sampling is denser where the curvature is larger.

In a similar manner, the mean for the second algorithm or limit notation, omitting the summation notation, is:

$$\begin{aligned} m^{B2}(t) &= \frac{1}{\pi}\int_0^T e^{j\psi(t)}\Re\{e^{-j\psi(t)}x(t)\}\frac{d\psi}{dt}dt \\ &= m^{B1}(t) + \frac{1}{2\pi}\int_0^T e^{ej\psi(t)}x^*(t)\frac{d\psi}{dt}dt \end{aligned} \tag{51}$$

This equation leads to $m^{B2}(t) = m^{B1}(t)$ due to:

$$\begin{aligned} \int_0^T e^{ej\psi(t)}x^*(t)\frac{d\psi}{dt}dt &= \frac{j}{2}\left(\left[-e^{2j\psi(t)}x^*(t)\right]_0^T + \int_0^T \frac{dx^*}{dt}e^{2j\psi(t)}dt\right) \\ &= \frac{j}{2}\int_0^T r(t)e^{j\psi(t)}dt = \frac{j}{2}\int_0^T \frac{dx}{dt}dt = 0. \end{aligned} \tag{52}$$

The mean is equivalent for both BEMD algorithms and is also a fixed point of both sifting operators if and only if the integral in (50) is close to zero. More generally,

the outputs of the two complex algorithms are similar when there are rotating components inherent to the complex data, but may differ when the algorithms fail to extract the rotations.

3.3.3. The Hilbert Transform

A real function, $f(t)$, and its Hilbert transform, $\hat{f}(t)$, are related where, together, they create an analytic signal. This analytic signal can be represented as amplitude and phase, with the derivative of the phase called the instantaneous frequency [20]. By taking the Fourier transform of a strong analytic signal as described above, the "negative" frequencies are discarded and the spectrum becomes one-sided in the frequency domain.

The Hilbert transform in the time domain is a convolution between the Hilbert transformer, $1/\pi t$, and the function, $f(t)$. The Hilbert transform, $H[f(t)]$, of $f(t)$ defined as:

$$H[f(t)] = f(t) * \frac{1}{\pi t} = \frac{1}{\pi}\int_{-\infty}^{\infty} \frac{f(\tau)}{t-\tau} d\tau = \frac{1}{\pi}\int_{-\infty}^{\infty} \frac{f(t-\tau)}{\tau} d\tau . \tag{53}$$

This convolution represents the response to $f(t)$ of a linear time invariant filter having the impulse response, $1/\pi t$ [21]. The Hilbert transform was expressed as:

$$H[f(t)] = \hat{f}(t) = \frac{1}{\pi} P\int_{-\infty}^{\infty} \frac{f(\tau)}{t-\tau} d\tau . \tag{54}$$

The integral in the Hilbert transform description in (54) is, by definition, improper. The integrand contains a singularity, but has infinite limits of integration [21]. The P in front of the integral represents the Cauchy principal value, defined by the following equation:

$$H[f(t)] = \frac{1}{\pi}\lim_{\varepsilon \to 0^+}\left(\int_{t-1/\varepsilon}^{t-\varepsilon}\frac{f(\tau)}{t-\tau}d\tau + \int_{t+\varepsilon}^{t+1/\varepsilon}\frac{f(\tau)}{t-\tau}d\tau\right). \quad (55)$$

The Cauchy principal value was obtained by considering a finite range of integrate, symmetric about the singularity, if and when it exists [21].

3.3.3.1 Mathematical Motivations

The signal $1/\pi t$ has a Fourier transform of:

$$-j\,\mathrm{sgn}(\omega) = \begin{Bmatrix} -j, if\ \omega > 0 \\ 0, if\ \omega = 0 \\ j, if\ \omega < 0 \end{Bmatrix}. \quad (56)$$

If the signal $f(t)$ has the Fourier transform of $F(\omega)$, then the Hilbert transform, $\hat{f}(t)$, has the Fourier transform of [21]

$$\hat{F}(\omega) = -j\,\mathrm{sgn}(\omega)F(\omega). \quad (57)$$

The Hilbert transform is more easily understood in the frequency domain. The magnitude of $F(\omega)$ does not change; however, the phase of $F(\omega)$ does change. The positive frequencies of the Fourier transform values are multiplied by $-j$ (or a phase change of $-\pi/2$), while the negative frequencies of the Fourier transform values are multiplied by j (or a phase change of $+\pi/2$). Therefore, given the signal spectrum $F(\omega) = a + jb$, the Hilbert transform is $\hat{F}(\omega) = b - ja$ for $\omega > 0$ and $\hat{F}(\omega) = -b + ja$ for $\omega < 0$. The Hilbert transform exchanges the real and imaginary parts of the signal $F(\omega) = a + jb$, while changing one of the signs in the signal [21].

A table of common Hilbert transform pairs is detailed below in Table 7 [21].

Table 7: Hilbert Transform Pairs

Signal, $f(t)$	**Hilbert transform, $\hat{f}(t)$**
$a_1 g_1(t) + a_2 g_2(t); a_1, a_2 \in \mathbb{C}$	$a_1 \hat{g}_1(t) + a_2 \hat{g}_2(t)$
$h(t - t_0)$	$\hat{h}(t - t_0)$
$h(at); a \neq 0$	$\text{sgn}(a)\hat{h}(at)$
$\frac{d}{dt} h(t)$	$\frac{d}{dt} \hat{h}(t)$
$\delta(t)$	$\frac{1}{\pi t}$
e^{jt}	$-je^{jt}$
e^{-jt}	je^{-jt}
$\cos(t)$	$\sin(t)$
$rect(t)$	$\frac{1}{\pi} \ln \left\| \frac{2t+1}{2t-1} \right\|$
$\sin c(t)$	$\frac{\pi t}{2} \sin c^2(t) = \sin\left(\frac{\pi t}{2}\right) \sin c\left(\frac{t}{2}\right)$
$\frac{1}{1+t^2}$	$\frac{t}{1+t^2}$

The Fourier transform is important for signal processing. When given a real function $f(t)$, only the positive frequency axis is of interest because spectrum is symmetric about zero. The negative frequency axis is not needed and the Hilbert transform is employed to remove the negative frequency axis [20].

The Hilbert transform of a strong analytic signal is:

$$H[f(t)] = H[f(t) + j\hat{f}(t)] = \hat{f}(t) - jf(t) = -jz(t). \quad (58)$$

The Hilbert transform can be used to create an analytic signal from a real signal [20].

Therefore, it is possible to study the signal as a rotating vector with an instantaneous phase $\rho(t)$ and instantaneous amplitude $A(t)$ in the time domain:

$$z(t) = f(t) + j\hat{f}(t) = A(t)e^{j\rho(t)}. \tag{59}$$

The final portion of (59) represents the signal in polar notation, where

$$A(t) = \sqrt{f^2(t) + \hat{f}^2(t)}. \tag{60}$$

and

$$\theta(t) = \arctan\left(\frac{\hat{f}(t)}{f(t)}\right). \tag{61}$$

Finally, the notion of instantaneous frequency is introduced as:

$$\omega(t) = \frac{d\theta(t)}{dt}. \tag{62}$$

3.3.3.2 MATLAB® Hilbert Transform Function

MATLAB® has a function that will perform the Hilbert transform as defined in this section. Under the help section for the `hilbert()` function in MATLAB®, the explanation of the input values and the outputs are described in great detail. The `hilbert()` function returns a complex sequence, or the analytic signal, from a real-valued sequence. The real-valued part of the signal contains the original signal of the input data and the imaginary-valued part of the signal contains the Hilbert transform of the input data [22]. The imaginary-valued portion represents a 90 degree phase shift of the original real-valued data sequence. In addition, "the Hilbert transformed series has the same amplitude and frequency content as the original real data and includes phase information that depends on the phase of the original data" [22].

MATLAB® details the algorithm inherent to the MATLAB® `hilbert()` function, as the following:

> "The analytic signal for a sequence `x` has a *one-sided Fourier transform*, that is, negative frequencies are 0. To approximate the analytic signal, `hilbert` calculates the FFT of the input sequence, replaces those FFT coefficients that correspond to negative frequencies with zeros, and calculates the inverse FFT of the result" [22].

In greater detail, the `hilbert()` function employs the following four-step algorithm in Table 8:

Table 8: MATLAB® Hilbert Algorithm [22]

1. It calculates the FFT of the input sequence, storing the result in a vector **`x`**.
2. It creates a vector **`h`** whose elements `h(k)` have the values, where `n` represents the number of elements: • 1 for `k = 1, (n/2)+1` • 2 for `k = 2, 3, ... , (n/2)` • 0 for `k = (n/2)+2, ... , n`
3. It calculates the element-wise product of **`x`** and **`h`**.
4. It calculates the inverse FFT of the sequence obtained in step 3 and returns the first `n` elements of the result.

Furthermore, MATLAB® also explains the uses of the Hilbert transform for calculations. The Hilbert transform can be used in calculating two important instantaneous attributes of a signal: the amplitude and frequency. The instantaneous amplitude is the amplitude of the complex-valued Hilbert transform, whereas the instantaneous frequency is the rate of change of the instantaneous phase angle with respect to time [22].

3.3.4. The Fourier Transform

The Fourier transform is important in many fields of study, such as mathematics, engineering, and physical sciences. Fourier transforms are key components in data

processing and instruments, as well as the cornerstone of interferometry and aperture synthesis [23]. The Discrete Fourier transform (DFT), and more specifically the FFT, has revolutionized the data processing and digital electronics industry.

3.4.4.1. Fourier Transform Basics

The Fourier transform is a reversible and linear transform with a number of important properties, such as time shifting and scaling. For any time-domain function $f(t)$ (either real- or complex-valued), the Fourier transform in the frequency domain is denoted by $F(\omega)$ [23].

The forward transform of the Fourier transform is defined as:

$$F(\omega) = \int_{-\infty}^{\infty} f(t) e^{-j\omega t} dt \tag{63}$$

and the inverse transform of the Fourier transform is represented as:

$$f(t) = \frac{1}{2\pi} \int_{-\infty}^{\infty} F(\omega) e^{j\omega t} d\omega . \tag{64}$$

The complex exponential plays a key role in the Fourier transform.

A complex exponential is defined as a complex number consisting of sinusoids. Euler's formula embodies the relationship:

$$e^{j\theta} = \cos(\theta) + j \sin(\theta) . \tag{65}$$

Because of the fact that complex exponentials are complete and orthogonal, the Fourier transform can represent any piecewise continuous function and to minimize the error between the function and its transform representation [23].

3.4.4.2 The Discrete Fourier Transform

While the continuous Fourier transform converts a time-domain signal of a continuous spectrum of an infinite number of sinusoids, the DFT is composed of a finite number of sinusoids. The DFT is extremely important in the area of frequency analysis, primarily due to how it approaches a discrete signal in the time-domain and transforms the signal into its frequency domain representation [24]. The DFT of a signal of sampled data points, x_n, is defined by:

$$X_k = \sum_{n=0}^{N-1} x_n e^{-j2\pi nk/N} . \tag{66}$$

and its inverse by:

$$x_n = \frac{1}{N} \sum_{k=0}^{N-1} X_k e^{j2\pi nk/N} . \tag{67}$$

A DFT of N-point time series results in an N-point frequency spectrum. When the input signal is real-valued, the DFT contains an even real-part and an odd imaginary-part of the spectrum. Therefore, the "negative" Fourier transform frequencies provide no new information, leading to the conclusion that no information is created nor destroyed by the DFT [23].

3.4.4.3. The Fast-Fourier Transform

The FFT is a faster version of the DFT. While the FFT performs the same task as the DFT, it utilizes algorithms to accomplish the objectives in less time. The discrete property and speed of the FFT allows the use of MATLAB® to analyze signals [24]. MATLAB®'s `fft()` function is effective for computing the DFT of the input signal.

The FFT functions in MATLAB® are based on the MATLAB® library, Fastest Fourier Transform in the West (FFTW), is used to increase the Fourier transform speed.

To compute the DFT of a signal, the FFTW library decomposes the problem using the Cooley-Tukey algorithm [22], resulting in the values for the DFT of the given signal. The `fft(X)` outputs the DFT of the input data in the form of a vector. The output vector is computed using the FFT algorithm, through selection using the FFTW library [22]. To further understand the FFT, the steps of the MATLAB® function `fft()` can be helpful. The function `Y= fft(X)` implements the transform for a vector of length N as detailed in below:

$$X[k] = \sum_{m=1}^{N} x[m]\omega_N^{(m-1)(k-1)}, \tag{68}$$

with

$$\omega_N = e^{(-2\pi j)/N}, \tag{69}$$

representing the N th root of unity [22].

3.5. Implementation of the Algorithms

In the previous section, the components and algorithms employed were explained. After an understanding of the components was gained, solutions for satisfying the objectives of this research were implemented as code in MATLAB®. Before the final code was implemented and used to generate the results, there were failed coding attempts explored. These attempts were detailed in the following sub-section, followed by the final BEMD coding written for the final results generated, and finishing the section with a detailed explanation of the implemented BEMD code.

3.5.1. Unsuccessful Coding Attempts

There were two unsuccessful coding attempts to create the graphs to compare in the data analysis and results section. The first attempt was to compare the FFT with the HHT directly. Yet, upon further research, it was discovered that the FFT exists in the frequency domain, whereas the HHT exists in the time domain. Therefore, the direct comparison attempt led to a dead end due to the inability to compare the graphs to each other since they existed in different domains.

The next attempt was to change the FFT into the time domain using the inverse FFT to compare directly with the HHT in the same domain. The inverse FFT graphs presented an incorrect interpretation of the FFT signal when transformed into the time domain. So, again, this second attempt was unsuccessful in generating the graphs and comparisons needed to successfully create the graphs for data analysis.

3.5.2. Bivariate Empirical Mode Decomposition Explanation

The first component implemented in the code was the complex extension of the EMD algorithm BEMD [11], described in section 3.3.2, to calculate the complex IMFs. Dr. Patrick Flandrin, one of the primary authors, worked to create his own code for implementing the method proposed by Rilling et al. Through reading the BEMD paper and proceeding to the website listed in the paper (http://perso.ens-lyon.fr/patrick.flandrin), coding for the BEMD algorithm was available in the emd.zip file. Dr. Flandrin's original BEMD example was detailed in Appendix A.

3.5.3. Final CEMD Algorithm Implementation

Even though code was written for the BEMD method, a couple changes were made to satisfy the objectives for this research. One of the first changes was to plot the

magnitude and phase of the signal, rather than the real and imaginary components. The input complex RCS data set required a change of domain to produce useful phase and magnitude data for graphical comparison. Another modification was made to present two subplots on each figure, meaning that the magnitude and phase of the decomposed signal were plotted as their independent figure. This modification allowed the computer to run without using much memory with respect to the computer used to run the code, as well as allowed for a quicker side-by-side comparison of the magnitude and phase plots of both before and after the application of the Hilbert transform. A final change was the labeling of the title and axes, since they need to fit the real-world signal rather than the example provided by Dr. Flandrin. The modification of the code written by Dr. Flandrin is presented in Appendix B.

3.5.3.1. Loading the Data and Calculation of the IMFs

Section B.1, of Appendix B, represented the loading and the remodeling of BEMD code to run the data. Once the data was loaded, the BEMD algorithm was applied to the remodeled data. The specific `cemdc2()` function was presented in Appendix C, where the definition of the function was described in detail, such as the inputs and the outputs of the function. After the `cemdc2()` function was employed, the function outputted two separate values. The first, called `imf`, was a matrix where the IMFs were stored for each radar return measurement of the real-world data set. The second, called `NB_ITERATIONS`, represented the effective number of sifting iterations for each IMF.

3.5.3.2 Plots of IMFs: CEMD and HHT

In section B.3 of Appendix B, the IMFs that were calculated and stored in section B.2 were plotted. First, the original signal was plotted with the magnitude on the top

portion of the subplot and the unwrapped phase on the lower portion of the subplot. The magnitude was plotted using the `abs()` function, whereas the phase was plotted using the `angle()` function after the value for the angle was unwrapped. The `unwrap()` function corrected the phase angles of the input signal to produce a smoother phase plot [22]. MATLAB® defines the `unwrap()` function as a function that corrects the radian phase angles in a vector by adding multiples of $\pm 2\pi$ [22]. Once the original signal was plotted, the IMFs and residue of the decomposed signal were plotted. The decomposed plots were displayed in the same layout as the original signal. The x-axis of the magnitude plot represented the time scale, while the y-axis represented the RCS value in decibel per square meter (dBsm). This measurement represents the decibel measure for the RCS of a target relative to one square meter. The x-axis was represented on the phase plot as the time scale as well, and the y-axis represented the angle value of the signal in radians.

In section B.4 of Appendix B, the Hilbert transform was applied to the real and imaginary components of the real-world data set. Rather than plot the real and imaginary parts of the data set, the magnitude and phase after the application of the Hilbert transform were plotted. The magnitude plot represented the RCS value in dBsm on the y-axis, with the time scale represented on the x-axis. Similarly, the phase plot represented time on the x-axis, while the y-axis represented the angle of the signal in radians. After the Hilbert transform of the original signal was plotted, the Hilbert transform was applied to the IMFs and the residue decomposed from the original data set, in which the magnitude and phase of the Hilbert transform of the IMFs and the residue were plotted. Because the `hilbert()` function ignores the imaginary part of a signal, the phase plot represents the imaginary component and the magnitude plot analyzed the real component

of the signal. Similar to the CEMD plots in section B.3, the axes of the Hilbert transform of the signal was RCS in dBsm with respect to time for the magnitude plot and was angle in radians with respect to time for the phase plot.

3.5.3.3. Plots of IMFs: FFT of CEMD and HHT

The FFT of the decomposed signal before the application of the Hilbert transform was calculated and plotted in section B.5 of Appendix B. In a similar manner to the previous two comparisons, the original and decomposed signals were plotted for the real-world data set. Prior to generating the plots, the `fft()` function was applied to the real-world data set. Then, the magnitude and phase were separately calculated. Finally, the magnitude and unwrapped phase were plotted. Since the FFT was applied to the data set, the magnitude graph represented frequency in GHz on the x-axis with the RCS value in dBsm plotted on the y-axis. Additionally, the magnitude plot represented the absolute value of the FFT of the real-world data set, while using the `fftshift()` function applied to the real-world data set to shift the zero-frequency component of the data to the center of the spectrum. By using the `fftshift()` function, interpretation of the generated plot was easier. MATLAB® states that the `fftshift()` function "rearranged the outputs of the [FFT of the data] by moving the zero-frequency component to the center of the array…[and]…is useful for visualizing a Fourier transform with the zero-frequency component in the middle of the spectrum" [22]. The phase plot of the FFT of the real-world data set was also represented by frequency along the x-axis and the angle value in radians on the y-axis.

After the original signal was plotted, the plots of the IMFs and residue were generated through implementation of a `for()` loop. The plots of the IMFs were created

similar to the original signal, with the only exception of input value. Rather than the original data set, the input signals were the modes of the decomposed signal of the real-world data set. The magnitude plot represented the absolute value of the FFT of the decomposed signal, with the `fftshift()` applied to the resulting FFT of the IMFs and residue. For the magnitude plot, the x-axis represented the frequency present in the modes of the decomposed signal and the y-axis represented the RCS value in dBsm. Additionally, the phase plot represented the angle of the FFT of the modes of the decomposed signal. Frequency was represented along the x-axis and the angle in radians was represented along the y-axis.

Section B.6 detailed the process of applying the FFT to the decomposed signal after the application of the Hilbert transform. The first plots generated were the representations of: (1) the magnitude of the FFT after the Hilbert transform application and (2) the phase of the FFT after the Hilbert transform application. All plots in this section represented the FFT after the application of the Hilbert transform of the input data. To generate the magnitude graph, the `fftshift()` of the real-valued data of the FFT after the application of the Hilbert transform was plotted. The x-axis represented the frequency component present in the signal in GHz, while the y-axis represented the amplitude of the RCS value in dBsm. For the phase plot, the unwrapped angle of the imaginary-valued components FFT after the Hilbert transform application of the data was plotted. The x-axis represented the amount of each frequency present in the signal in GHz and the y-axis represented the angle value of the signal in radians.

After the original signal of the FFT after the application of the Hilbert transform was generated, the magnitude and phase plots for the decomposed signal modes of the

FFT after the Hilbert transform application were plotted. The magnitude graph was generated using the `fftshift()` of the real-valued components of the FFT after the Hilbert transform application to the respective mode. On the magnitude graph, the x-axis represented the frequency present in the signal and the y-axis represented the RCS value in dBsm. Additionally, the phase plot was generated through use of the `unwrap()` and `angle()` functions from the FFT after the Hilbert transform application of the imaginary-valued components of the respective mode. For the phase plot, the x-axis represented the frequency present in the signal, while the y-axis represented the angle of the signal in radians.

3.5.3.4. Plots of IMFs: DTI of CEMD and HHT

For the Doppler-Time-Intensity (DTI) plots, only the magnitude plot was of interest. The DTI plots are represented on a `pcolor()`, or pseudocolor, plot. A pseudocolor plot is a rectangular array of cells with colors determined by the input data [22]. The x-axis and y-axis limits were defined using the `linspace()` function and MATLAB® defines as a function used to "generate linearly spaced vectors" [22]. To graph a `pcolor()` plot, there are three dimensions. The x-axis of the DTI was represented by the time value, the y-axis represented the frequency content in the signal in GHz, and the color axis represented the FFT intensity at each time and frequency value in the matrix spanning the x-y linear space. The third dimension was represented through the intensity of the color of the absolute value of the windowed FFT both before and after the application of the Hilbert transform on a logarithmic scale.

Section B.7 in Appendix B presented the application of the windowed FFT to the original signal, IMFs, and the residue to generate the DTI plots. While a traditional FFT

would also provide similar analysis, the FFT employed in this section of the code was a windowed FFT implemented by the user, rather than a function embedded in the MATLAB® program. The windowed FFT replaces the Fourier transform's sinusoidal wave by the product of a sinusoid and a window which is localized in time. In addition, windowed Fourier Transforms are important in providing simultaneous insight in time and frequency behavior of the functions. The first step was to define the step resolution and the amount of seconds for the resolution of the windowed FFT. Next, the windowed FFT was applied and the DTI plot of the FFT of the original signal was generated.

Subsequently, the windowed FFT of the decomposed signal modes were calculated and stored. Then, the FFT of the decomposed signal modes were graphed on a `pcolor()` plot. These two objectives were accomplished using an embedded `for()` loop. First, the windowed FFT value of the IMF was calculated and the magnitude of the FFT was graphed. The `fftshift()` of the absolute value of the windowed FFT was graphed on the `pcolor()` plot using a logarithmic scale. The DTI plot was represented with time on the x-axis, frequency on the y-axis, and the color axis representing the intensity of the FFT of the decomposed signal.

Section B.8 of Appendix B represented the calculation of the windowed FFT of the original signal and the modes of the decomposed signal after the application of the Hilbert transform, as well as generated the DTI. The first step was to define the step resolution and the amount of seconds for the resolution of the windowed FFT. Next, the windowed FFT after the Hilbert transform application of the original signal was calculated and stored. Once the windowed FFT was calculated and store, the windowed FFT was plotted.

The windowed FFT of each mode of the decomposed signal was calculated and stored. Then, the FFT after the Hilbert transform application of the decomposed signal graphed on a `pcolor()` plot. These two objectives were accomplished using an embedded `for()` loop. First, the Hilbert transform of each component of the decomposed signal was calculated and the windowed FFT value after the Hilbert transform application was calculated. Next, the magnitude of the FFT after the Hilbert transform application was plotted. The `fftshift()` of the absolute value of the windowed FFT after the Hilbert transform application was graphed on the `pcolor()` plot using a logarithmic scale. The DTI plot was represented with time on the x-axis, frequency on the y-axis, and the color axis representing the intensity of the FFT after the Hilbert transform application of the decomposed signal.

3.6. Chapter Summary

An exploration of the various components necessary to implement the MATLAB® code and satisfy the objectives presented in Chapter I was performed. The applied BEMD algorithm was explained and relevant data collection was detailed. Four specific components were investigated for employing the algorithm presented by Rilling et al. [11]: (1) the EMD algorithm, (2) the CEMD algorithm, (3) the Hilbert transform (leading to the HHT representation), and (4) the FFT. Finally, algorithm was implemented and discussed with detailed MATLAB® code as presented in Appendices A, B, and C.

IV. Results and Data Analysis

4.1. Overview

The results and analysis for the comparisons of the data generated in Chapter III, after applying the CEMD algorithm and the two mathematical transforms, the Hilbert transform and FFT, are presented and analyzed in detail. The results are organized into four sections. The first section compares the decomposed real-world data set with the RCS signal of various canonical shapes collected in the RCS range at AFIT, often encountered in real-world signals. Next, the decomposed real-world signal is compared with its Hilbert transform of the decomposed real-world signal. In addition, the application of the FFT to both the decomposed signal and the application of the Hilbert transform to the decomposed signal are compared. Finally, the windowed FFT of the decomposed signal and the Hilbert transform application to the decomposed signal are compared. In other words, the Doppler-Time-Intensity (DTI) representation of the signals were analyzed and compared, noting the differences and similarities in the generated graphical representation.

4.2. Evaluation of CEMD Method

To assess how well the CEMD method performed, the decomposed signal of the real-world data set was compared with four common shapes inherent to dynamic objects similar to the one represented by the real-world data set. First, the graph of the original signal of a closed-cap cylinder was compared to the various IMFs of the decomposed real-world signal. After comparing the RCS of the closed-cap cylinder with the IMFs,

the most similar IMF to the original signal of the closed-cap cylinder was IMF #2, as displayed in Figures 8 and 9.

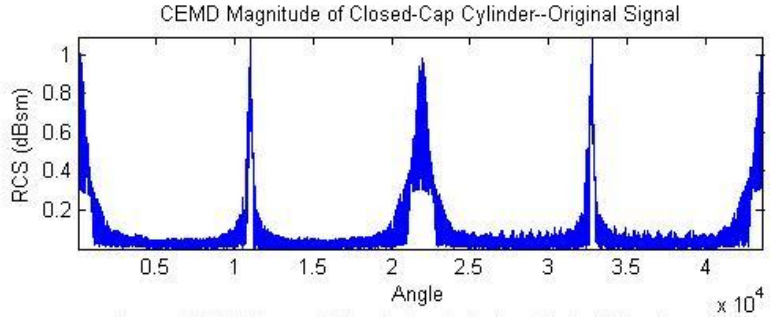

Figure 8: CEMD Magnitude of Closed-Cap Cylinder

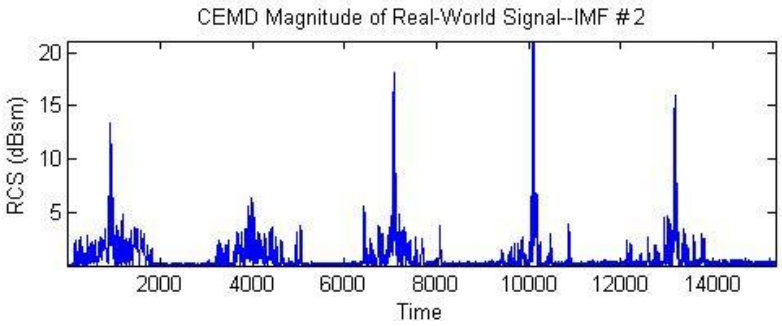

Figure 9: CEMD Magnitude of Real-World Signal--IMF #2

The peaks in the RCS values of the two plots occurred at analogous fixed points in the analysis of the complex time series. However, the amplitude of the peak return values differ by a factor of 20 dB. Even though this difference exists, the RCS value of the original signal of the closed-cap cylinder behaved most like IMF #2 of the decomposed real-world signal through comparing the plots.

The second comparison occurred between the RCS of a cavity cylinder and the decomposed real-world signal. The cavity cylinder results were similar to the closed-cap cylinder RCS return plot. Additionally, the peaks of the cavity cylinder and IMF #2

occur at approximately the same instances in time on the graph, shown in Figures 10 and 11.

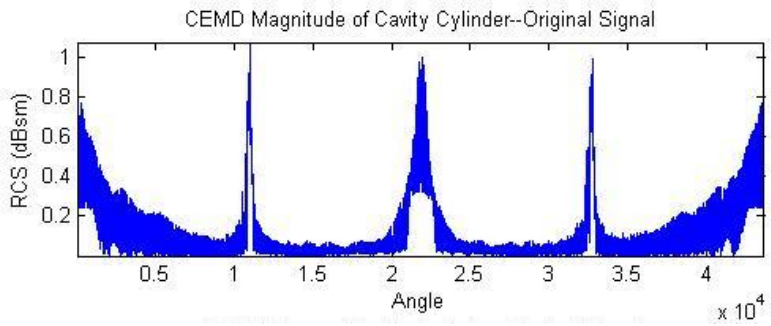

Figure 10: CEMD Magnitude of Closed-Cap Cylinder

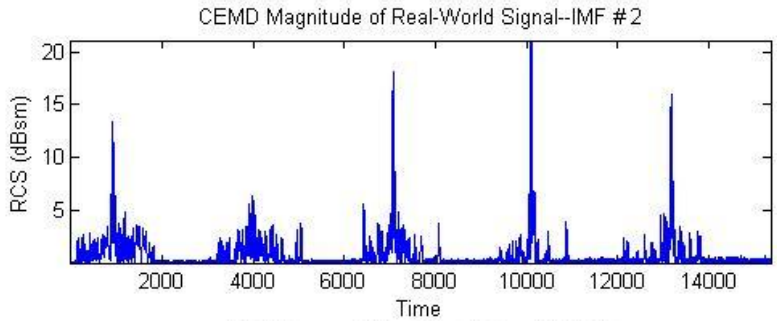

Figure 11: CEMD Magnitude of Real-World Signal--IMF #2

The amplitude of the peaks was also different by a factor of 20 dB; although there was a difference, the cavity cylinder behaved most like IMF #2 of the decomposed real-world signal.

Third, the RCS plot of the cone-sphere was compared with the IMFs of the real world signal. Yet, unlike the first two shape comparisons, there was no IMF of the decomposed real-world signal that behaved most like the RCS plot of the cone-sphere signal.

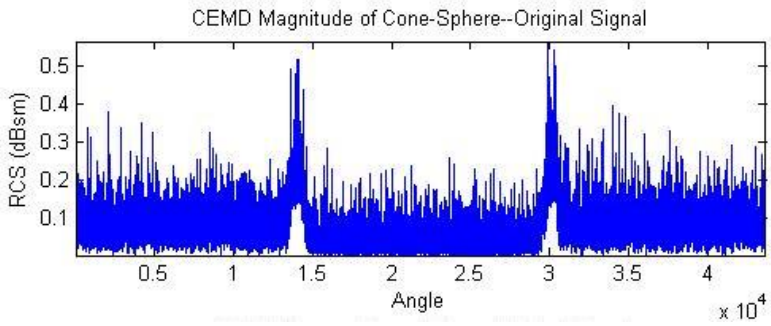

Figure 12: CEMD Magnitude of Cone-Sphere

Finally, the RCS plot of the original signal of the dihedral corner reflector was compared to the IMFs of the decomposed real-world signal. Comparing these two plots side-by-side, the dihedral corner reflector behaved most like IMF #3, with a magnitude difference by a factor of seven. One possible explanation for the difference in the magnitude factors is the amount of space between the dynamic object and the radar measuring the RCS value. Finally, the peaks of each plot occurred at approximately the same proportional time interval, and the smaller radar returns also occurred at the approximate same time intervals.

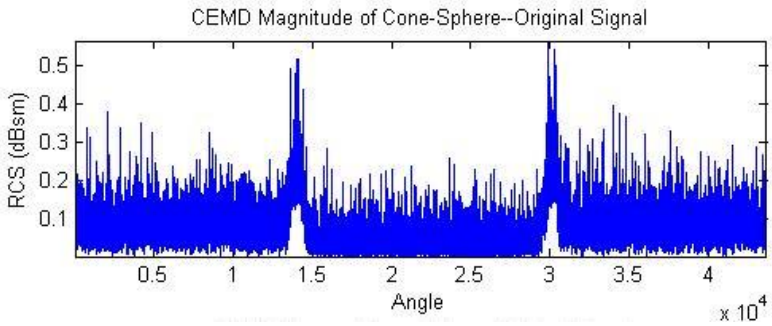

Figure 13: CEMD Magnitude of Dihedral Corner Reflector

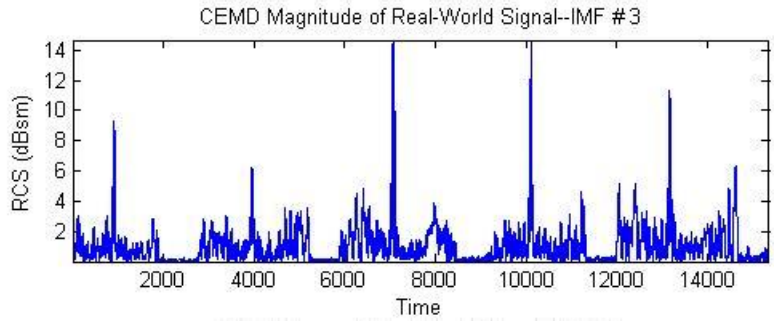

Figure 14: CEMD Magnitude of Real-World Signal—IMF #3

Overall, the comparisons discussed reinforced the fact that the CEMD method effectively decomposed the real-world data set provided for this evaluation into its IMFs. Therefore, the CEMD method could be a viable tool for analysis of RCS signals in the future.

4.3. Analysis of Decomposed Data Before and After the Hilbert Transform

The second analysis was the comparison of the graphical results generated of the original signal and the Hilbert transform application to the original signal using the CEMD algorithm. There was not any quantitative data to analyze; rather, the graphs were qualitatively compared and discussed.

4.3.1. Original Signal Plot Analysis

Firstly, the magnitude of the original signal and the Hilbert transform application to the original signal were displayed in Figures 15 and 16 and represented by the graph of RCS value in dBsm with respect to time.

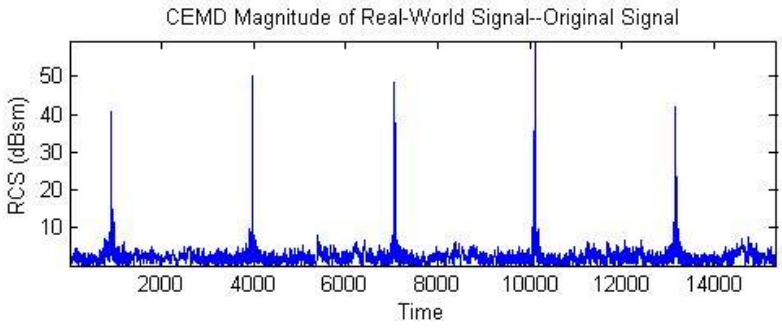

Figure 15: CEMD Magnitude of Original Signal

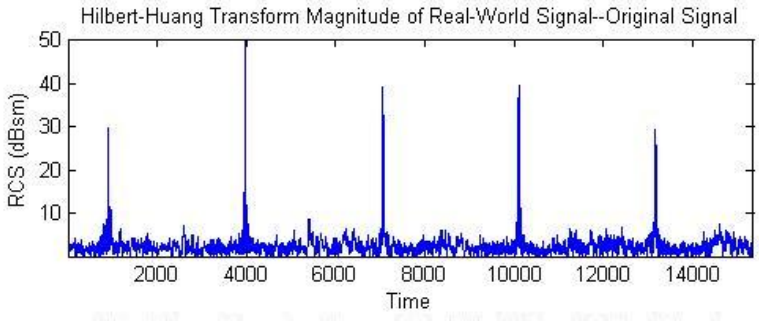

Figure 16: HHT Magnitude of Original Signal

The graphs both displayed five large returns, where the original signal had a slightly higher return at each spike than after the application of the Hilbert transform. Other than the differences in the peaks, there was no noticeable difference in the original signal when compared with the signal after the application of the Hilbert transform.

However, the phase plots, shown in Figures 17 and 18, displayed a much larger difference. Namely, the scale on the y-axis displayed a large difference in amplitude, as well as the smoothness of the curve. The plots needed to be viewed on the same scale to

determine if there was a difference in the curve because the plots were on such different scales.

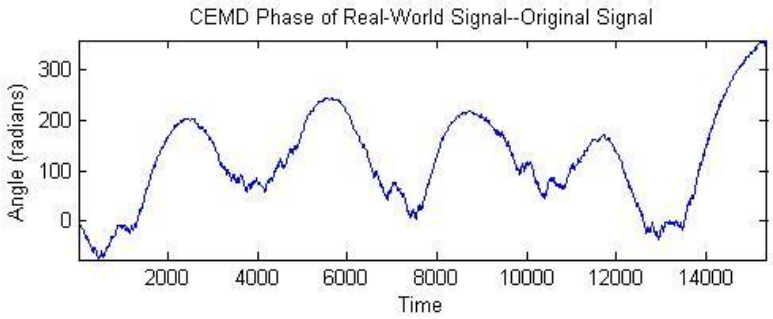

Figure 17: CEMD Phase of Original Signal

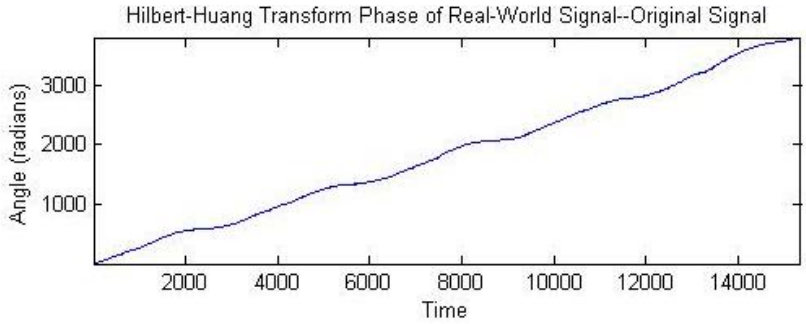

Figure 18: HHT Phase of Original Signal

However, these differences and possible causes fell outside the scope of this evaluation and would require more research to determine whether the phase portion of the CEMD algorithm provided significant analysis.

Comparatively to the magnitude plots of the original signal, there were not noticeable differences between the before and after the application of the Hilbert transform. Consequently, more information and noticeable changes might occur after analysis of specific IMFs.

4.3.2. IMF Plot Analysis

The plots of IMF #1 showed only a small difference between the two plots both before and after the application of the Hilbert transform, in Figures 19 and 20. Therefore, no helpful information could be determined by comparison of these two plots.

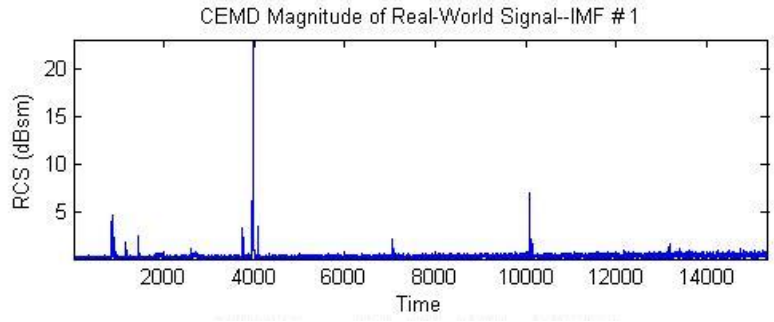

Figure 19: EMD Magnitude of IMF #1

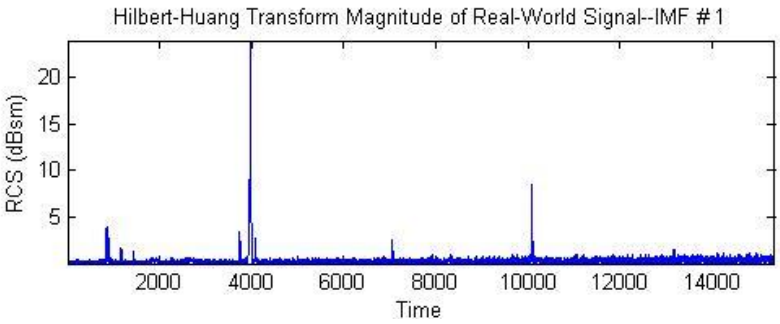

Figure 20: HHT Magnitude of IMF #1

By comparing the two IMF #2 plots in Figures 21 and 22, there was a slight difference in the intensity of each return value with respect to time. On the graph of the IMF #2 signal before the application of the Hilbert transform, there was approximately double the intensity in time when compared with the signal after the application of the Hilbert transform. Although there was a slight magnitude difference, the primary and most noticeable difference was the intensity at each time value before the application of the Hilbert transform signal. After application of the Hilbert transform, the negative

frequency values were set to equal zero and could account for the less intense plot value after the Hilbert transform application. For a more detailed representation of what the Hilbert transform does to an input signal, please refer to Chapter III, section 3.3.3.

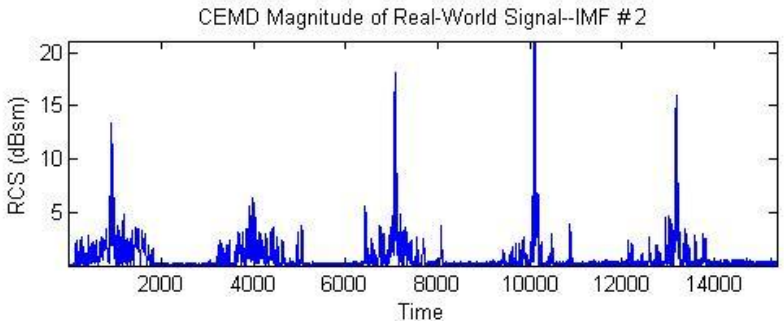

Figure 21: CEMD Magnitude of IMF #2

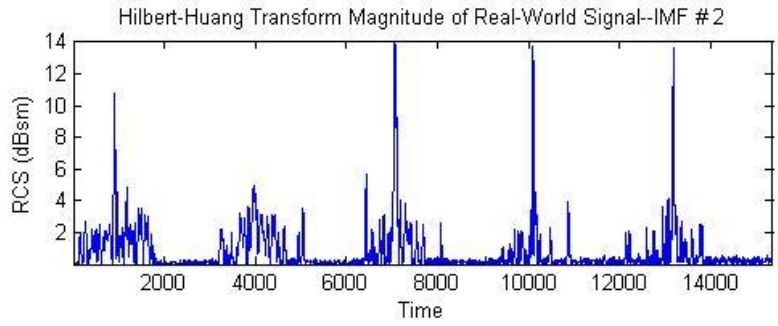

Figure 22: HHT Magnitude of IMF #2

Beginning with IMF #5, displayed in Figures 23 and 24, the curve after application of the Hilbert transform presented a more smooth representation than previous IMFs, as well as displayed a more precise value representation of the original signal. IMF #5 provided a cleaner representation of the decomposed real-world signal, even though the amplitude scale was slightly different between two plots.

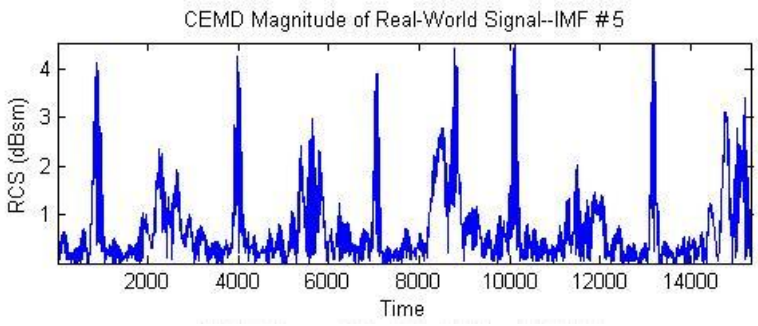

Figure 23: CEMD Magnitude of IMF #5

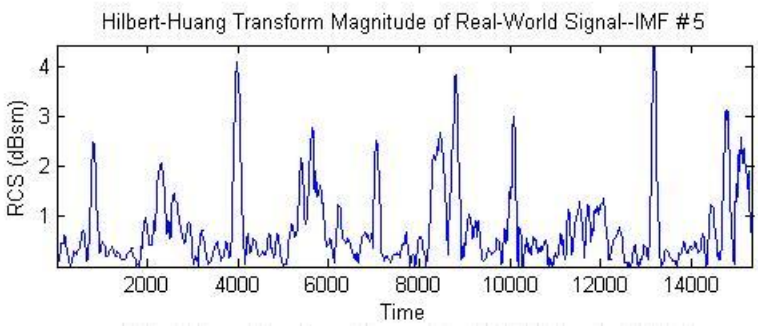

Figure 24: HHT Magnitude of IMF #5

From comparing the plots of IMF #6, in Figures 25 and 26, this IMF allowed for direct comparison and showed that, after application of the Hilbert transform, the plot was more fluid than before the application of the Hilbert transform. The same characteristics were present in both plots and, through application of the Hilbert transform, the plot of IMF #6 of the real-world signal was more focused and displayed a cleaner representation. The "cleaned-up" version makes analysis of the time value representation in RCS value easier and may have provided more accurate analysis of the decomposed signal after the application of the Hilbert transform.

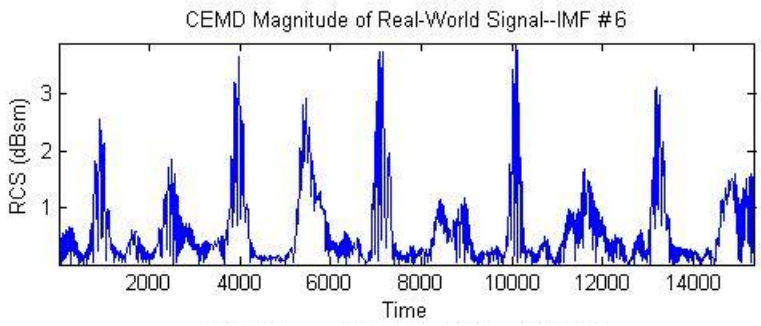

Figure 25: CEMD Magnitude of IMF #6

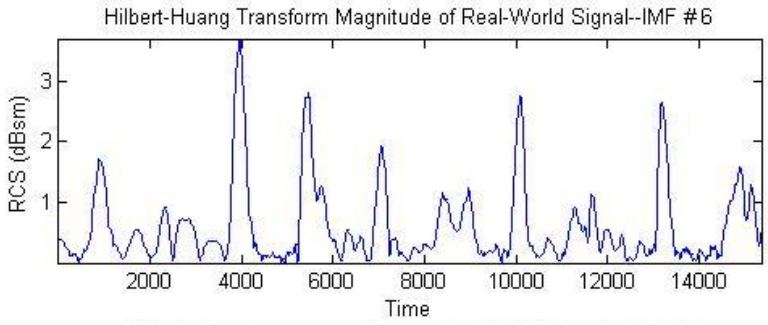

Figure 26: HHT Magnitude of IMF #6

IMFs #7 through #11 provided additional support for the conclusions and characteristics discussed about IMF #6.

The decomposition displayed in Figures 27 through 36 showed the sinusoidal nature of the CEMD method; however, the sinusoid became more noticeable after application of the Hilbert transform. Before the application of the Hilbert transform, the decomposition of the signal appeared noisier and possibly contained extraneous signal values of the decomposed signal representation. Based on the aforementioned conclusions, it is hypothesized in later plot representations that the removal of negative frequencies might prove be either helpful or harmful, especially when used for analysis in the intelligence community.

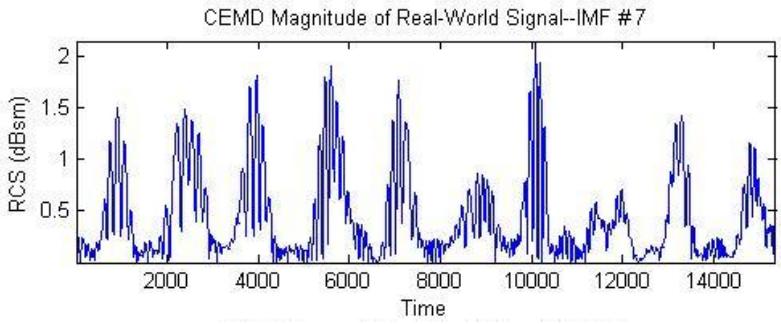

Figure 27: CEMD Magnitude of IMF #7

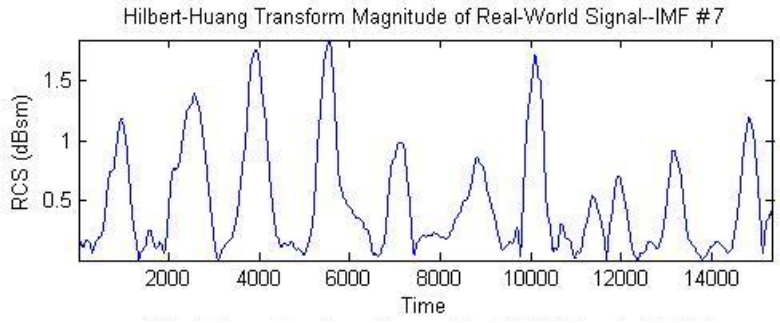

Figure 28: HHT Magnitude of IMF #7

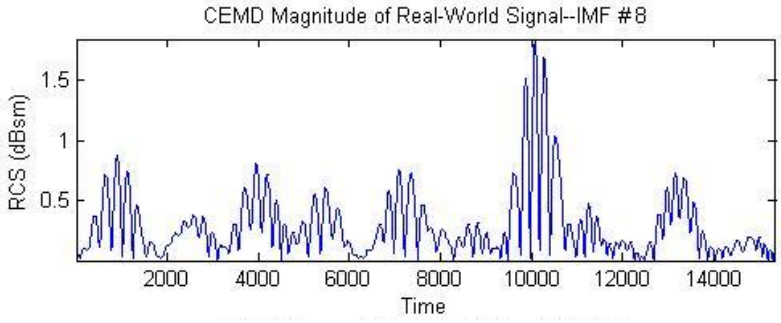

Figure 29: CEMD Magnitude of IMF #8

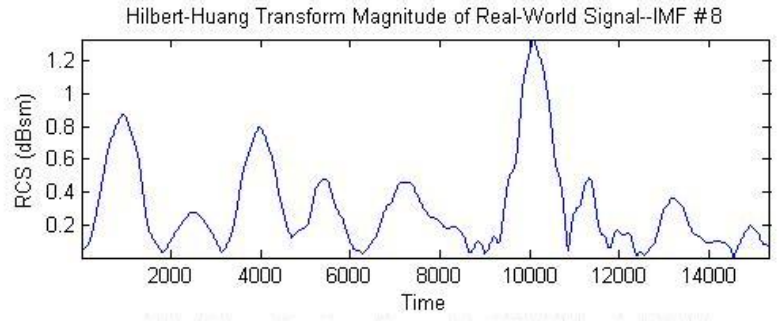

Figure 30: HHT Magnitude of IMF #8

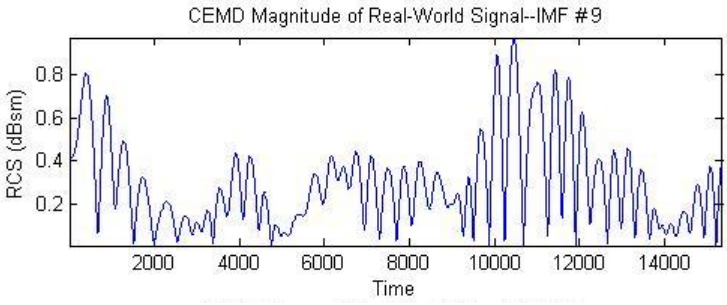

Figure 31: CEMD Magnitude of IMF #9

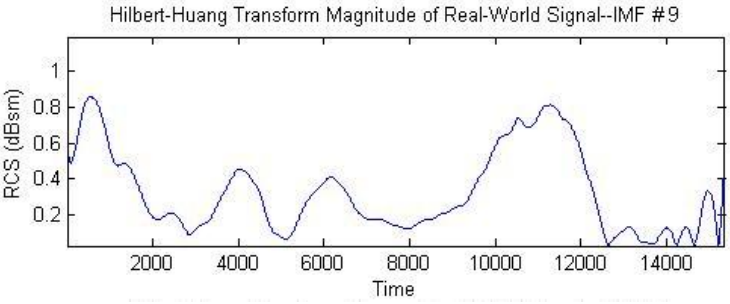

Figure 32: HHT Magnitude of IMF #9

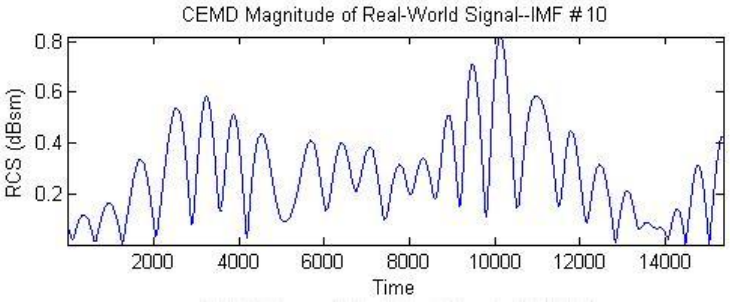

Figure 33: CEMD Magnitude of IMF #10

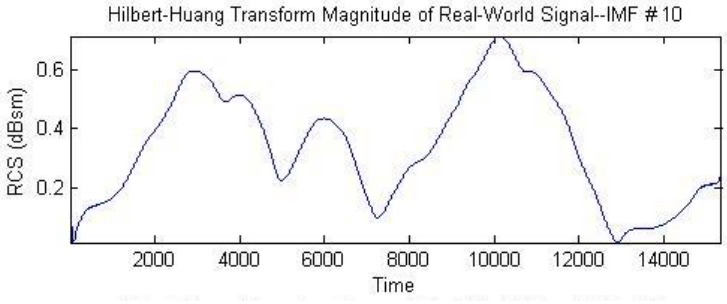

Figure 34: HHT Magnitude of IMF #10

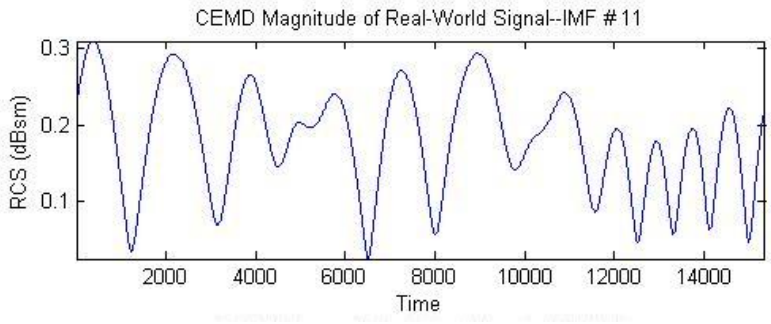

Figure 35: CEMD Magnitude of IMF #11

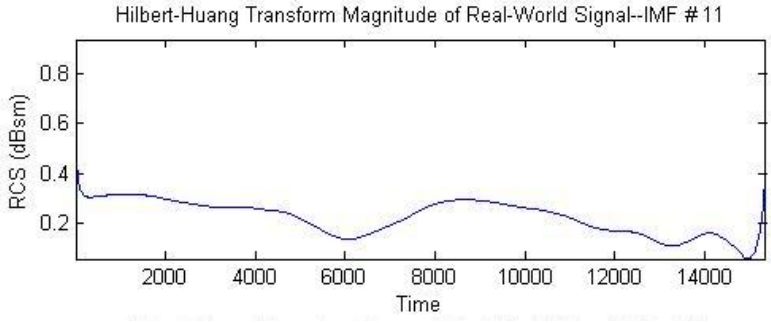

Figure 36: HHT Magnitude of IMF #11

4.4. Analysis of the FFT Plots Before and After the Hilbert Transform Application

Traditionally, the FFT has been the main signal analysis tool for analyzing RCS data. The application of the FFT allowed the researcher to determine at what frequency values the signal was most dominant, as well as represented the signal for analysis in the frequency domain. For each of the graphs generated to represent the magnitude of the FFT in the frequency domain, the frequencies represented by 7685 Hz and below were the negative frequencies, while the positive frequencies were between 7686 Hz and 15370 Hz on the frequency axis. In addition to the magnitude plot being generated, the phase of the signal was represented by angle in radians with respect to the frequency of the signal.

4.4.1. Original Signal FFT Plot Comparisons

The first plots compared the effect of the Hilbert transform applied to the real-world signal. The magnitude plots of the original signal before and after applying the Hilbert transform, prior to decomposition using the CEMD algorithm, are represented below in Figures 37 and 38.

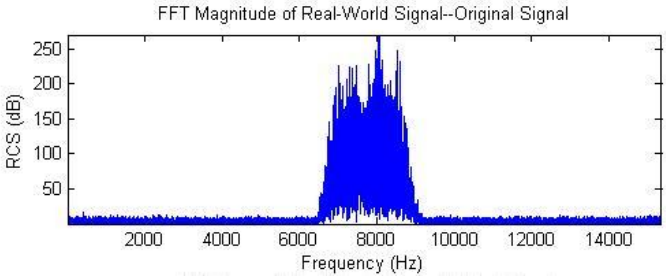

Figure 37: FFT of CEMD Magnitude of Original Signal

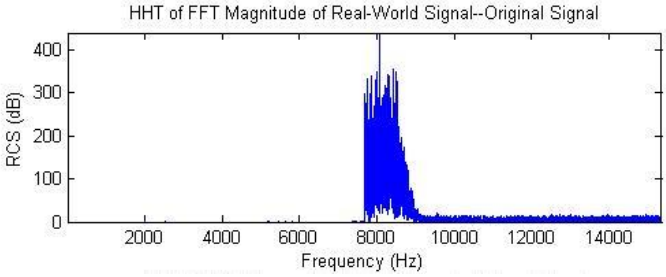

Figure 38: FFT of HHT Magnitude of Original Signal

First, the comparison of the magnitude plot of the FFT before and after the Hilbert transform application displayed a characteristic inherent to the Hilbert transform. The characteristic inherent to the Hilbert transform resulted in the negative frequencies of the signal being removed, leading the negative frequency values to equal zero. The FFT of the signal before the Hilbert transform application showed the plot contained both negative and positive frequencies, with the signal appearing approximately symmetric along the frequency axis with respect to its RCS value in dBsm. The removal of the negative frequencies on the plot was not the only difference present in the generated

graph. The RCS return values that were present in the positive frequencies after the application of the Hilbert transform and the graph had a larger magnitude value by a factor of approximately two as compared with the RCS return values before the application of the Hilbert transform. The difference in amplitude of the RCS return value led to the possibility that the negative frequency returns were preserved in the graph and resulted in the larger magnitude present on the positive frequency portion of the plot. One possible explanation is based on the conservation of energy principle, which states that the amount of energy put into the signal must equal that exiting after application of the Hilbert transform.

Additionally, the phase plots of the original signal of the FFT plot both before and after the Hilbert transform application did not appear to provide any new or possibly significant information due to them displaying approximately equal angle measurements, presented in Figures 39 and 40.

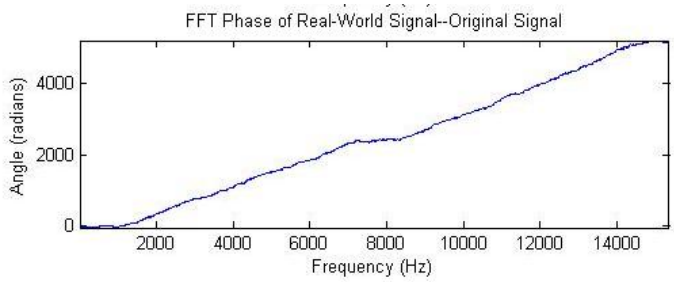

Figure 39: FFT of CEMD Phase of Original Signal

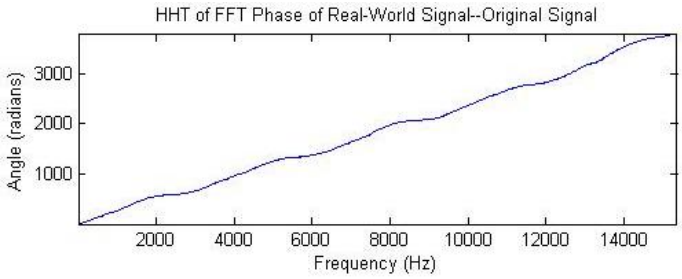

Figure 40: FFT of HHT Phase of Original Signal

4.4.2. IMF FFT Plot Comparisons

In a similar fashion to the plots of the original signal, comparisons between the IMFs of the FFT after application of the Hilbert transform of the decomposed signal yield different results and noted graphical differences. The plots representing the IMFs of the FFT were detailed below in Figures 41 through 50.

The main difference between the IMF plots of the FFT plot before and after the Hilbert transform was the disappearance of the negative frequencies after the application of the Hilbert transform, whereas before the application of the Hilbert transform, the full frequency spectrum displayed the radar return signal. Removal of the negative frequencies of the signal after application of the Hilbert transform is a property of the FFT of the Hilbert transform and discussed in Section 3.3.3. In addition to the difference along the frequency axis, the magnitude of the radar return varied between the graphs generated before and after the application of the Hilbert transform.

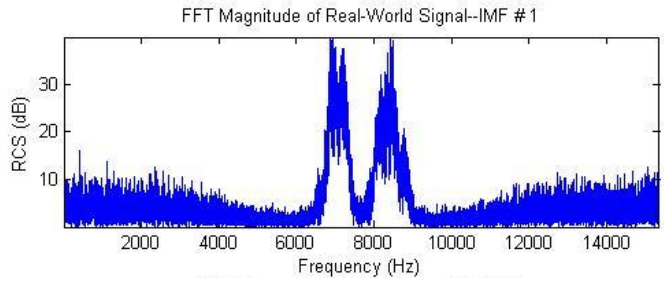

Figure 41: FFT of CEMD Magnitude of IMF #1

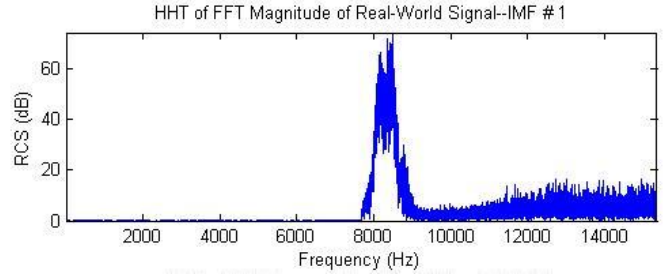

Figure 42: FFT of HHT Magnitude of IMF #1

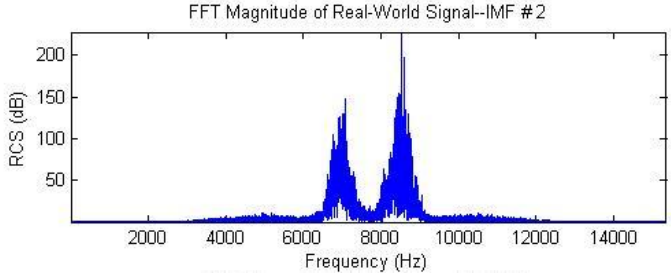

Figure 43: FFT of CEMD Magnitude of IMF #2

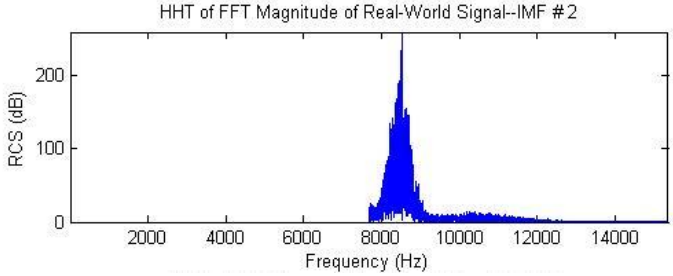

Figure 44: FFT of HHT Magnitude of IMF #2

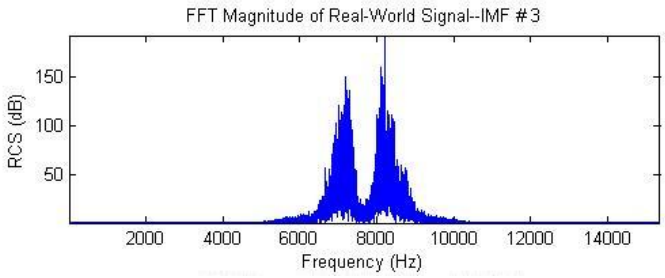

Figure 45: FFT of CEMD Magnitude of IMF #3

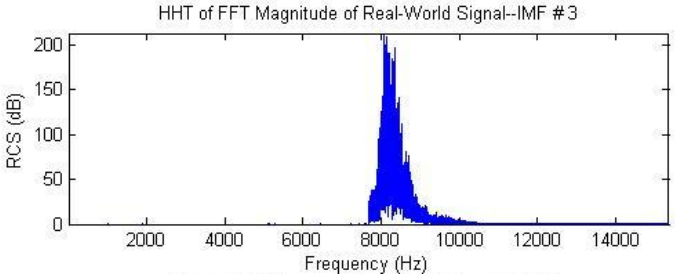

Figure 46: FFT of HHT Magnitude of IMF #3

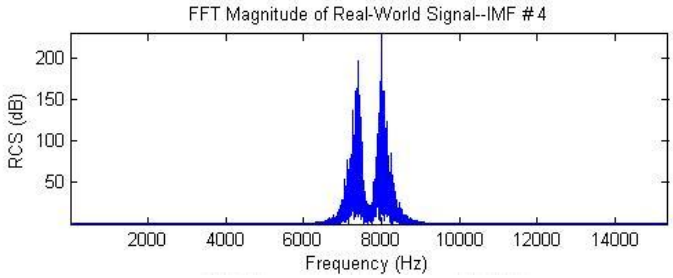

Figure 47: FFT of CEMD Magnitude of IMF #4

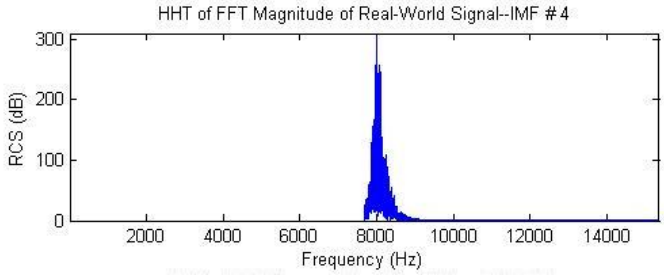

Figure 48: FFT of HHT Magnitude of IMF #4

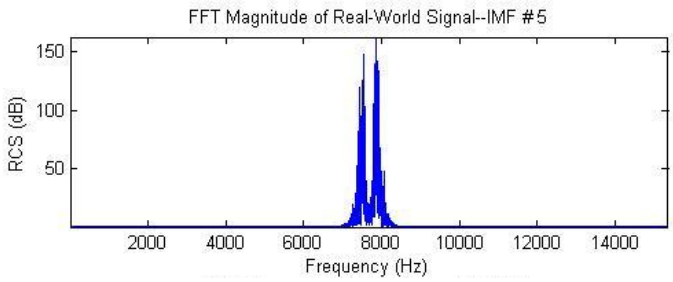

Figure 49: FFT of CEMD Magnitude of IMF #5

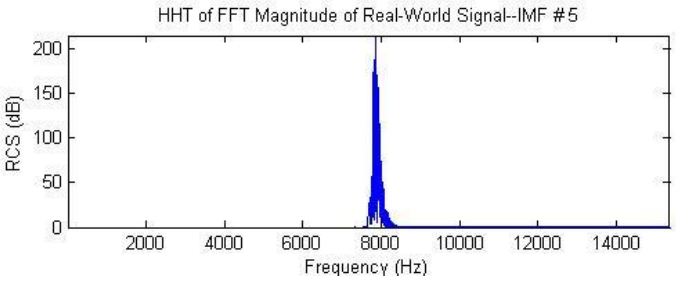

Figure 50: FFT of HHT Magnitude of IMF #5

Prior to the Hilbert transform application, IMF plots were consistent with a high-end limit of the complex RCS return value between 40 dB and approximately 250 dB from IMF #1 to IMF #11. Also, the magnitude plots after the Hilbert transform plots ranged with a high-end limit from 75 dB to 310 dB, with IMFs #6 through #11 are detailed in Figures 51 through 62. The difference in magnitude was indicative of the conclusion that the HHT was not a useful analysis tool in comparison with the FFT for the real-world data set provided for this project. A deeper understanding of exactly what the Hilbert transform application yields from a similar complex RCS data set is necessary for determining the usability of the HHT as a tool for complex RCS data used in the intelligence community, when analyzed in the frequency domain.

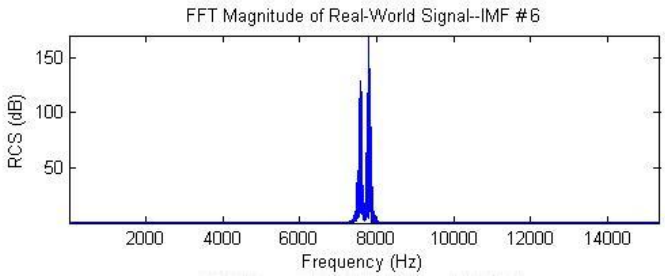

Figure 51: FFT of CEMD Magnitude of IMF #6

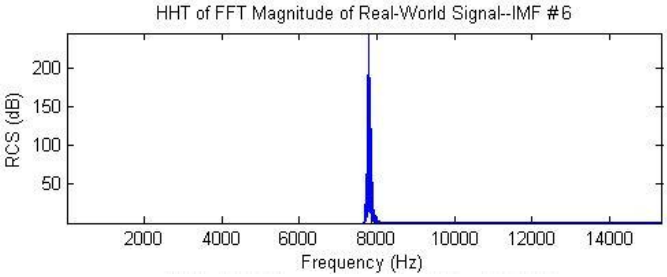

Figure 52: FFT of HHT Magnitude of IMF #6

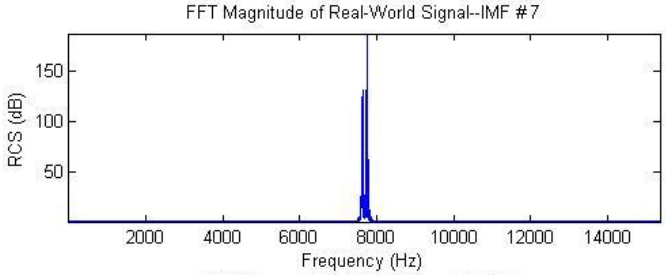

Figure 53: FFT of CEMD Magnitude of IMF #7

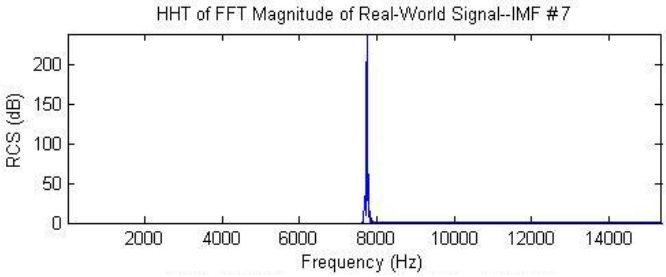

Figure 54: FFT of HHT Magnitude of IMF #7

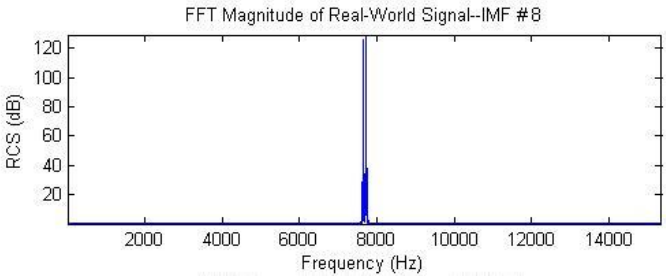

Figure 55: FFT of CEMD Magnitude of IMF #8

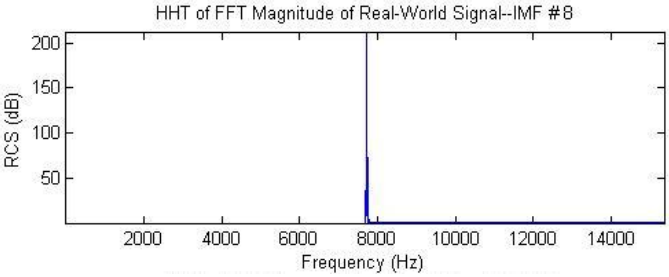

Figure 56: FFT of HHT Magnitude of IMF #8

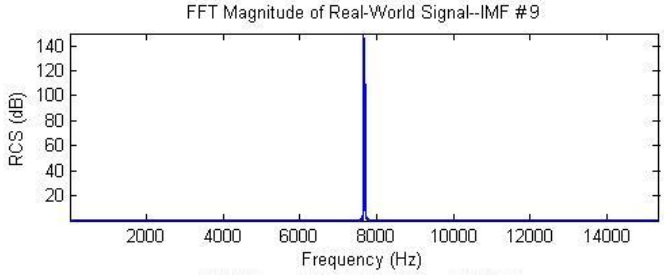

Figure 57: FFT of CEMD Magnitude of IMF #9

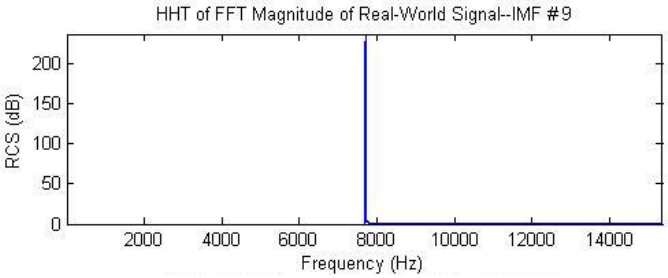

Figure 58: FFT of HHT Magnitude of IMF #9

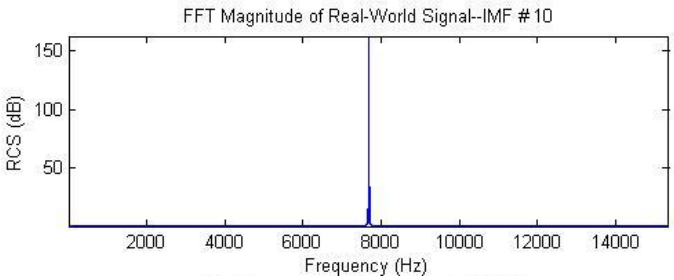

Figure 59: FFT of CEMD Magnitude of IMF #10

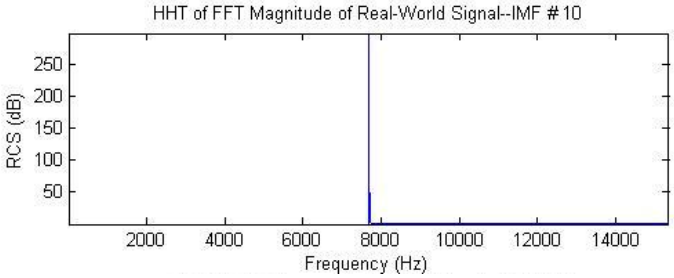

Figure 60: FFT of HHT Magnitude of IMF #10

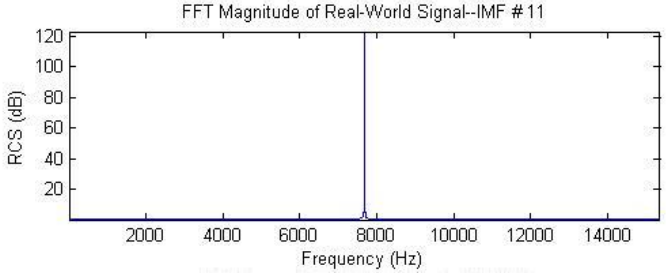

Figure 61: FFT of CEMD Magnitude of IMF #11

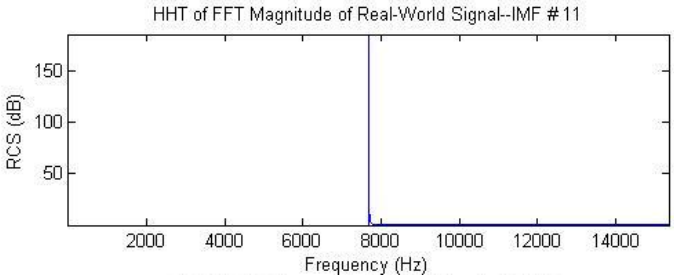

Figure 62: FFT of HHT Magnitude of IMF #11

The phase plots of the IMFs of the FFT plot of before and after the Hilbert transform application provided limited new or possibly significant data, although the

plots displayed a significant difference between the two mathematical transforms, with the IMFs represented in Figures 63 through 70.

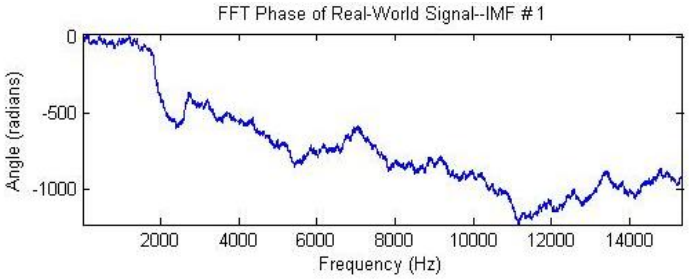

Figure 63: FFT of CEMD Phase of IMF #1

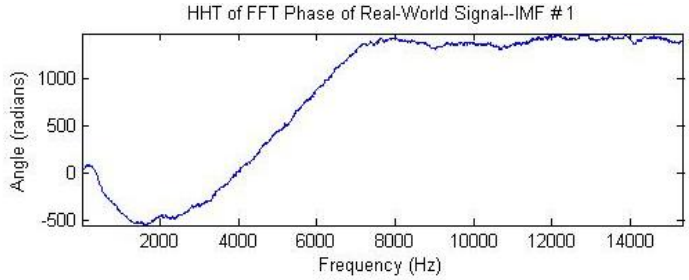

Figure 64: FFT of HHT Phase of IMF #1

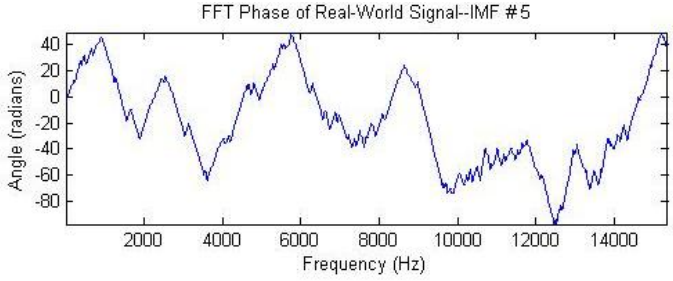

Figure 65: FFT of CEMD Phase of IMF #5

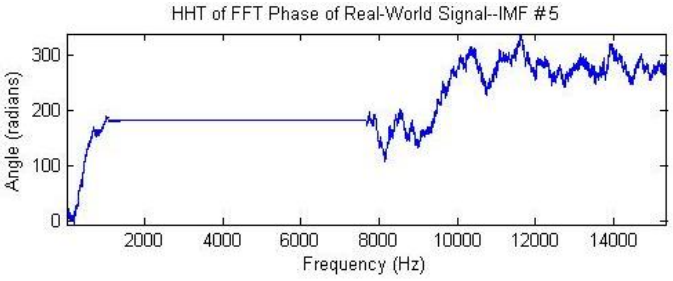

Figure 66: FFT of HHT Phase of IMF #5

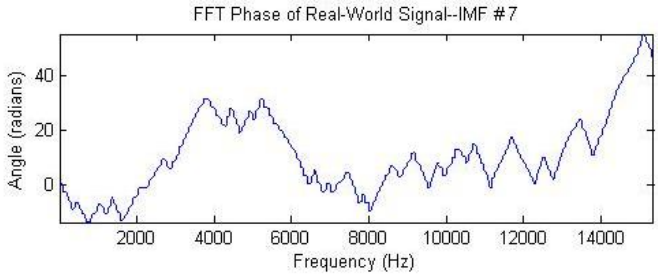

Figure 67: FFT of CEMD Phase of IMF #7

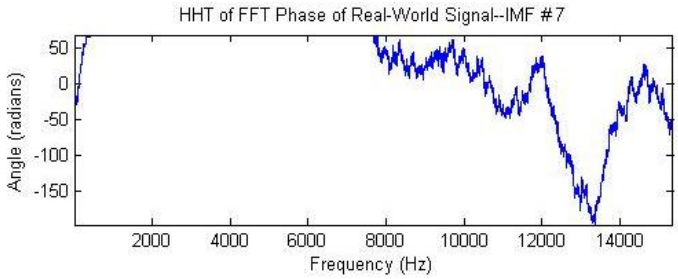

Figure 68: FFT of HHT Phase of IMF #7

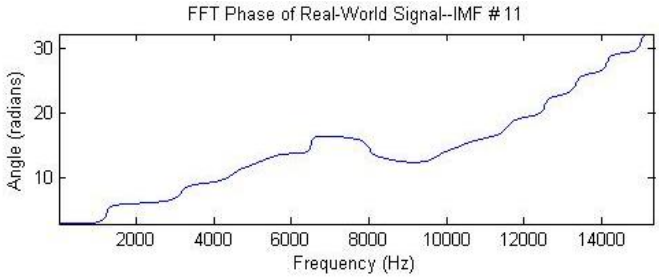

Figure 69: FFT of CEMD Phase of IMF #11

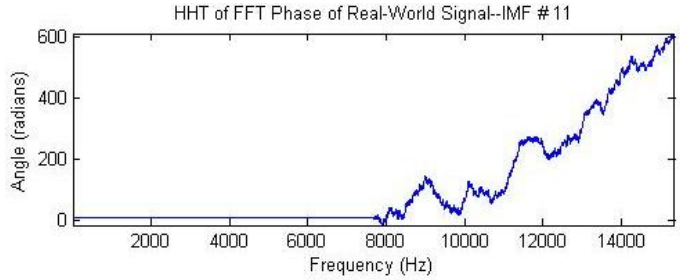

Figure 70: FFT of HHT Phase of IMF #11

A distinct difference between these phase plots both before and after the application of the Hilbert transform existed; however, the understanding needed to determine the significance or lack thereof of these plots is outside the scope of this

inquiry. Further understanding of the phase plots and the interpretation of these plots is necessary to determine new or significant information.

4.5. Analysis of Doppler-Time-Intensity Plots Prior to and After the Hilbert Transform

4.5.1. Doppler-Time-Intensity (DTI) Plots

For intelligence analysts, the DTI plot is of interest for understanding what occurred at each frequency and time interval, as well as displaying the amount of energy being transmitted at that moment. This plot is created using a windowed Fourier transform and is an accepted tool in the analyst community. More information concerning DTI plots are in Section 3.5.3.4.

4.5.2. Original Signal DTI Plot Comparison

Immediately, a major difference was noticed in the plots between the original DTI plots of before and after the Hilbert transform application, in Figures 71 and 72. Prior to the application of the Hilbert transform, the signal displayed a symmetric signal along the frequency axis, whereas the negative frequency values after the Hilbert transform application were no longer symmetric and did not allow for analysis capabilities in the known intelligence community. Representation of the HHT as a DTI plot yielded reason to believe the application of the Hilbert transform did not allow for the proper analysis needed for RCS data.

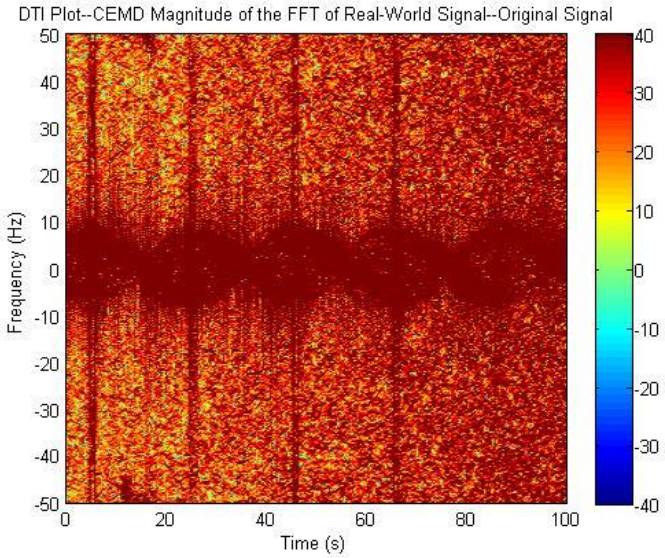

Figure 71: DTI Magnitude of Original Signal

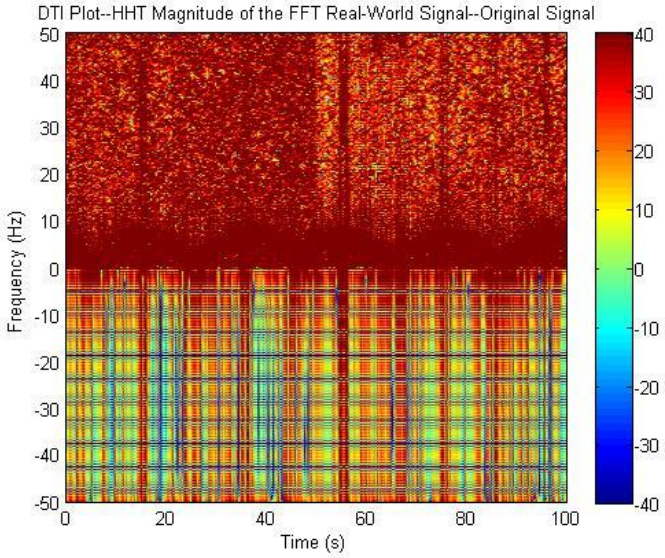

Figure 72: DTI HHT Magnitude of Original Signal

The time axis from 0 to 50 displayed a more intense return on the DTI plot after the Hilbert transform application, according to the color representation. When compared with the DTI plot of before the application of the Hilbert transform signal, the plot representation after the application of the Hilbert transform provided a possibly incorrect interpretation of the signal. Thus, the only useable portion of the DTI plot after the

Hilbert transform application of the pre-decomposed signal was the positive frequency between time 50 and time 100. Nevertheless, before the decomposition of the signal using the CEMD algorithm, the application of the Hilbert transform did not provide a DTI plot that yielded useful results.

4.5.3. IMF DTI Plot Comparisons

When comparing the two plots of IMF #1, represented in Figures 73 and 74, the same characteristics and differences present in the comparison of the original signal were also present in this specific IMF. Again, after the application of the Hilbert transform, the negative frequencies were non-existent and little useful information was displayed on the plot of IMF #1. The large returns, normally indicative of broadside flashes in RCS data, were shifted in the DTI plot after the Hilbert transform application and potentially resulted from the `fftshift()` or the `fft()` functions in MATLAB®. This shifting was not noticeable until IMF #1 and many techniques were employed to attempt to fix this shifting; however, the `fftshift()` and the `ifftshift()` functions were not helpful with shifting the time scale, where the problem appeared to occur. The time shifting occurred after the application of the Hilbert transform presented another reason why the Hilbert transform application to the real-world signal did not produce a more enhanced fidelity or a better analysis tool for RCS data.

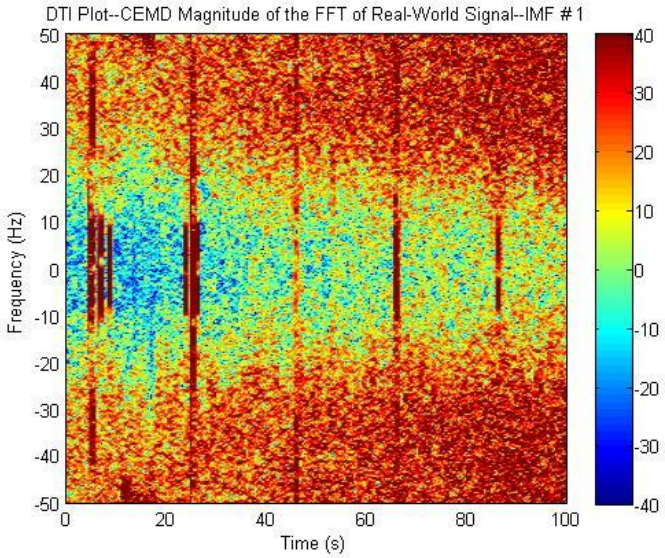

Figure 73: DTI Magnitude of IMF #1

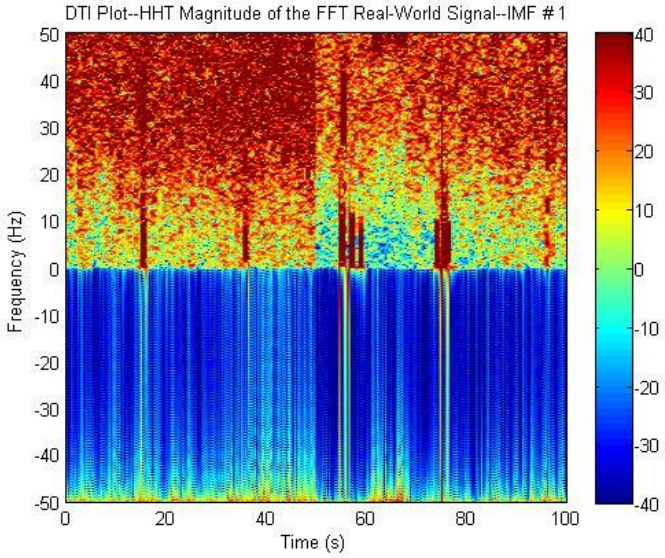

Figure 74: DTI HHT Magnitude of IMF #1

From the DTI plots for IMF #2, in Figures 75 and 76, both before and after the Hilbert transform application, the plots displayed differences detectable between the before and after the application of the Hilbert transform plots. The negative frequencies were unusable, even though the plot started looking more like a mirror image of the positive frequencies. The characteristic of growing intensity on the negative frequency

portion of the graph may represent the higher, more intense mode being sifted out of the decomposed signal on the plot. The time axis was still shifted after the application of the Hilbert transform. The shifting might be caused by a function inherent to the Hilbert transform, which displayed another reason that the application of the Hilbert transform may not provide new or enhanced information than the application of the FFT.

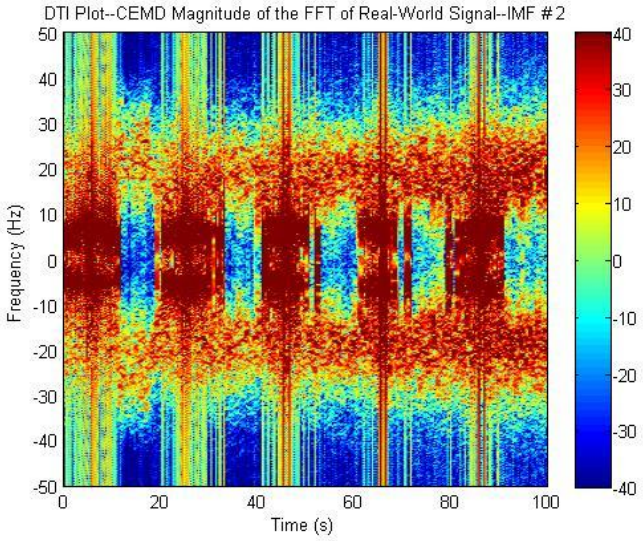

Figure 75: DTI Magnitude of IMF #2

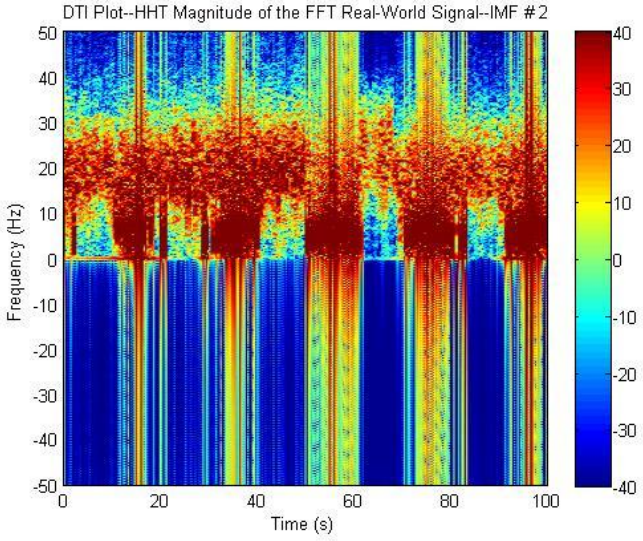

Figure 76: DTI HHT Magnitude of IMF #2

By comparing IMFs #5 through #8, the negative frequencies after the Hilbert transform application on the plots became less intense, represented by Figures 77 through 84; however, the higher and more intense RCS values were being sifted out using the CEMD algorithm, and provided positive frequencies mirrored as negative frequencies. When comparing the DTI plots before the Hilbert transform and the signal after the application of the Hilbert transform characteristics present prior to the application of the Hilbert transform were not represented. Therefore, if the Hilbert transform is applied to the data, data is lost, leading to the conclusion that the analysis would not represent the true signal. By analyzing these six IMFs, the Hilbert transform application appeared to ineffectively represent the data decomposed using the CEMD algorithm.

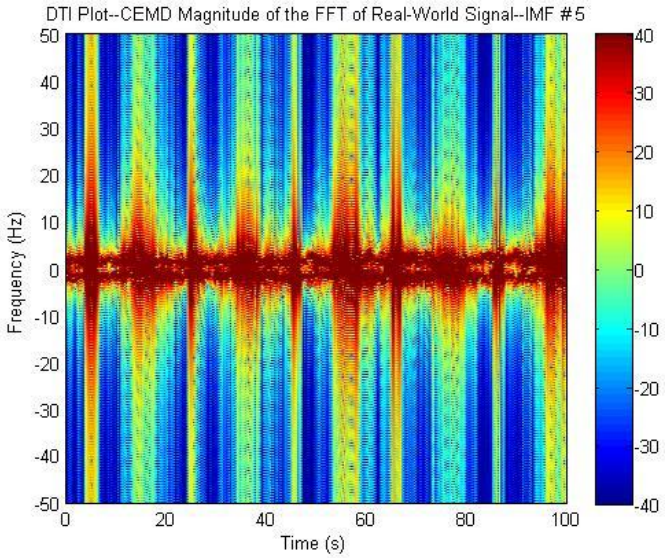

Figure 77: DTI Magnitude of IMF #5

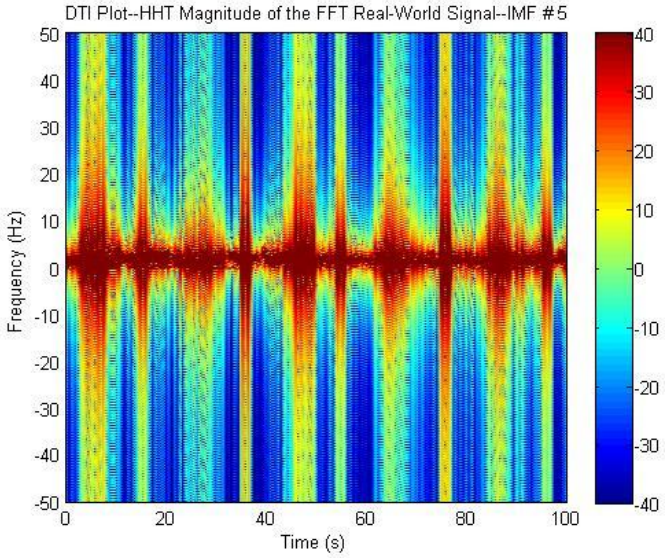

Figure 78: DTI HHT Magnitude of IMF #5

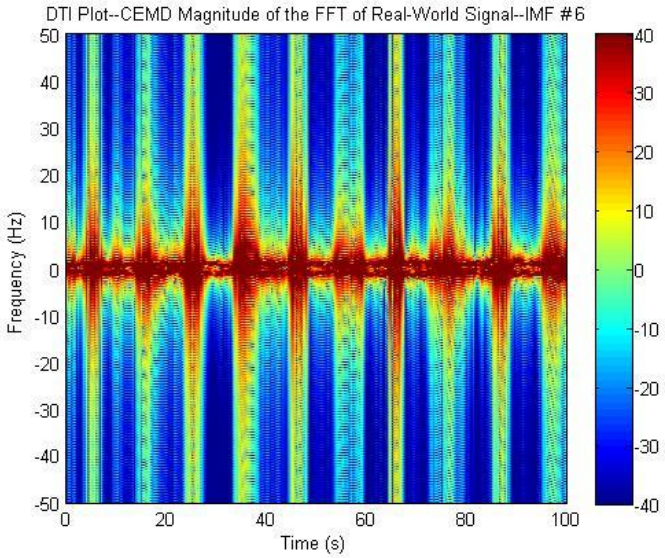

Figure 79: DTI Magnitude of IMF #6

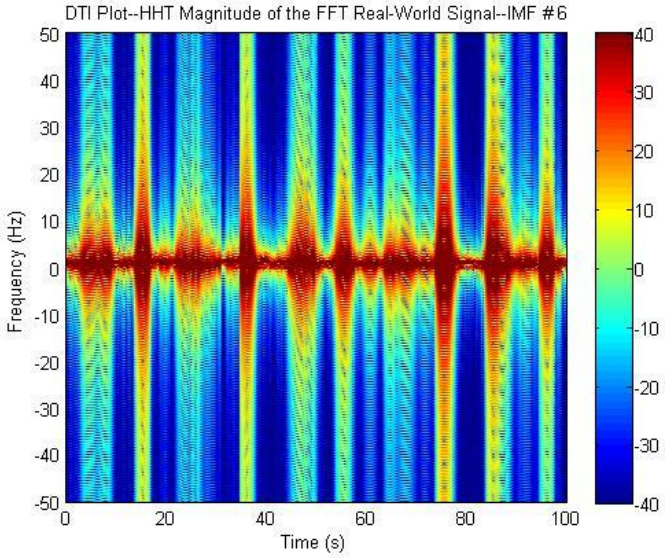

Figure 80: DTI HHT Magnitude of IMF #6

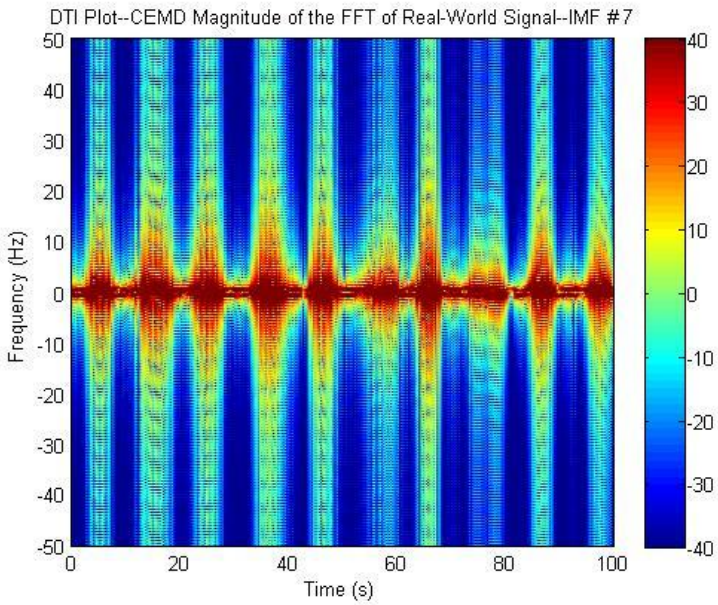

Figure 81: DTI Magnitude of IMF #7

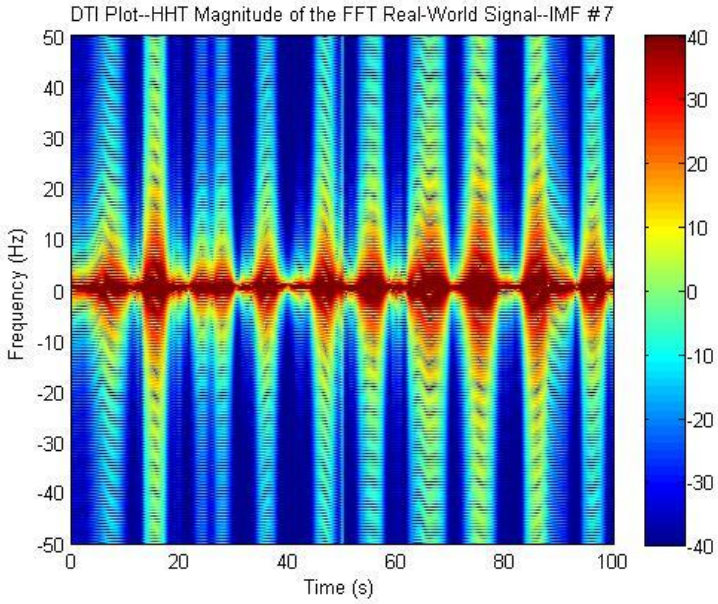

Figure 82: DTI HHT Magnitude of IMF #7

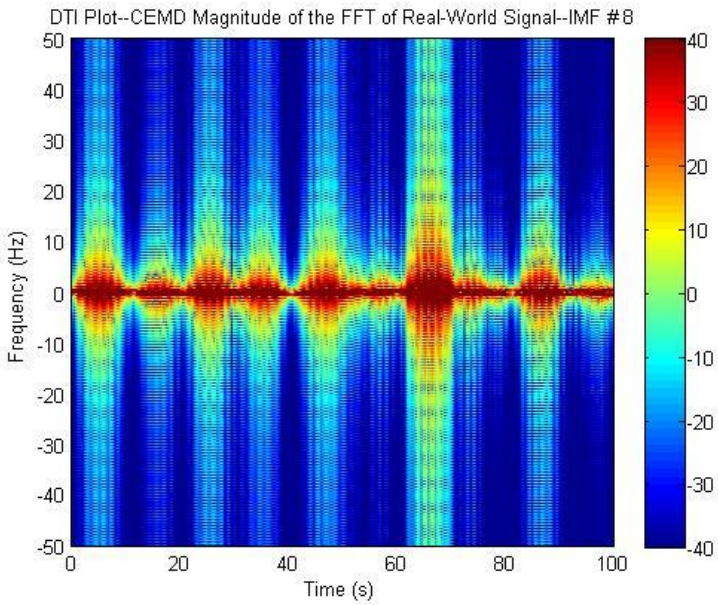

Figure 83: DTI Magnitude of IMF #8

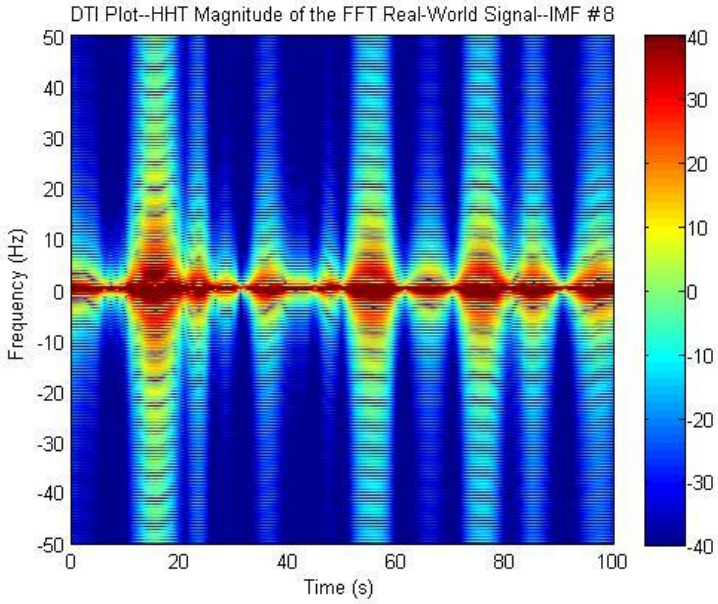

Figure 84: DTI HHT Magnitude of IMF #8

IMFs #9 through #11 display major differences in the DTI plots before and after the Hilbert transform application, shown in Figures 85 through 90.

First, the shift of the time axis was noticeable in IMF #9 due to the vertical line present at time equal to 50. Secondly, the signal displayed before the Hilbert transform was more focused and displayed all data points, whereas the graph after the application of the Hilbert transform was smoother and overlooked the individual spikes from the signal decomposition. Finally, it was concluded that the signal after the Hilbert transform application was not representative of the originally decomposed signal.

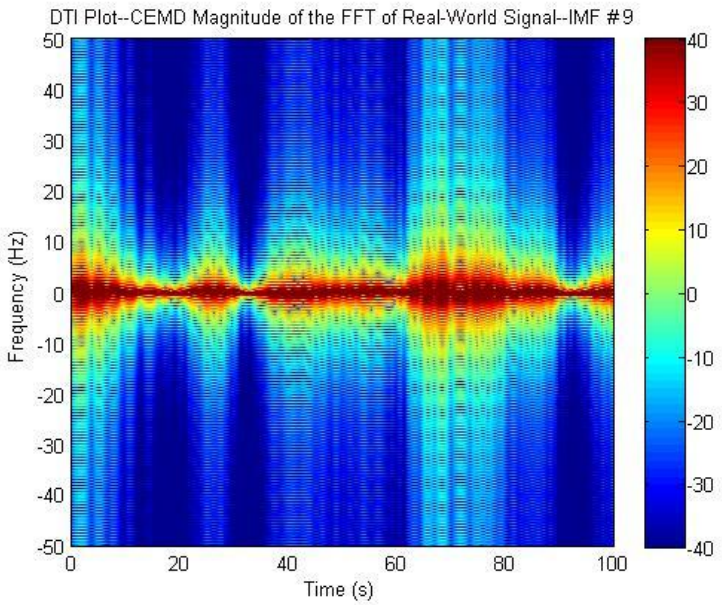

Figure 85: DTI Magnitude of IMF #9

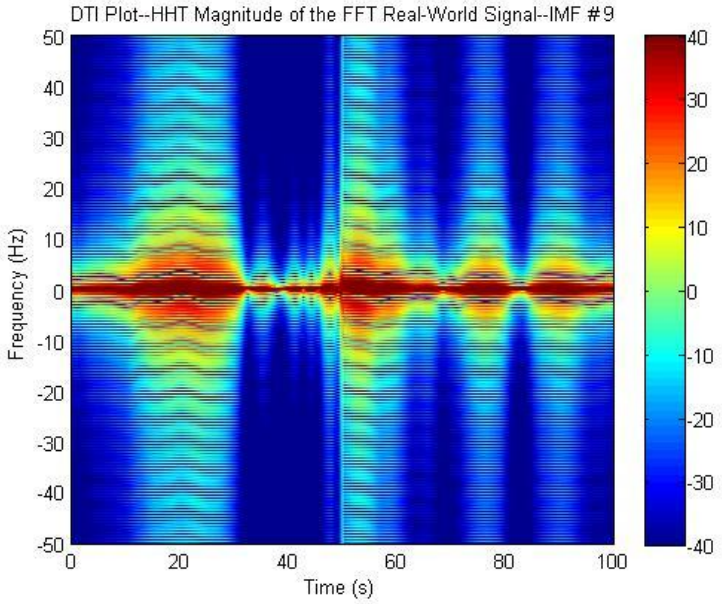

Figure 86: DTI HHT Magnitude of IMF #9

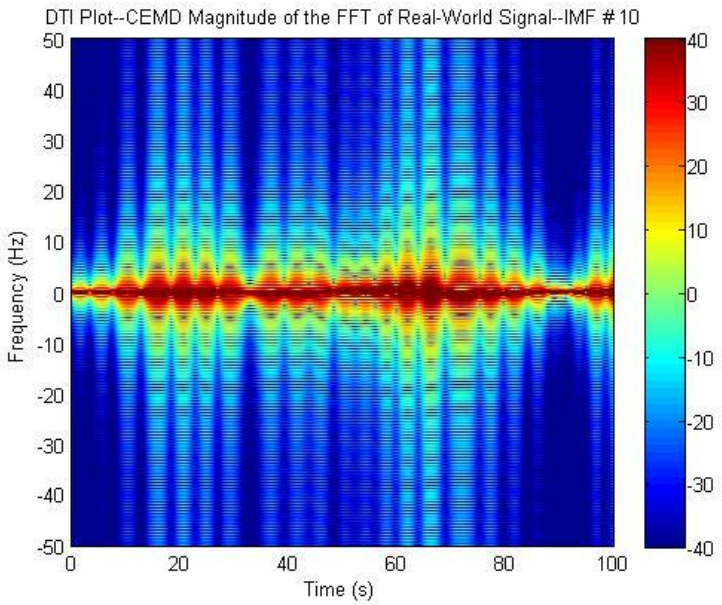

Figure 87: DTI Magnitude of IMF #10

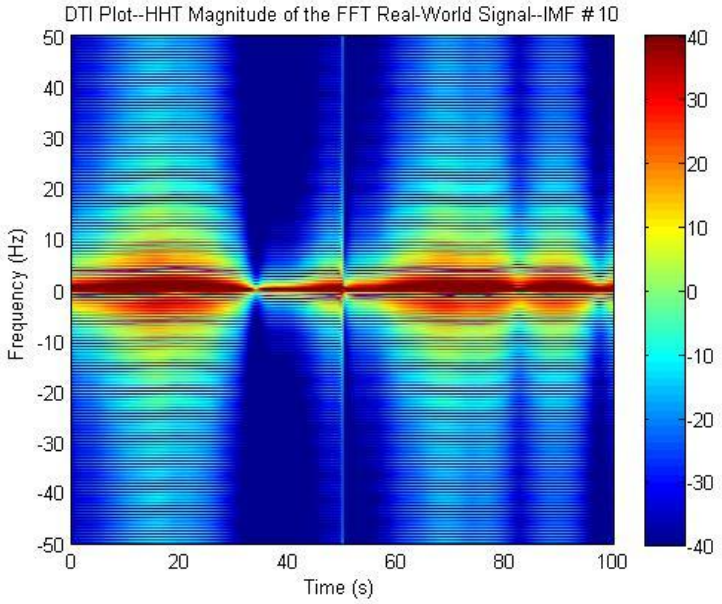

Figure 88: DTI HHT Magnitude of IMF #10

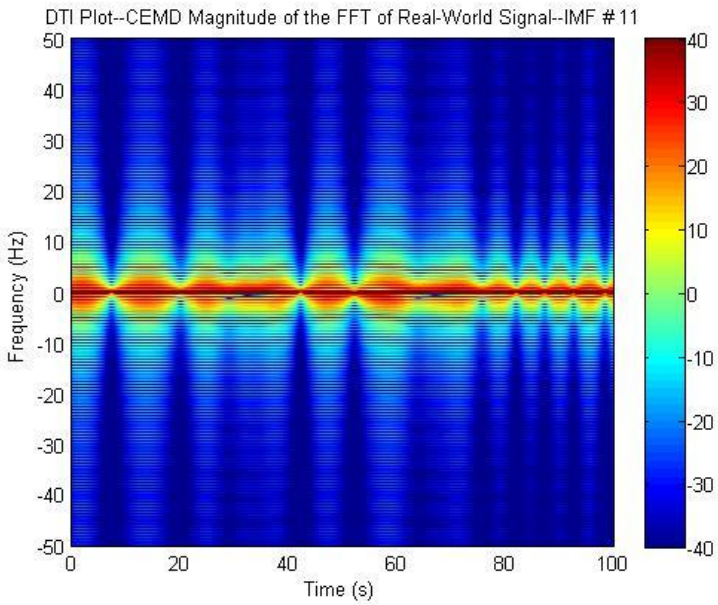

Figure 89: DTI Magnitude of IMF #11

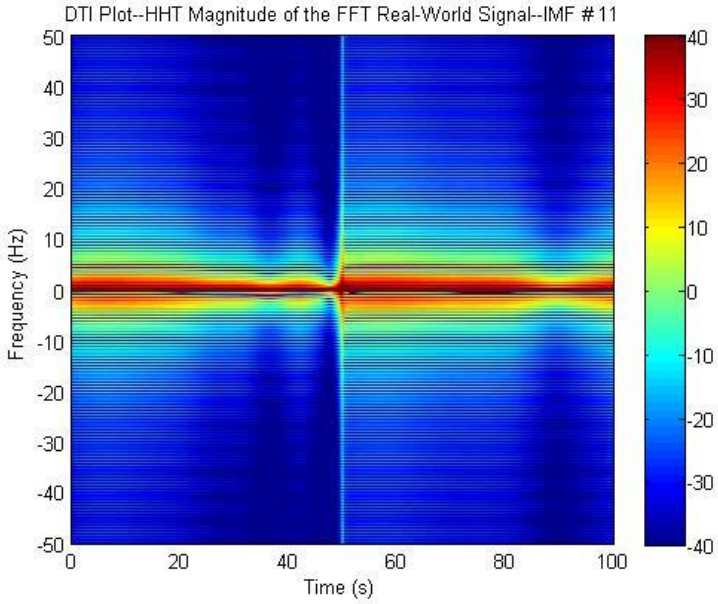

Figure 90: DTI HHT Magnitude of IMF #11

4.5.4. DTI Plot Comparison Conclusions

By comparing the DTI plots both before and after the application of the Hilbert transform to the original signal and decomposed data, it was concluded the application of

the HHT did not provide new or significant enhancements to the analysis of the data. After the detailed comparison of each IMF, the Hilbert transform application seemed to delete approximately half of the original frequency data, as well as incorrectly represented the signal along the time scale axis. It is hypothesized that the HHT might provide a more enhanced fidelity and new or useful information of the input RCS signal. However, this application of the Hilbert transform did not provide a more enhanced fidelity than the application of the FFT. Additionally, the Hilbert transform removed important data and did not display the correct amount of fidelity compared to the application of the FFT. It cannot be clearly determined whether the HHT was a useful signal analysis tool for RCS data. Furthermore, it could not be determined that, when compared with the application of the FFT, the Hilbert transform was a better representation of the data and was more a hindrance than helpful tool for the analysis of the DTI plots.

4.6. Chapter Summary

First, the magnitude of the decomposed signal was compared with various canonical RCS graphs to assess the CEMD algorithm in decomposing the real-world data set. Next, the magnitude of the decomposed signal was compared both before and after the application of the Hilbert transform. Similarly, the magnitude of the FFT of the decomposed signal was compared both before and after the application of the Hilbert transform. Finally, the generated magnitude DTI plots of the decomposed signal before and after the application of the Hilbert transform were compared. In addition, the phase plots for the decomposed signal and the FFT of the decompose signal were compared

with their respective graphs after the application of the Hilbert transform. For all four graphical comparisons, the similarities and differences were discussed, as well as possible implications for application of signal processing.

V. Conclusions and Future Work

The activities of this research and the results obtained were detailed as follows. The comparisons and conclusions drawn from the graphs generated were highlighted. Also, overall concluding thoughts related to the objectives of this evaluation were detailed and discussed to determine the implications of the results. The research conclusions were also the basis for future work concerning RCS data analysis and possible helpful future signal analysis tools, including the HHT.

5.1. Overall Summary

Chapter I detailed the objectives of this research used to assess the effectiveness of using the CEMD method to analyze RCS data, as well as compared the application of the Hilbert transform and the FFT on the decomposed data sets after the CEMD technique. To meet the research objectives, the CEMD algorithm code was found and modified. The code was also used to apply the FFT, Hilbert transform, and windowed FFT to produce graphical results for comparison. Comparative analysis of the four graphically generated results was performed. In addition, the generated plots were analyzed to determine the algorithm's ability to meet the objectives of this research effort.

5.2. Key Results

Results and conclusions from the work performed in this thesis are presented as follows.

1. *Results for the ability of the CEMD algorithm to decompose the RCS real-world data set.*

Overall, the comparison discussed in this section displayed the functionality of the CEMD method for the decomposition of a real-world data set. The CEMD method is a possible tool for decomposition of RCS signals, when compared in the time domain.

2. *Results from the comparison of the CEMD algorithm before and after the application of the Hilbert transform.*

From the original signal, few differences were noticed between the pre and post Hilbert transform application magnitude plots. No new information could be determined by comparison of the plots represented by IMF #1.

After comparing the two IMF #2 plots, a slight difference in the intensity of each return value was noticed with respect to time. On the graph of the IMF #2 of the signal before the application of the Hilbert transform, there was approximately double the intensity in time as compared to the plot after the application of the Hilbert transform. There was a slight magnitude difference, with the primary and most noticeable difference exhibited by the intensity at each time value before the application of the Hilbert transform.

Beginning with IMF #5, the curve after the application of the Hilbert transform showed a more fluid representation than previous IMFs, as well as displayed a more specific value representation of the real-world signal. After comparing the plots of IMF #6, this plot showed that, after the application of the Hilbert transform, the plot was more fluid than before the application of the Hilbert transform. The same characteristics were present in both plots and, through application of the Hilbert transform, the plot of IMF #6

was more focused and displayed a cleaner representation of the real-world signal than previous IMF plots.

The signal decomposition displayed in IMFs #7 through #11 showed the sinusoidal nature of the CEMD method; nevertheless, the sinusoid was more distinguishable after application of the Hilbert transform. Prior to the application of the Hilbert transform, the decomposition of the signal demonstrated noisier and contained possible extraneous signal values of the decomposed signal interpretation.

3. *Results from the comparison of the FFT plots of the CEMD algorithm before and after the application of the Hilbert transform.*

The main difference between the FFT plot before and after the Hilbert transform was noted by the disappearance of the negative frequencies after the application of the Hilbert transform. Yet, before the application of the Hilbert transform, the full frequency spectrum displayed the radar return signal. It was found that the characteristics of the graphical results occurred due to an inherent property of the Hilbert transform.

Another difference occurred with the magnitude and was indicative of the HHT not being a useful analysis tool in comparison with the FFT for the real-world data set provided for analysis. A deeper understanding of exactly what the Hilbert transform application yields from an RCS data set is necessary to determine the usability of the HHT in continued RCS data or to determine whether the use of the HHT is or is not a valid tool for the type of data used in the intelligence community.

4. *Results from the comparison of the DTI plots of the CEMD algorithm before and after the application of the Hilbert transform.*

Through the comparison of the DTI plots both before and after the application of the Hilbert transform to the original signal and decomposed data, it was concluded the application of the Hilbert transform did not provide new or significant analysis of the data. After the detailed comparison of each IMF, the Hilbert transform application seemed to delete approximately half of the original frequency data, as well as incorrectly represented the signal along the time axis.

5.3. Concluding Thoughts

Various generated graphical results were analyzed and evaluated throughout the course of this research effort. The two principle objectives were investigated. These two objectives were: (1) to assess the effectiveness of the CEMD method and HHT as signal analysis tools for complex RCS data and (2) to determine whether the HHT provided an enhanced fidelity and improved analysis of complex RCS data than through use of the FFT as the analysis tool. Through the four comparative analyses, these objectives were met. The four comparisons performed were: (1) the comparison of the decomposed data using the CEMD with various canonical shapes, (2) the comparison of the decomposed data using the CEMD with the decomposed data after the application of the Hilbert transform, (3) the comparison of the FFT of the decomposed data using the CEMD both before and after the Hilbert transform was applied, and (4) the comparison of the DTI plots of the decomposed data using the CEMD both before and after the application of the Hilbert transform.

The first graphical comparison displayed that the CEMD method inherent to the HHT effectively decomposed the RCS data and exhibited the IMFs of the real-world signal in a correct manner. The second, third, and fourth comparisons were used to determine whether the hypothesis that the HHT might provide an enhanced fidelity and new or useful information of the input RCS signal was proven. From the comparative analyses, the application of the Hilbert transform did not provide an enhanced fidelity than the application of the FFT. The Hilbert transform even appeared to remove important data and incorrectly displayed the desired amount of fidelity the application of the FFT provided. Nevertheless, it could not be determined whether the complete HHT was a useful signal analysis tool for RCS data; it was concluded that the CEMD method inherent to the HHT provided a useful analysis tool for RCS data. Finally, compared with the application of the FFT, the Hilbert transform inadequately represented the data and was more of a hindrance to the analysis of the various plots generated of the real-world data set.

5.4. Future Work

A list of possible areas for future research concerning the usability of the CEMD and EMD algorithms, as well as the HHT and other mathematical transforms as possible analysis tools, are described as follows.

- Investigation of blind studies of the CEMD algorithm should be performed. It is essential to establish the validity of the CEMD for determining objects and the shape of those objects without prior knowledge.

- Investigations of comparing various rocket bodies should be conducted to distinguish between similar shapes through decomposing and analyzing the IMFs. It is important to know the minute details for expedited analysis of the rocket bodies.
- Implementation of real-valued RCS data as opposed to complex-valued data should be used to determine if similar results occur as with the CEMD algorithm.
- Investigation of the using time-frequency transforms as possible new signal analysis tools on decomposed signals should be examined compared to current results of use of the HHT and FFT.

Appendix A

Appendix A displays Dr. Flandrin's original BEMD algorithm code, as applied to an example complex data set.

```
%bivariate_EMD_illustration.m
%illustration of the bivariate EMD extension on a real-world
oceanographic signal
%reproduces Fig. 3 in "Bivariate Empirical Mode Decomposition", G.
Rilling,
%P. Flandrin, P. Goncalves and J. M. Lilly, IEEE Signal Processing
Letters
%
%G. Rilling 3/2007 email:  gabriel.rilling@ens-lyon.fr

load('float_position_record.mat','x');

[imf,nb] = cemdc2_fix([],x,10,[],32);

x = hilbert(x)

n = size(imf,1);

figtitle1 = 'Float position record';
figure('name',figtitle1)
plot(x);
xlabel('Displacement East (km) --- Real part')
ylabel('Displacement North (km) --- Imaginary part')
title(figtitle1)
axis equal;
set(gca,'Ylim',[-250,300])

figtitle2 = 'Bivariate Empirical Mode Decomposition of Float signal';
figure('name',figtitle2)
subplot(n+1,1,1)
plot(real(x))
hold on
plot(imag(x),'k--')
axis tight
ylabel('signal')
title(figtitle2)
set(gca,'XTickLabel',{})
minmin = @(x)min(x(:));
maxmax = @(x)max(x(:));
m = minmin([real(imf(1:end-1,:));imag(imf(1:end-1,:))]);
M = maxmax([real(imf(1:end-1,:));imag(imf(1:end-1,:))]);
for k = 1:n
  subplot(n+1,1,k+1)
```

```
  plot(real(imf(k,:)))
  hold on
  plot(imag(imf(k,:)),'k--')
  axis([1,length(x),m,M])
  ylabel(['d_',int2str(k)])
  if k<n
    set(gca,'XTickLabel',{})
  end
end
ylabel('res.')
xlabel('Time (days)')
axis tight
```

Figure 91: BEMD Algorithm by Dr. Flandrin

Appendix B

Appendix B shows the detailed code used for producing the graphical results.

```
%% Section B.1
%% Load all the data and remake it to work for the algorithm

load('data.mat');
dataR = nb_data.nb_rcs_r';
dataI = nb_data.nb_rcs_i';
prf=round(nb_data.nb_avg_prf);
Ts = round(nb_data.nb_avg_prf);
data = (dataR+i*dataI).';
lengthData=length(data);
```

Figure 92: Section B.1 Modified BEMD Algorithm

```
%% Section B.2
%% Apply the CEMD to the inputted signal

[imf,nb] = cemdc2([],data,[],[]);
n = size(imf,1);
```

Figure 93: Section B.2 Modified BEMD Algorithm

```
%% Section B.3
%% Plots the Complex Empirical Mode Decomposition of the signal

figure ();
subplot(2,1,1)
plot(abs(data))
title('CEMD Magnitude of Real-World Signal--Original Signal');
xlabel('Time')
ylabel('RCS (dBsm)')
axis tight;
subplot(2,1,2)
plot(unwrap(angle(data)))
title('CEMD Phase of Real-World Signal--Original Signal');
xlabel('Time')
ylabel('Angle (radians)')
axis tight;

for k = 1:n-1
  figure();
  subplot(2,1,1)
  plot(abs(imf(k,:)))
  title(['CEMD Magnitude of Real-World Signal--IMF # ',int2str(k)]);
  xlabel('Time')
  ylabel('RCS (dBsm)')
  axis tight;
  subplot(2,1,2)
```

```
  plot(unwrap(angle(imf(k,:))))
  title(['CEMD Phase of Real-World Signal--IMF # ',int2str(k)]);
  xlabel('Time')
  ylabel('Angle (radians)')
  axis tight;
end

for k=n:n
figure();
subplot(2,1,1)
plot(abs(imf(k,:)))
title('CEMD Magnitude of Real-World Signal--Residue');
xlabel('Time')
ylabel('RCS (dBsm)')
axis tight;
subplot(2,1,2)
plot(unwrap(angle(imf(k,:))))
title('CEMD Phase of Real-World Signal--Residue');
xlabel('Time')
ylabel('Angle (radians)')
axis tight;
end
```

Figure 94: Section B.3 Modified BEMD Algorithm

```
%% Section B.4
%% Take the HT of the Decomposed data and plot the HT of the CEMD of
the
%% data

figure ();
hilbertOriginal=hilbert(data);
hilbertMagOriginal=abs(hilbert(real(data)));
hilbertPhaseOriginal=unwrap(angle(hilbert(imag(data))));
subplot(2,1,1)
plot(hilbertMagOriginal)
title('Hilbert-Huang Transform Magnitude of Real-World Signal--Original
Signal');
xlabel('Time')
ylabel('RCS (dBsm)')
axis tight;
subplot(2,1,2)
plot(hilbertPhaseOriginal)
title('Hilbert-Huang Transform Phase of Real-World Signal--Original
Signal');
xlabel('Time')
ylabel('Angle (radians)')
axis tight;

for k = 1:n-1
   hilbertMag(k,:)=abs(hilbert(real(imf(k,:))));
   hilbertPhase(k,:)=unwrap(angle(hilbert(imag(imf(k,:)))));
```

```
      figure ()
   subplot(2,1,1)
   plot(hilbertMag(k,:))
   title(['Hilbert-Huang Transform Magnitude of Real-World Signal--IMF
# ', int2str(k)])
   ylabel('RCS (dBsm)')
   xlabel('Time')axis tight;
   subplot(2,1,2)
   plot(hilbertPhase(k,:))
   title(['Hilbert-Huang Transform Phase of Real-World Signal--IMF # ',
int2str(k)])
   ylabel('Angle (radians)')
   xlabel('Time')
   axis tight;
end

for k = n:n
   hilbertMag(k,:)=abs(hilbert(real(imf(k,:))));
   hilbertPhase(k,:)=unwrap(angle(hilbert(imag(imf(k,:)))));
   figure ()
   subplot(2,1,1)
   plot(hilbertMag(k,:))
   title('Hilbert-Huang Transform Magnitude of Real-World Signal--
Residue')
   ylabel('RCS (dBsm)')
   xlabel('Time')
   axis tight;
   subplot(2,1,2)
   plot(hilbertPhase(k,:))
   title('Hilbert-Huang Transform Phase of Real-World Signal--Residue')
   ylabel('Angle (radians)')
   xlabel('Time')
   axis tight;
end
```

Figure 95: Section B.4 Modified BEMD Algorithm

```
%% Section B.5
%% Take the FFT of the decomposed signal before HT and plot the graphs

figure ();
fftOriginal=(1/n).*fft(data);
fftMagOriginal=abs(fftOriginal);
fftPhaseOriginal=unwrap(angle(fftOriginal));
subplot(2,1,1)
plot(fftshift(fftMagOriginal))
title('FFT Magnitude of Real-World Signal--Original Signal');
xlabel('Frequency')
ylabel('RCS (dBsm)')
axis tight;
subplot(2,1,2)
plot(fftPhaseOriginal)
title('FFT Phase of Real-World Signal--Original Signal');
```

```
xlabel('Frequency')
ylabel('Angle (radians)')
axis tight;

for k = 1:n-1
  figure();
  fftCEMD(k,:)=(1/n).*fft(imf(k,:));
  fftMagCEMD(k,:)=abs(fftCEMD(k,:));
  fftPhaseCEMD(k,:)=unwrap(angle(imf(k,:)));
  subplot(2,1,1)
  plot(fftshift(fftMagCEMD(k,:)))
  title(['FFT Magnitude of Real-World Signal--IMF # ',int2str(k)]);
  xlabel('Frequency')
  ylabel('RCS (dBsm)')
  axis tight;
  subplot(2,1,2)
  plot(fftPhaseCEMD(k,:))
  title(['FFT Phase of Real-World Signal--IMF # ',int2str(k)]);
  xlabel('Frequency')
  ylabel('Angle (radians)')
  axis tight;
end

for k=n:n
  figure();
  fftCEMD(k,:)=(1/n)*fft(imf(k,:));
  fftMagCEMD(k,:)=abs(fftCEMD(k,:));
  fftPhaseCEMD(k,:)=unwrap(angle(imf(k,:)));
  subplot(2,1,1)
  plot(fftshift(fftMagCEMD(k,:)))
  title('FFT Magnitude of Real-World Signal--Residue');
  xlabel('Frequency')
  ylabel('RCS (dBsm)')
  axis tight;
  subplot(2,1,2)
  plot(fftPhaseCEMD(k,:))
  title('FFT Phase of Real-World Signal--Residue');
  xlabel('Frequency')
  ylabel('Angle (radians)')
  axis tight;
end
```

Figure 96: Section B.5 Modified BEMD Algorithm

```
%% Section B.6
%% Take the FFT of the decomposed signal after HT and plot the graphs

figure ();
fftOriginalHilbert=fft(hilbert(data));
fftMagOriginalHilbert=abs((1/n).*fft(hilbert(real(data))));
fftPhaseOriginalHilbert=unwrap(angle((hilbert(imag(data)))));
subplot(2,1,1)
```

```
plot((fftshift(fftMagOriginalHilbert)))
title('HHT of FFT Magnitude of Real-World Signal--Original Signal');
xlabel('Frequency')
ylabel('RCS (dBsm)')
axis tight;
subplot(2,1,2)
plot(fftPhaseOriginalHilbert)
title('HHT of FFT Phase of Real-World Signal--Original Signal');
xlabel('Frequency')
ylabel('Angle (radians)')
axis tight;

for k = 1:n-1
  figure();
  fftMagHilbert(k,:)=abs((1/n).*fft(hilbert(real(imf(k,:))))));
  fftPhaseHilbert(k,:)=unwrap(angle(fft(hilbert(imag(imf(k,:))))));
  subplot(2,1,1)
  plot(fftshift(fftMagHilbert(k,:)))
  title(['HHT of FFT Magnitude of Real-World Signal--IMF #
',int2str(k)]);
  xlabel('Frequency')
  ylabel('RCS (dBsm)')
  axis tight;
  subplot(2,1,2)
  plot(fftPhaseHilbert(k,:))
  title(['HHT of FFT Phase of Real-World Signal--IMF # ',int2str(k)]);
  xlabel('Frequency')
  ylabel('Angle (radians)')
  axis tight;
end

for k=n:n
  figure();
  fftMagHilbert(k,:)=abs((1/n).*fft(hilbert(real(imf(k,:))))));
  fftPhaseHilbert(k,:)=unwrap(angle(fft(hilbert(imag(imf(k,:))))));
  subplot(2,1,1)
  plot(fftshift(fftMagHilbert(k,:)))
  title('HHT of FFT Magnitude of Real-World Signal--Residue');
  xlabel('Frequency')
  ylabel('RCS (dBsm)')
  axis tight;
  subplot(2,1,2)
  plot(fftPhaseHilbert(k,:))
  title('HHT of FFT Phase of Real-World Signal--Residue');
  xlabel('Frequency')
  ylabel('Angle (radians)')
  axis tight;
end
```

Figure 97: Section B.6 Modified BEMD Algorithm

```
%% Section B.7
%% Take the windowed FFT of the decomposed signal before HT to generate
the
%% DTI plots

%Define resolution for the windowed FFT
step_res=50;
sec=96;

%Calculate and store the windowed FFT value of the original signal
counter=0;
for b=1:prf*(sec-1)/step_res+1

original(b,:)=fft([data(counter*step_res+1:counter*step_res+1+prf),...
        zeros(1,1024-prf)]);
  counter=counter+1;
end

%Graph the windowed FFT of the original signal
y=linspace(-50,50, 1025);
x=linspace(0, 100, prf*(sec-1)/step_res+1);
figure()
pcolor(x, y, fftshift(20*log(abs(original)'), 1));
shading interp
title('DTI Plot--CEMD Magnitude of the FFT of Real-World Signal--
Original Signal')
xlabel('Time')
ylabel('Frequency (GHz)')
axis tight;
caxis([-40 40]);
colorbar;

%Get the windowed FFT of each of the IMFs and plot the windowed FFT of
each
%IMF
 for a = 1:n-1
    sig=imf(a,:);
    counter=0;
    for b=1:prf*(sec-1)/step_res+1

    ff(b,:) = fft([sig(counter*step_res+1:counter*step_res+1+prf),...
        zeros(1,1024-prf)]);
    counter=counter+1;
    end
 figure()
 pcolor(x,y, fftshift(20*log(abs(ff)'),1));
 shading interp;
 title(['DTI Plot--CEMD Magnitude of the FFT of Real-World Signal--IMF
# '...
     , int2str(a)])
 xlabel('Time')
 ylabel('Frequency (GHz)')
 axis tight;
 caxis([-40 40]);
```

```
colorbar;
 end

 %Windowed FFT of the residue of the signal
 for a = n:n
    sig=imf(a,:);
    counter=0;
    for b=1:prf*(sec-1)/step_res+1

    ff(b,:) = fft([sig(counter*step_res+1:counter*step_res+1+prf),...
        zeros(1,1024-prf)]);
    counter=counter+1;
    end
 figure()
pcolor(x,y, fftshift(20*log(abs(ff)'),1));
 shading interp;
 title('DTI Plot--CEMD Magnitude of the FFT of Real-World Signal--
Residue ')
 xlabel('Time')
 ylabel('Frequency (GHz)')
 axis tight;
  caxis([-40 40]);
  colorbar;
 end
```

Figure 98: Section B.7 Modified BEMD Algorithm

```
%% Section B.8
 %% Take the windowed FFT of the decomposed signal after HT to generate
the DTI plots

%Define resolution for the fft
step_res=50;
sec=96;

%Calculate and store the windowed FFT value of the original signal
counter=0;
for b=1:prf*(sec-1)/step_res+1
    originalH(b,:)=fft([hilbert(data(counter*step_res+1:...
        counter*step_res+1+prf)),zeros(1,1024-prf)]);
    counter=counter+1;
end

%Graph the windowed FFT of the original signal
fftMagOriginalHilbert=fftshift(20*log(abs(originalH')));
y=linspace(-50,50, 1025);
x=linspace(0, 100, prf*(sec-1)/step_res+1);
figure()
pcolor(x,y,fftMagOriginalHilbert)
shading interp
title('DTI Plot--HHT Magnitude of the FFT Real-World Signal--Original
Signal')
xlabel('Time')
```

```
ylabel('Frequency (GHz)')
axis tight;
caxis([-40 40]);
colorbar;

%Get the windowed FFT of each of the IMFs after the HT has been applied
to the signal and plot the windowed FFT of each IMF
 for a = 1:n-1
    sigH=hilbert(imf(a,:));
    counter=0;
    for b=1:prf*(sec-1)/step_res+1

    ffH(b,:) = fft([sigH(counter*step_res+1:counter*step_res+1+prf),...
        zeros(1,1024-prf)]);
    counter=counter+1;
 end
 figure()
 fftDTIMagHilbert=fftshift(20*log(abs(ffH')));
 pcolor(x,y, fftDTIMagHilbert);
 shading interp;
 title(['DTI Plot--HHT Magnitude of the FFT Real-World Signal--IMF #
'...
     , int2str(a)])
 xlabel('Time')
 ylabel('Frequency (GHz)')
 axis tight;
 caxis([-40 40]);
 colorbar;
 end

%Windowed FFT of the residue of the signal
 for a = n:n
    sigH=hilbert(imf(a,:));
    counter=0;
    for b=1:prf*(sec-1)/step_res+1

    ffH(b,:) = fft([sigH(counter*step_res+1:counter*step_res+1+prf),...
        zeros(1,1024-prf)]);
    counter=counter+1;
    end
 figure()
 fftDTIMagHilbert=fftshift(20*log(abs(ffH')));
 pcolor(x,y, fftDTIMagHilbert);
 shading interp;
 title('DTI Plot--HHT Magnitude of the FFT Real-World Signal--Residue')
 xlabel('Time')
 ylabel('Frequency (GHz)')
 axis tight;
 caxis([-40 40]);
 colorbar;
 end
```

Figure 99: Section B.7 Modified BEMD Algorithm

Appendix C

Appendix C explains the inputs and outputs of `cemdc_fix()` and explains what task each part of the function performs.

```
%CEMDC_FIX  bivariate Empirical Mode Decomposition, first algorithm
%
%
%   Syntax
%
%
% [IMF,NB_ITERATIONS]=CEMDC_FIX(T,X,NB_ITERATIONS,MAX_IMFS,NDIRS);
%
%
%   Description
%
%
% computes bivariate EMD, first algorithm [1] with NB_ITERATONS sifting
% iterations for each IMF
%
%   mean of boolean array {(mean_amplitude)/(envelope_amplitude) >
THRESHOLD} < TOLERANCE
%
% inputs:
%       - T: sampling times. If T=[], the signal is assumed uniformly
sampled.
%       - X: analyzed signal
%       - NB_ITERATIONS: number of sifting iterations to be performed
to
%         extract each IMF. If NB_ITERATIONS is empty or unspecified,
10 iterations
%         are performed by default.
%         Note: The effective number of sifting iterations might be
less
%         than NB_ITERATIONS for the last modes if the sifting process
has
%         to be stopped because of a lack of extrema.
%       - MAX_IMFS: maximum number of IMFs to be extracted. If MAX_IMFS
is
%         zero, empty or unspecified, the default behavior is to
extract as
%         many IMFs as possible.
%       - NDIRS: number of directions used to compute the local mean.
%         If unspecified, the default value is 4.
%         rem: the actual number of directions (according to [1]) is
2*NDIRS
%
% outputs:
%       - IMF: intrinsic mode functions (IMFs) (last line = residual)
%       - NB_ITERATIONS: effective number of sifting iterations for
each mode
%
```

```
%
%   Examples:
%
%
% workspace %  T: 1xN time instants
%  X: 1xN signal data
%
%>>IMF = CEMDC_FIX(T,X);
%>>[IMF,NB_IT] = CEMDC_FIX([],X);
%>>IMF = CEMDC_FIX(T,X,20);
%>>[IMF,NB_IT] = CEMDC_FIX([],X,[],4);
%
%
%   References
%
%
% [1] G. Rilling, P. Flandrin, P. Gonçalves and J. M. Lilly.,
% "Bivariate Empirical Mode Decomposition",
% Signal Processing Letters (submitted)
%
%
% See also
%  (c)emd_visu (visualization),
%  emd (slow but has many options),
%  cemdc, cemdc2, cemdc2_fix (other fast implementations of bivariate
EMD)
%
%
% G. Rilling, last modification: 3.2007
% gabriel.rilling@ens-lyon.fr
%
% code based on a student project by T. Boustane and G. Quellec,
11.03.2004
% supervised by P. Chainais (ISIMA - LIMOS - Universite Blaise Pascal -
Clermont II
% email : pchainai@isima.fr).
```

Figure 100: CEMD_FIX function

Appendix D

The IMF #3 and #4 plots of DTI before and after the Hilbert transform application.

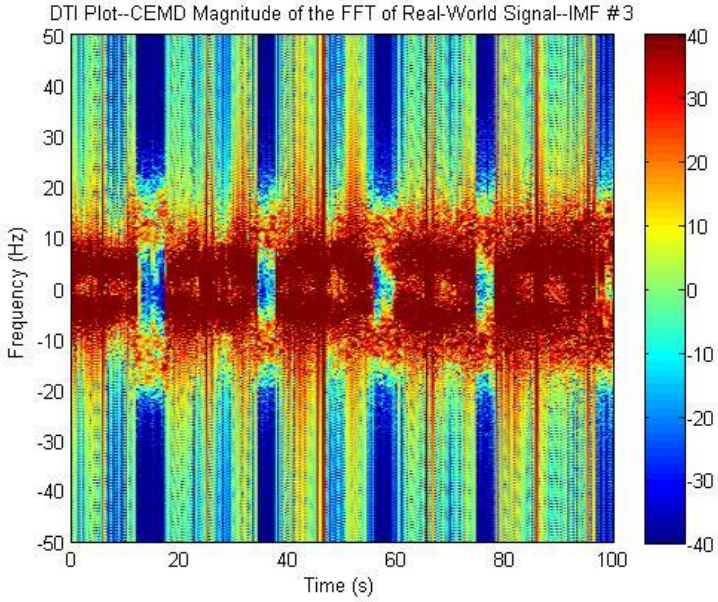

Figure 101: DTI Magnitude of IMF #3

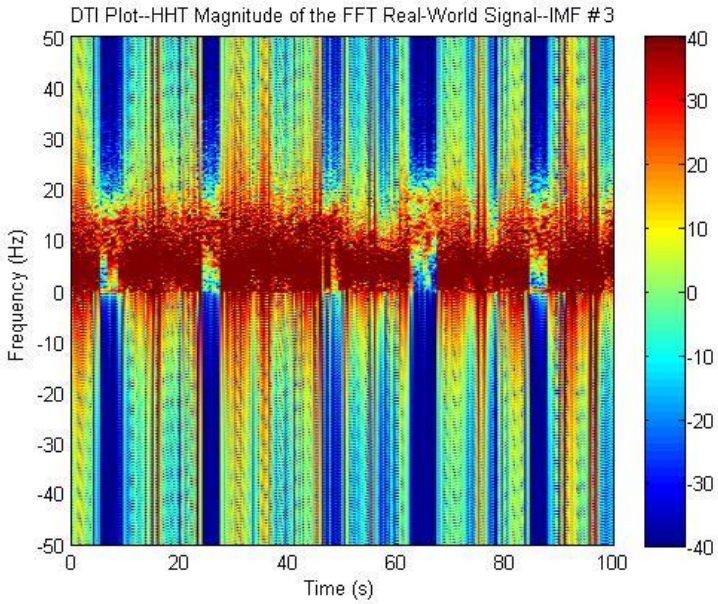

Figure 102: DTI HHT Magnitude of IMF #3

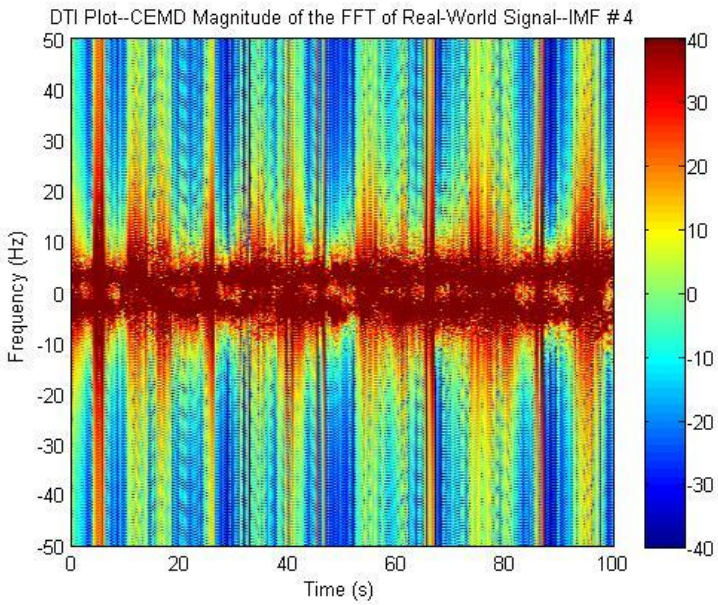

Figure 103: DTI Magnitude of IMF #4

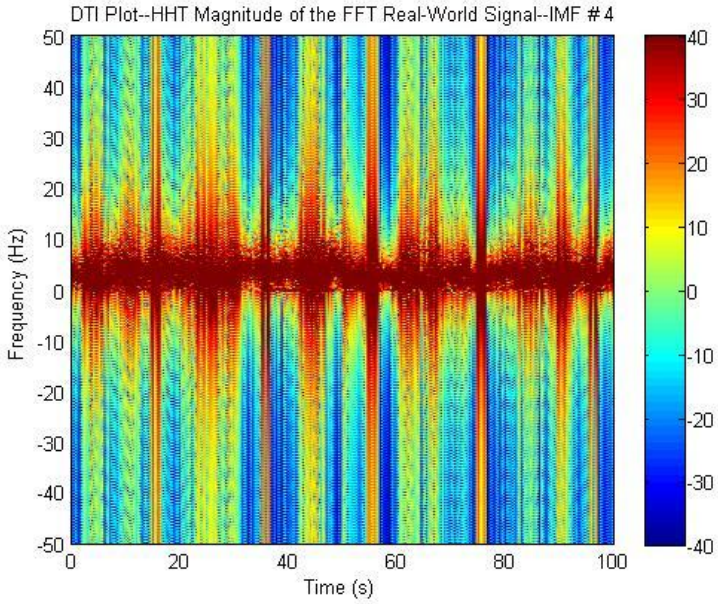

Figure 104: DTI HHT Magnitude of IMF #4

Bibliography

1. N. E. Huang, Z. Shen, S. R. Long, M. L. Wu, H. H. Shih, Q. Zheng, N. C. Yen, C. C. Tung, and H. H. Liu, "The Empirical Mode Decomposition and Hilbert spectrum for nonlinear and non-stationary time series analysis," *Proc. Roy. Soc. London A,* vol. 454, pp. 903-995, 1998.

2. D. P. Mandic, G. Souretis, W. Y. Leong, D. Looney, M. M. Van Hulle, and T. Tanaka, "Complex Empirical Mode Decomposition for Multichannel Information Fusion," in *Signal processing techniques for knowledge extraction and information fusion,* 1st ed. New York: Spring Science+Business Media, LLC, 2008, pp. 243-259.

3. R. Balocchi, D. Menicucci, E. Santarcangelo, L. Sebastiani, A. Gemignani, B. Ghelarducci, and M. Varanini, "Deriving the respiratory sinus arrhythmia from the heartbeat time series using Empirical Mode Decomposition," *Elsevier Science,* 5 February 2008

4. J. Huang and B. Milkereit, "Empirical Mode Decomposition Based Instantaneous Spectral Analysis and its Applications to Heterogeneous Petrophysical Model Construction," *Frontiers + Innovation—2009 CSPG CSEG CWLS Convention,* pp. 205-210, 2009.

5. G. Rilling, P. Flandrin, and P. Goncalves, "On Empirical Mode Decomposition and its Algorithms," 2003.

6. B. M. Battista, C. Knapp, T. McGee, and V. Goebel, "Application of the empirical mode decomposition and Hilbert-Huang transform to seismic reflection data," *Geophysics,* vol. 72, no. 2, pp. H29-H37, March-April 2007.

7. I. Magrin-Chagnolleau and R. G. Baraniuk, "Empirical mode decomposition based time-frequency attributes," 1998.

8. P. Flandrin, G. Rilling, and P. Goncalves, "Empirical Mode Decomposition as a Filter Bank," *IEEE Signal Processing Letters,* vol. 11, no. 2, pp. 112-114, February 2004.

9. T. Tanaka and D. P. Mandic, "Complex Empirical Mode Decomposition," *IEEE Signal Processing Letters,* vol. 14, no. 2, pp. 101-104, February 2007.

10. M. Umair Bin Altaf, T. Gautama, T. Tanaka, and D. P. Mandic, "Rotation Invariant Complex Empirical Mode Decomposition," *IEEE International Conference on Acoustics, Speech and Signal Processing,* pp. 1009-1012, April 2007.

11. G. Rilling, P. Flandrin, P. Gonclaves, and J. M. Lilly, "Bivariate Empirical Mode Decomposition," *IEEE Signal Processing Letters,* submitted, pp. 1-10, March 2007.

12. A. Y. Mutlu and S. Aviyente, "Multivariate Empirical Mode Decomposition for Quantifying Multivariate Phase Synchronization," *EURASIP Journal on Advances in Signal Processing,* vol. 2011, pp. 1-13, November 2010.

13. D. Kim and H. Oh, "EMD: A Package for Empirical Mode Decomposition and Hilbert Spectrum," *Contributed Research Articles*, pp. 40-46, 2008.

14. J. F. Ehlers and R. Way, "Empirical Mode Decomposition: A novel approach for cycle and trend mode detection," *MESA Software*, 2009.

15. G. Yunchao, S. Enfang, and S. Zhengyan, "Comparison of EMD and Complex EMD in Signal Processing," *2008 Congress on Image and Signal Processing*, pp. 141-145, 2008.

16. G. Yunchao, S. Enfang, L. Baifeng, and S. Zhengyan, "Application of Complex Empirical Mode Decomposition in Separation of Multiple Targets Using a Single Vector Sensor," *IEEE International Conference Neural Networks & Signal Processing*, pp. 294-298, June 2008.

17. D. Looney and D. P. Mandic, "Multiscale Image Fusion Using Complex Extensions of EMD," *IEEE Transactions on Signal Processing*, vol. 57, no. 4, pp. 1626-1630, April 2009.

18. P. J. Collins, Class report, EENG 627, ALPINE© Manual, Version 3.1.1, Department of Electrical & Computer Engineering, Air Force Institute of Technology (AU), Wright-Patterson AFB OH, Summer Quarter 2011.

19. E. W. Weisstein, (2011, November), "Cubic Spline: *MathWorld*—A Wolfram Web Resource," [Online], Available: http://mathworld.wolfram.com/CubicSpline.html.

20. M. Johansson, "The Hilbert transform," M.S. thesis, Växjö University, Sweden, 2006.

21. F.R. Kschischang, "The Hilbert Transform," Supplementary Notes for ECE 316, The Edward S. Rogers Sr. Department of Electrical and Computer Engineering, University of Toronto, Oct. 22, 2006.

22. MATLAB® version 7.8.0.347. Natick, Massachusetts: The MathWorks, Inc., 2009.

23. J. J. Condon and S. M. Ransom, "Fourier Transforms," Supplementary Notes for Essential Radio Astronomy, The National Radio Astronomy Observatory, University of Virginia, Sep. 13, 2010.

24. J. R. Graham, “FFT Tutorial,” Notes for ELE 436: Communication Systems, Department of Electrical and Computer Engineering, University of Rhode Island, July 2, 1999.

Vita

Second Lieutenant Kristen L. Wallis graduated from Westfield High School in Chantilly, Virginia with an Advanced Program diploma. She began her undergraduate studies in Fall 2006 at Clemson University in Clemson, South Carolina, where she majored in Electrical Engineering with a concentration in Electronics and minored in Mathematics. She received an AFROTC scholarship while attending Clemson University. She graduated with a Bachelor of Science degree in May 2010. She was commissioned through Detachment 770—The Flyin' Tigers AFROTC at Clemson University.

Her first assignment, which began August 2010, was to attend the Graduate School of Engineering and Management at the Air Force Institute of Technology on Wright-Patterson Air Force Base in Dayton, Ohio, where she studied Electrical Engineering with a concentration in Electromagnetics. Upon graduating, she will be assigned to the National Air and Space Intelligence Community (NASIC) at Wright-Patterson Air Force Base.

REPORT DOCUMENTATION PAGE

Form Approved
OMB No. 074-0188

PLEASE DO NOT RETURN YOUR FORM TO THE ABOVE ADDRESS.

1. REPORT DATE *(DD-MM-YYYY)*	2. REPORT TYPE	3. DATES COVERED *(From – To)*
22-Mar-2012	Master's Thesis	August 2010 – March 2012

4. TITLE AND SUBTITLE
An Inquiry: Effectiveness of the Complex Empirical Mode Decomposition Method, the Hilbert-Huang Transform, and the Fast-Fourier Transform for Analysis of Dynamic Objects

5a. CONTRACT NUMBER

5b. GRANT NUMBER

5c. PROGRAM ELEMENT NUMBER

6. AUTHOR(S)
Wallis, Kristen L., Second Lieutenant, USAF

5d. PROJECT NUMBER
N/A

5e. TASK NUMBER

5f. WORK UNIT NUMBER

7. PERFORMING ORGANIZATION NAMES(S) AND ADDRESS(S)
Air Force Institute of Technology
Graduate School of Engineering and Management (AFIT/ENG)
2950 Hobson Way, Building 640
WPAFB OH 45433-8865

8. PERFORMING ORGANIZATION REPORT NUMBER
AFIT/GE/ENG/12-42

9. SPONSORING/MONITORING AGENCY NAME(S) AND ADDRESS(ES)
Air Force Research Laboratory
Richard Davis and Alan Frazier, RF Engineer, Radar Section
2241 Avionics Circle, WPAFB, OH 45433
(937) 938-4441, richard.davis2@wpafb.af.mil

10. SPONSOR/MONITOR'S ACRONYM(S)
AFRL/RYMR

11. SPONSOR/MONITOR'S REPORT NUMBER(S)

12. DISTRIBUTION/AVAILABILITY STATEMENT
DISTRIBUTION STATEMENT A. APPROVED FOR PUBLIC RELEASE; DISTRIBUTION IS UNLIMITED.

13. SUPPLEMENTARY NOTES
This material is declared a work of the U.S. Government and is not subject to copyright protection in the United States

14. ABSTRACT
A review of current signal analysis tools show that new techniques are required for an enhanced fidelity or data integrity. Recently, the Hilbert-Huang transform (HHT) and its inherent property, the Empirical Mode Decomposition (EMD) technique, have been formerly investigated. The technique of Complex EMD (CEMD) was also explored. The scope of this work was to assess the CEMD technique as an innovative analysis tool. Subsequent to this, comparisons between applications of the Hilbert transform (HT) and the Fast-Fourier transform (FFT) were analyzed. MATLAB® was implemented to model signal decomposition and the execution of mathematical transforms for generating results. The CEMD technique successfully decomposed the data into its oscillatory modes. After comparative graphical analysis of the HT and FFT, application of the HT provided marginal enhancements of the data modeled previously by the FFT. Altogether, the HHT could not be determined as a helpful analysis tool. Nevertheless, the CEMD technique, an inherent component of the HHT, exhibited a possible improvement as an analysis tool for signal processing data. Further evaluation of the CEMD technique and the HHT is needed for ultimate determination of their usefulness as an analysis tool.

15. SUBJECT TERMS
Signal analysis, mathematical transforms, radar-cross section, empirical mode decomposition, Hilbert-Huang transform

16. SECURITY CLASSIFICATION OF:			17. LIMITATION OF ABSTRACT	18. NUMBER OF PAGES	19a. NAME OF RESPONSIBLE PERSON
a. REPORT	b. ABSTRACT	c. THIS PAGE			Terzuoli, Andrew J., PhD
U	U	U	UU	160	19b. TELEPHONE NUMBER *(Include area code)* (937) 255-3636 x 4717 (Andrew.terzuoli@afit.edu)